Title
Design, Synthesis and Characterization of Novel Zwitterionic Lipids for Drug and siRNA Delivery Applications

Author
Walsh, Colin

Publication Date
2012

Peer reviewed|Thesis/dissertation

Design, Synthesis, and Characterization of Novel Zwitterionic Lipids for Drug and siRNA Delivery Applications.

by

Colin L. Walsh

DISSERTATION

Submitted in partial satisfaction of the requirements for the degree of

DOCTOR OF PHILOSOPHY

in

Bioengineering

in the

GRADUATE DIVISION

of the

UNIVERSITY OF CALIFORNIA, SAN FRANCISCO

AND

UNIVERSITY OF CALIFORNIA, BERKELEY

Acknowledgements

The text of Chapter 2 is a partial reprint of materials that appear in the journal *Chemical Communications.* Colin L. Walsh wrote the paper, F.C. Szoka revised the manuscript, and Juliane Nguyen assisted with liposomal formulations and *in vivo* experiments.

> Walsh, C. L., Nguyen, J. & Szoka, F. C. Synthesis and characterization of novel zwitterionic lipids with pH-responsive biophysical properties. *Chemical Communications* **48**, 5575–5577 (2012).

The text of Chapter 3 is co-authored by Aditya Kohli, who assisted in synthesizing and characterizing lipids, biophysical characterization experiments, and animal experiments, and manuscript writing. The text of Chapter 3 is in part a reprint of materials that appear in the journal *Chemistry and Physics of Lipids*. F.C. Szoka revised the manuscript.

> Kohli, A. G., Walsh, C. L. & Szoka, F. C. Synthesis and characterization of betaine-like diacyl lipids: zwitterionic lipids with the cationic amine at the bilayer interface. *Chemistry and Physics of Lipids* **165**, 252–259 (2012).

The text of Chapter 4 is a partial reprint of materials to appear in the journal *Bioconjugate Chemistry*. Colin L. Walsh wrote the paper and F.C. Szoka revised the manuscript. Juliane Nguyen and Matthew R. Tiffany assisted with liposomal formulations, *in vitro* transfection studies, and *in vivo* experiments.

The contribution of Colin L. Walsh is comparable to that of a standard thesis.

Acknowledgements

It is impossible for me to fully acknowledge the impact that all of my mentors, colleagues, family, and friends have had on my journey to this point. I can honestly say I had no idea what to expect when I packed up and moved to California five years ago, but the people I've met and the experiences I've had have shaped my life more than I ever could have expected.

I would first like to acknowledge the incredible support and guidance of my advisor, Dr. Frank Szoka, whose passion and enthusiasm for his work is truly inspiring. I thoroughly appreciate his scientific perspective, limitless curiosity, and willingness to tackle hard problems in unique ways. Most of all, I appreciate his borderline irrational confidence in me, even when we both knew that I had no idea what I was doing.

I would like to sincerely thank Dr. Tejal Desai and Dr. Kevin Healy for serving on my dissertation committee. I would also like to thank Dr. Chris Diederich, Dr. Chris Cullander, Dr. Frances Brodsky, and Dr. Dorian Liepmann for serving on my qualifying exam committee.

I would also like to thank all of the talented people who helped make this work possible: Dr. Zhaohua Huang, Dr. Emily Perttu, Dr. Derek van der Poll, Dr. Bo Chen, and Dr. Zhen Yao for their help with all things chemistry; Dr. Juliane Nguyen for significant contributions to nearly all aspects of my project; Darren Chan and Kat Jerger for their extensive efforts assisting me with *in vitro* and *in vivo* experiments; and Dr. Rich Cohen for his friendship and mentorship since joining the Szoka lab.

Thank you to all of my Szoka Labmates, past and present, for making this such a great place to come to everyday: Dr. Zhaohua Huang, Dr. Juliane Nguyen, Dr. Bo Chen, Dr. Emily Perttu, Dr. Kareen Riviere, Dr. Virginia Platt, Dr. Rich Cohen, Dr. Michael Motion, Jonathan Sockolosky, Darren Chan, Kat Jerger, Steve Ha, and Nikki Macaraeg.

A special thanks goes to Matthew Tiffany, Aditya Kohli, Dr. Vince Venditto, and Dr. Derek van der Poll for their friendship and scientific insight, I really could not have asked for a better group of people to spend almost every waking hour of my life with, and I can only hope that in the future I get to work with a group of people that are as smart, talented, funny, and easy to get along with as all of you.

Finally, I would like to thank my family and loved ones. To my parents and stepparents, thank you for your unconditional support and encouragement during the last five years, and for instilling upon me the value of hard work and perseverance. To my brother, thank you for your advice, friendship, and love. Your experiences paved the way for me, and there is simply no chance that I would be where I am today without you. Lastly, I owe a special thanks to Ms. Laura Panos, whose support and positivity helped keep me sane throughout this entire experience.

This work was supported by the National Science Foundation Graduate Research Fellowship Program, NIH grant EB003008, and a UCSF-QB3 Pfizer grant.

Abstract

Lipid-based nanoparticles have long been used to deliver biologically active molecules such as drugs, proteins, peptides, DNA, and siRNA *in vivo*. Liposomes and lipoplexes alter the biodistribution, pharmacokinetics, and cellular uptake of their encapsulated or associated cargo. This can increase drug efficacy while reducing toxicity, resulting in an improved therapeutic index and better clinical outcomes. Unlike small molecule drugs, which passively diffuse through lipid membranes, nucleic acids and proteins require an active, carrier mediated escape mechanism to reach their site of action. As such, the therapeutic application and drug properties dictate the required biophysical characteristics of the lipid nanoparticle. These carrier properties depend on the structure and biophysical characteristics of the lipids and other components used to formulate them.

This dissertation presents a series of studies related to the development of novel synthetic lipids for use in drug and siRNA delivery systems. First, we developed a novel class of zwitterionic lipids with head groups containing a cationic amine and anionic carboxylate and ester-linked oleic acid tails. These lipids exhibit structure-dependent, pH-responsive biophysical properties, and may be useful components for next-generation drug delivery systems. Second, we extended the idea of amine/carboxylate containing zwitterionic head groups and synthesized a series of acetate terminated diacyl lipids containing a quaternary amine. These lipids have an inverted headgroup orientation compared to naturally occurring zwitterionic lipids, and show interesting salt-dependent biophysical properties. Third, we synthesized and characterized a series of ionizable lysine-based lipids, which contain a lysine head group linked to a long-chain dialkylamine. A focused library was synthesized to determine the impact of hydrophobic fluidity, lipid net

charge, and lipid pKa on the biophysical and siRNA transfection characteristics of these lipids. Our results indicate that structural variations significantly impact the biophysical and transfection behavior of this class of lipids.

In summary, we have synthesized several new classes of lipids with biophysical characteristics that may be useful for drug delivery applications. Our results show that slight modifications to lipid structure impacts their biophysical behavior, which in turn dictates their potential utility in drug delivery systems. Further understanding lipid structure-activity relationships will allow for the rational design and engineering of lipids with appropriate properties for specific applications.

Table of Contents

List of Tables

List of Schemes

List of Figures

Abbreviations

ANTS - 8-aminonophthalene-1,3,6-trisulfonate
BMV – Biomembrane mimicking vesicle
Ca^{2+} - Calcium
CF – Carboxyfluorescein
$CHCl_3$ - Chloroform
Chol – Cholesterol
DiD - 1,1'-dioctadecyl-3,3,3',3'-tetramethylindodicarbocyanine
DMAP – 4-dimethylaminopyridine
DOPC - 1,2-dioleoyl-*sn*-glycero-3-phosphocholine
DOPE -1,2-dioleoyl-*sn*-glycero-3-phosphoethanolamine
DOPG - 1,2-dioleoyl-*sn*-glycero-3-phospho-(1'-rac-glycerol)
DOTAP - 1,2-dioleoyl-3-trimethylamonium-propane
DLinDMA - 1,2-dilinoleyloxy-3-N,N-dimethylaminopropane
DPX - p-xylene-bis-pyridinium bromide
DSC – Differential scanning calorimetry
DSPC - 1,2-distearoyl-*sn*-glycero-3-phosphocholine
EDC – 1-ethyl-3-(3-dimethylaminopropyl)carbodiimide
EtOAc – Ethyl Acetate
EtOH – Ethanol
FBS – Fetal bovine serum
hr – Hour
ILL – Ionizable lysine-based lipids
Luc – Luciferase
MALDI-TOF – Matrix assisted laser desorption/ionization time of flight
MEM – Minimum essential media
MeOH – Methanol
mg – Milligram
Mg^{2+} - Magnesium
Min - Minutes
μL – Microliter
Mol - mole
MTT - 3-(4,5-Dimethylthiazol-2-yl)-2,5-diphenyltetrazolium bromide
NaOAc – Sodium Acetate
NBD-PE - 1,2-dioleoyl-sn-glycero-3-phospho-L-serine-N-(7-nitro-2-1,3-benzoxadiazol-4-yl) (ammonium salt)
NMR – Nuclear magnetic resonance
PBS – Phosphate buffered saline without calcium and magnesium salts
PEG-DMG – 1-(monomethoxypolyethyleneglycol)-2,3-dimyrystoylglycerol
PK - Pharmacokinetics

Rho-PE - 1,2-dioleoyl-sn-glycero-3-phosphoethanolamine-N-(lissamine rhodamine B sulfonyl) (ammonium salt)
siRNA – Short interfering Ribonucleic Acids
TFA – Trifluoroacetic Acid
Tm – Melting temperature
TNS - Sodium 2-(p-toluidino)-6-naphthalenesulfonic acid
TRIS-HCl - tris(hydroxymethyl)aminomethane
ZL – Zwitterionic lipid

Chapter 1: Designing Novel Lipids for Drug Delivery Applications

1.1 Abstract

Mammalian, plant, and bacterial cells contain a diverse collection of zwitterionic and anionic lipids including phospholipids, sphingolipids, and glycerides. These lipids have defined biosynthetic pathways, and play essential roles in the structure, cellular signaling, and membrane trafficking inside the cell. In addition to their natural roles, lipids are widely used in the food, cosmetic, and pharmaceutical industries for the formulation and encapsulation of biologically active molecules. While naturally occurring lipids have a broad range of properties, synthetic chemistry allows for the development of non-natural lipids with novel characteristics suitable for clinical applications. Manipulation of the lipid head group, linker region, and hydrophobic domain alters the biological and biophysical behavior of the resulting superstructures. Unlike naturally occurring lipids, which are synthesized intracellularly from a defined set of precursors, synthetic lipids have an almost limitless number of possible structures due to the extensive collection of starting materials and linkages. Small changes to the chemical structure can drastically change the size, shape, activity, and stability of these molecules, allowing the lipid chemist to tailor the design of a lipid for a particular application.

Here, we discuss the role of lipid geometry in the design of bioactive lipids for drug delivery applications, identify "toolboxes" of common structural motifs found in natural and synthetic lipids, discuss how altering lipid regions impacts behavior, provide methods for designing or identifying lipids with a given set of biophysical and biological characteristics,

and present examples of how these ideas can be used to develop novel synthetic lipids for drug delivery.

1.2 Introduction

Lipid-based nanoparticles have a forty-year history for delivering biologically active molecules to target tissues *in vivo*. These systems are widely used to alter the pharmacokinetics, biodistribution, and uptake pathway of drugs, DNA, RNA, and proteins. Fine-tuning the molecular structures of the lipids used to formulate these nanoparticles allows for the control of the macrostructures they form, as well as their ability to associate with other molecules via electrostatic interactions, hydrogen bonding, pi-stacking, or other intermolecular forces.[1-11]

As a starting point, nature has provided a diverse library of lipids with chemical attributes that have evolved to satisfy a wide variety of functional and structural purposes. Additionally, synthetic efforts in the field of lipid chemistry have resulted in a myriad of new lipids that are not found in nature, but have interesting biological properties. Biophysical studies on these natural and synthetic lipids have revealed how molecular structure of the lipid influences its behavior in an ensemble.[10,12] Using this information, researchers can now rationally design and synthesize lipids, surfactants, and amphiphiles with specific chemical and biophysical properties.

One method for controlling lipid behavior is incorporating biologically active molecules such as drugs, nucleotides, nucleosides, and amino acids into the lipid structure, thereby imparting some of the characteristics and biological activity of these complex molecules to the lipid or the lipid ensemble. The resulting bioconjugate lipids can possess

properties that are distinctly different from those naturally synthesized in mammalian or bacterial cells, and have uses as drug or gene carriers, or even as drugs themselves.

The criteria discussed here provide information on the expected behavior of rationally designed synthetic lipids based on their structure, and serves as a starting point for the design and synthesis of lipids for a variety of drug delivery applications. However, the macromolecular structures formed by synthetic and natural lipids are extremely complex, and often even the most carefully designed lipid will not exhibit the desired properties. In these cases, it is important to understand that liposomal formulation and environmental conditions (pH, temperature, salt concentrations, divalent-cation concentration) can drastically change lipid or liposomal behavior.[13,14] In some cases, simply adjusting these parameters can result in different biophysical behavior. In others, empirical evidence and trial and error may be the only avenue to design the appropriate lipid. Under these circumstances, an iterative process including careful design, synthesis, and analysis of the biophysical properties in relation to the desired activity of the synthesized lipids will often lead to a successful outcome.

1.3 Lipid Structure, Geometry, and Phase Preference Dictate Behavior

In general, lipids consist of three distinct regions: the hydrophilic head group, a linker region, and the hydrophobic tail(s) (Figure 1.1). The size and molecular structure of each of these components plays an integral role in determining its biophysical behavior, stability, and utility in drug delivery systems. To fully understand the design of synthetic lipids for therapeutic applications, one must first understand how lipid structure affects the phase

preferences of the macromolecular structures formed, and how the properties of each structure impact the biophysical characteristics of the resulting drug carrier.

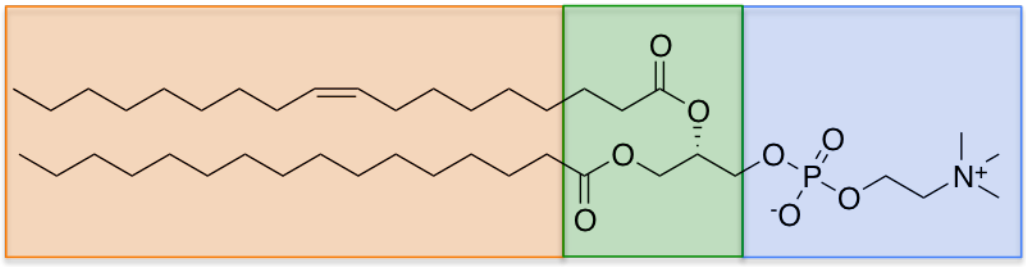

Figure 1.1: Structure of a phosphatidylcholine (PC) lipid, a common cellular membrane lipid, consisting of a phosphocholine head group (blue), glycerol linker region (green), and ester linked oleoyl and palmitoyl hydrophobic tails (orange).

One of the critical aspects of bioactive lipid design is lipid geometry, which plays a major role in the macromolecular structures formed in aqueous environments (Figure 1.2).[1-4,6,8,10,15] Amphiphilic lipid systems will self-assemble into thermodynamically favored phases that limit interactions between the hydrophobic lipid moieties and the surrounding aqueous environment. Cone shaped lipids, which contain a large head group and single hydrophobic tail, generally adopt a micellar structure with the large head groups assembling around a hydrophobic core (Figure 1.2, left). These structures are generally small (< 30 nm), and form because the hydrophobic tails occupy a smaller volume than the hydrophilic head group, allowing for tight packing in the hydrophobic core. Cylindrical lipids, generally consisting of a large head group and two hydrophobic tails, adopt the lamellar (L_α) phase and form bilayers and vesicles (Figure 1.2, center). These macrostructures possess an aqueous core, which can be used to encapsulate hydrophilic molecules. Inverted cone shaped lipids, characterized by a small head group and large (generally branched or unsaturated) hydrophobic region, form inverted micelles known as the inverse hexagonal (H_{II}) phase (Figure 1.2, right). These systems are generally unstable in water, and tend to form long assemblies of six cylindrical rods to exclude water from the exposed hydrophobic regions.

Lipids that prefer the inverted hexagonal phase are said to be "fusogenic," as they promote membrane collapse and fusion (formation of a continuous bilayer from two adjacent bilayers) upon interaction with another lipid membrane.[2,3,16-19]

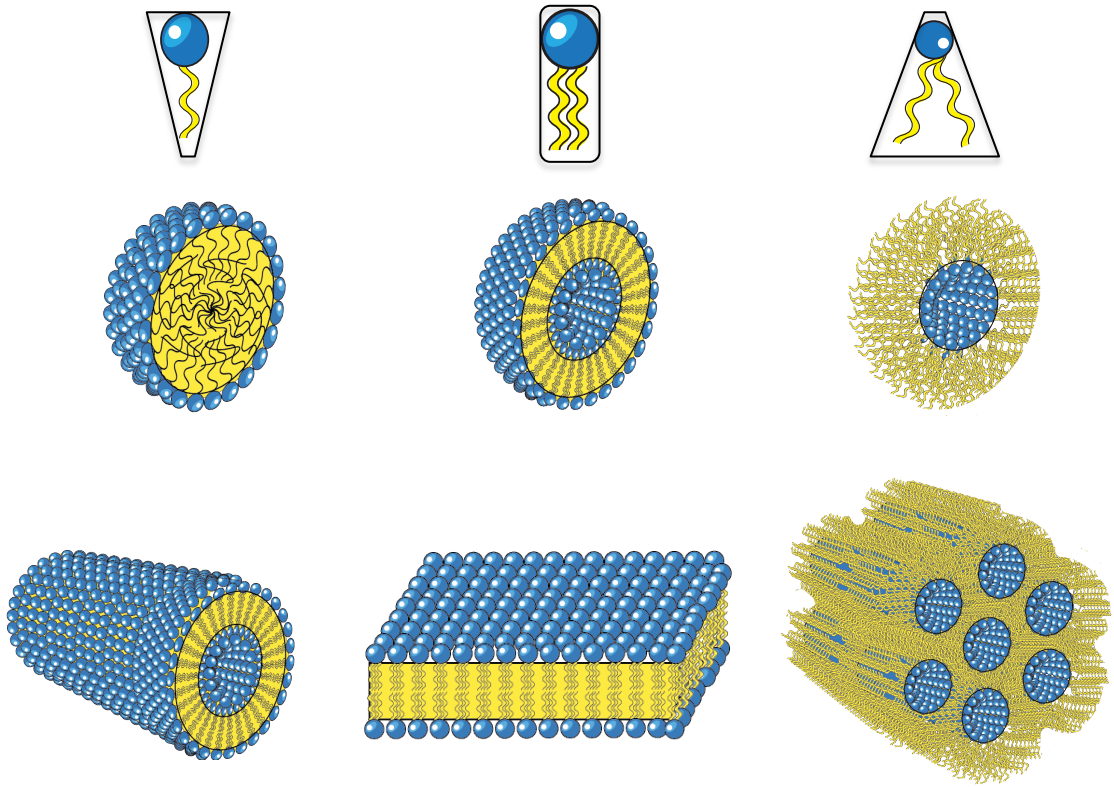

Figure 1.2: Schematic representations of lipid geometries and the macromolecular structures that they form. From left to right: cone-shaped lipids, cylindrical lipids, and inverted cone-shaped lipids.

It is important to note that liposomal formulation plays a critical role in the phase preference of the assembled macrostructure. Systems consisting of mixed lipids can adopt any of the described phases depending on lipid composition, and also show intramembrane phase separation under the appropriate conditions.[2,3,6,20] Incorporation of a large enough fraction of lipids that prefer the L_α phase can force lipids that prefer the H_{II} phase into a bilayer. Further, external stimuli, such as a change in environmental temperature or pH, or interactions of the carrier with other lipid membranes, proteins, or peptides can cause the system to spontaneously change phase and direct contents release or membrane fusion.

The phase preference of lipids in drug and gene delivery systems plays a role in the contents release kinetics and membrane interactions of the carrier. Here, we focus on lipids that adopt the L_α or H_{II} phase. Systems containing bilayer lipids tend to form stable liposomes that slowly leak their contents, and are therefore useful as long-circulating drug carriers for small molecule drugs. Systems with lipids that form inverted micelles tend to be less stable, and collapse or fuse upon interactions with other membranes. These systems are better suited for applications where the liposomal contents are unable to passively cross cellular membranes (DNA, RNA, proteins), and an active, carrier-mediated escape mechanism is required for contents release. Recently, significant work has focused on the development of lipids that adopt H_{II} phase at endosomal pH for the delivery of DNA and siRNA *in vivo*.[2,6,15,21]

1.3.1 Lipid head groups

The lipid head group imparts hydrophilicity, charge, and hydrogen bonding ability to the molecule, which affects the properties of the macromolecular structures it forms. Zwitterionic head groups, including phosphatidylcholine (PC) and phosphatidylethanolamine (PE), contain an anionic phosphate and a cationic amine. Lipids containing these head groups, which are neutral at physiological pH, are the main components of cellular membranes, and are essential to membrane stability and trafficking inside the cell. Recently, our group synthesized a series of zwitterionic lipids with an inverted charge configuration compared to PC lipids.[22-24] These systems exhibit interesting thermotropic and drug release behavior, which are salt-dependent, and likely related to the charge orientation at the bilayer interface. These properties make them interesting candidates for drug delivery applications.

Glycerides, which contain a glycerol head group linked to fatty acid tails, are neutral lipids with no formal charge that serve as energy sources and signaling molecules in mammalian cells. Naturally occurring anionic head groups, including phosphatidylglycerol (PG), phosphatidylinositol (PI), cardiolipin (CL), phosphatidic acid (PA), and phosphatidylserine (PS) are also found in mammalian cell membranes, and play a critical role in cellular signaling, lipid-protein interactions, and membrane trafficking.[17,20,25-27] These naturally occurring lipids have been used extensively for the delivery of drugs, including several FDA approved therapies such as Doxil, AmBisome, and DepoCyte.[28]

Conversely, cationic headgroups, including dimethylamine, trimethylamine, and guanidine are not found in mammalian cell membranes, but have shown promise in the drug delivery space.[5,29] Membrane incorporation of these lipids can be toxic as they can disrupt anionic cell membranes through electrostatic interactions, interfere with anionic proteins, and cause an inflammatory immune response.[5,6,25,27,30,31] However, their ability to associate with and disrupt cellular membranes makes them particularly interesting for use in gene and siRNA delivery vectors, and significant synthetic efforts have yielded a large library of lipids with cationic or ionizable head groups.[5-7,30-32]

In addition to charge, the structure of the head group plays a critical role in lipid behavior. The ability to form hydrogen bonds with other membrane lipids or molecules can significantly affect the phase behavior, transition temperature, and molecular interactions of synthetic lipids and amphiphiles in delivery systems. Including hydrogen-bonding groups tends to increase transition temperature, and allow for interactions with other H-bonding molecules like DNA and RNA. The size of the head group, along with other structural characteristics, impacts the stability and phase behavior of the lipid. Smaller head groups,

such as PE, tend to promote more membrane active, fusogenic lipids that adopt the H_{II} phase; larger head groups, including PC, PS, and PG promote the more stable L_{α} phase.

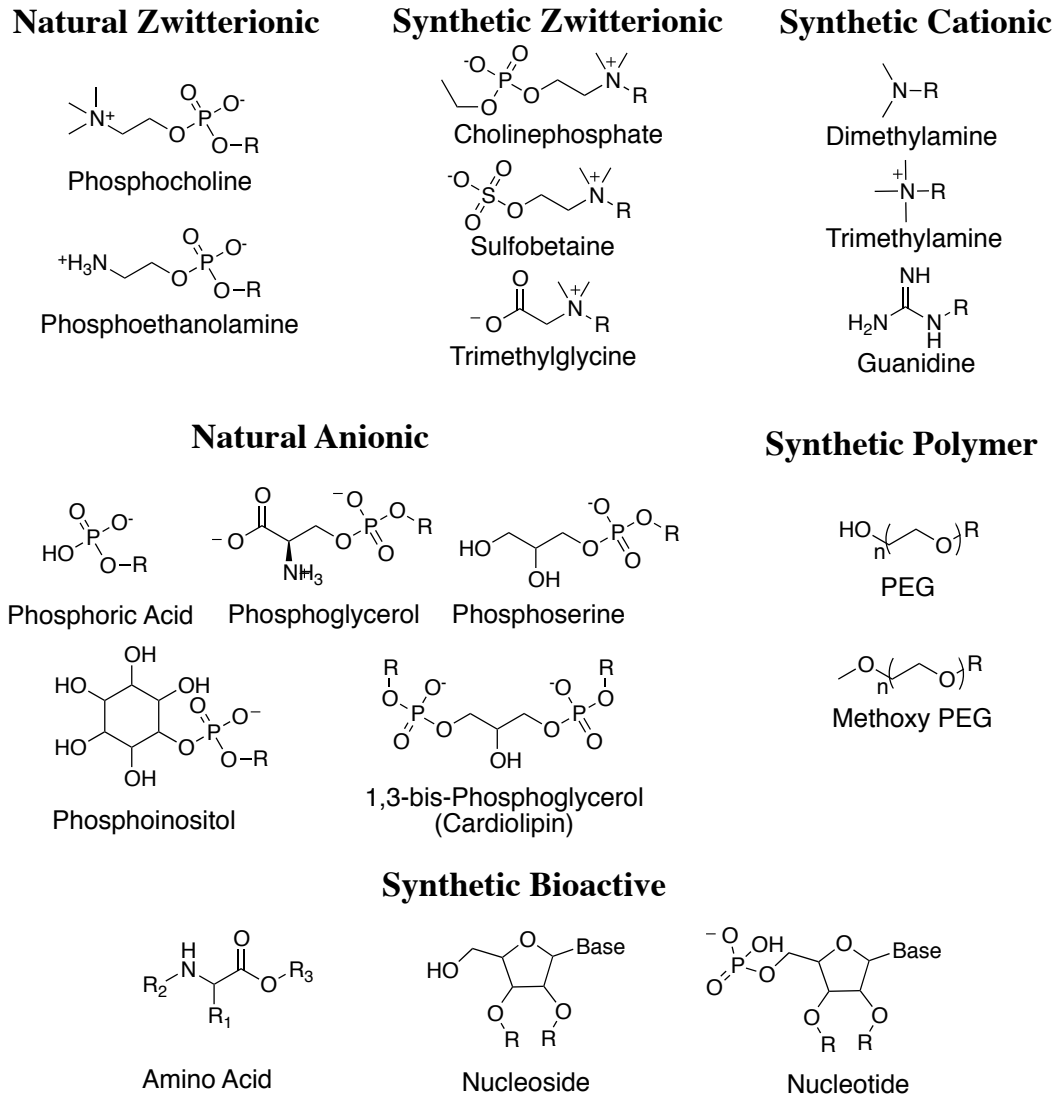

Figure 1.3: Molecular structures of common naturally occurring lipid head groups used in drug delivery, as well as a non-exhaustive list of potentially interesting hydrophilic groups that can be or have been used as synthetic lipid head groups. R = Hydrophobic group.

Unlike naturally occurring lipids, synthetic lipids can draw from a near infinite number of functionalized hydrophilic structures including drugs, polymers, amino acids, nucleotides, nucleosides, carbohydrates, acids, chelators, and cationic or ionizable amines.. Further, headgroups can be rationally designed to include multivalent functional

structures.[30,33-35] The structure and functional groups of the head group dictate both the synthetic pathway to the final product, as well as the properties that the completed amphiphile will possess.

One important synthetic head group to highlight is poly(ethylene) glycol (PEG), which is used extensively in drug delivery systems as a coating material to alter the pharmacokinetics of nanocarriers.[36] PEG can be conjugated to a number of different lipid backbones and incorporated into liposomes. The PEG molecules form a hydrophilic shell on the surface of the nanoparticle, preventing interactions with serum proteins and uptake by the mononuclear phagocyte system (MPS), thereby extending particle circulation time. The structure of the lipid anchor and size of the PEG head group dictate how stably these lipopolymers are incorporated into liposomes, which impacts clearance and distribution.

1.3.2 Lipid linkages

When designing lipids for drug delivery applications, it is important to consider the required delivery location (organ, tumor, intracellular, cytosolic), the mechanism by which the lipid will be processed to free the active encapsulated or conjugated molecule, as well as the possible byproducts of this degradation. The region linking the hydrophilic and hydrophobic moieties is of particular interest, as the degradation kinetics of this linkage can dictate the stability and release behavior of the drug carrier, as well as the toxicity of the lipids and their metabolic byproducts (Figure 1.4).

Hydrolytically degradable linkages such as esters, orthoesters, carbamates, carbonates, and ketals can provide rapid lipid degradation and subsequent release of liposomal contents in the presence of enzymes (ester, amide) or in the low-pH environment along the endocytic

pathway (orthoester, carbamate, carbonate, ketal). Delivery vehicles containing naturally occurring lipids, which generally contain ester linkages, are likely degraded by enzyme-catalyzed hydrolysis in the liver, serum, or along the endocytic pathway following internalization. Lipid hydrolases, such as phospholipase A2, selectively hydrolyze the ester bond linking fatty acids to the phospholipid backbone.[37] Alternatively, less specific enzymes such as carboxylesterases, which degrade esters, and cathepsins, which degrade amides, can also hydrolyze lipids containing these linkages, leading to rapid degradation of the carrier and subsequent release of the internal contents.[20]

When designing enzyme-sensitive lipids, particular consideration should be given to the enzyme activity, which will be dictated both by the molecular structure adjacent to the hydrolysis site, as well as the macromolecular structures formed. Lipids that form solid nanoparticles will be degraded slower than those that form bilayer structures. Additionally, degradation kinetics will depend upon the molecular structure surrounding the linker; for example, branched chain fatty acids, which sterically hinder enzymatic access to the cleavage site, can greatly reduce cleavage rates.[1-11,30,35,38-40] In addition to the enzyme and acid sensitive linkages described above, redox-sensitive disulfide linked lipids will degrade in the reducing intracellular environment. These systems can also be modified to change their shape and charge by replacing disulfide linked head group moiety with a cation, anion, or PEG.

More stable linkages, including ethers and alkylamines show limited degradation even under harsh lysosomal conditions, altering the release kinetics of the carrier. In addition to release kinetics, the stability of the linker region influences the degradation mechanism and cytotoxicity of synthetic lipids. Synthetic lipids containing biodegradable linkages are

Functional Group	Desired Linkage	Required Functional Group	Possible Chemistries
Alkyl Amine (1°, 2°) 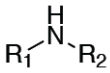	Amide 	Carboxylic Acid R_1–COOH	Coupling Activated Ester
		Acid Halide R_1–COX X = Cl, Br, I	Nucleophilic Reaction
	Alkyl Amine (2°,3°) 	Leaving Group R_1–X	S_N2
	Substituted Amino Acid (2°,3°) 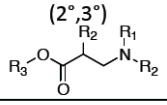	Acrylate 	Michael-Type Addition
Alkyl Amine (3°) 	Alkyl Amine (4°) 	Leaving Group R_1–X	S_N2
Hydroxyl 	Ester 	Carboxylic Acid R_1–COOH	Coupling
		Acid Halide R_1–COX X= Cl, Br, I	Nucleophilic Reaction
	Ether 	Leaving Group R_1–X	S_N2
	Phosphate 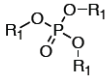	Phosphorous Halide 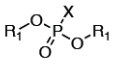	S_N2
Thiol 	Disulfide 	Thiol R_1–X	Oxidation
	Thioether 	Leaving Group R_1–SH	S_N2
		Alkene 	Thiolene Click Chemistry
Alkyne 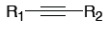	Triazole 	Azide 	Huisgen Cycloaddition
R_1= Any alkyl R_2= Any alkyl, H R_3= Any alkyl, carboxyl protecting group X = Cl, Br, I, OTs, OMs, OTf			

Figure 1.4: Schematic representation of several common functional groups and linkages used in synthetic lipid chemistry.

generally processed into low molecular weight byproducts that are cleared from the body through the renal system. Lipids with linkages that are not degraded tend to persist *in vivo*, potentially increasing their cytotoxic effects.[25,41-44] This is of particular importance for lipids with cationic or other potentially toxic moieties, as accumulation and persistence of these structures generally causes higher levels of cytotoxicity and inflammation than an equivalent anionic or neutral lipid. In fact, studies have shown that the cytotoxicity and immunostimulatory effects of cationic lipids is often directly linked to their stability. In many cases, delivery or transfection efficiency *in vivo* increases with lipid stability.[2,19,45-47] As such, it is important to understand the balance of efficacy and toxicity when designing synthetic lipids, particularly those that are cationic.

The linker region plays a critical role in the stability, toxicity, and degradation mechanism of natural and synthetic lipids. Hence, understanding the behavior of different linkages in an assortment of physiologically relevant environmental conditions enables the lipid chemist to select an appropriate linkage for a given application. This, along with other aspects of lipid design, allows for the control of contents release, degradation, and toxicity of lipid-based drug carriers.

1.3.3 Lipid hydrophobic groups

Lipid tails impart hydrophobicity to these amphipathic molecules. The size and structure of the hydrophobic region influences lipid geometry, phase preference, degradation, and drug release kinetics. As such, it is another critical aspect of synthetic lipid design that should be carefully considered.

Generally, two types of hydrophobic groups are used in synthetic lipid chemistry: aliphatic chains and sterols (Figure 1.5). Common aliphatic chains consist of saturated, unsaturated, and branched structures ranging from eight to twenty carbons in length; common sterols include cholesterol, cholesterol hemisuccinate, and tocopherol. These molecules are commercially available with a variety of functional groups, including acids, alcohols, amines, or thiols. The functional group used is dependent upon the synthetic scheme and the desired linkage.

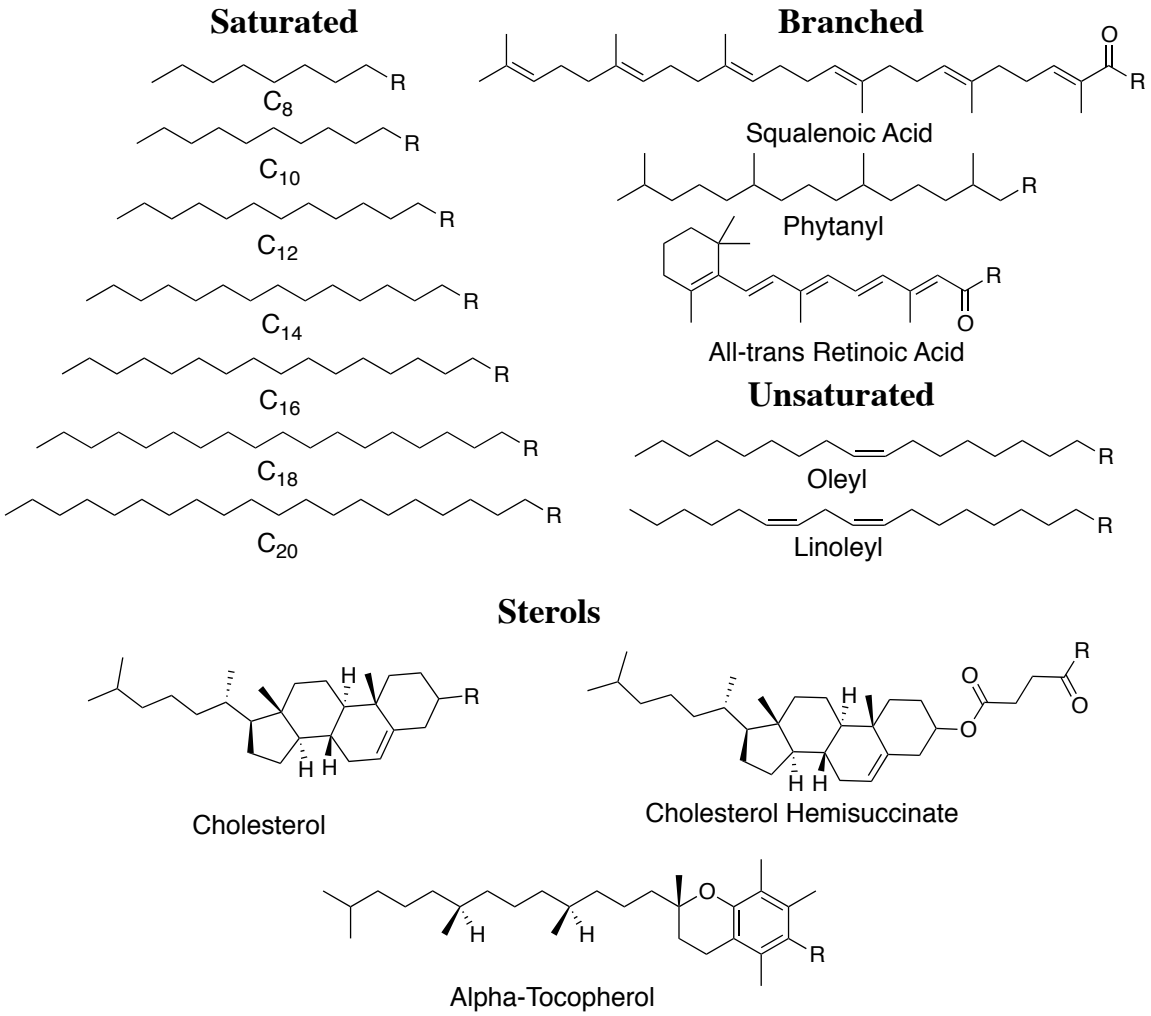

Figure 1.5: Examples of hydrophobic groups that are commonly found in naturally occurring lipids or used for synthetic lipid chemistry. Carefully selecting the appropriate number of chains with the appropriate structure should allow for the synthesis of a structure with the desired characteristics.

Similar to the lipid head group, the hydrophobic region plays an important role in the geometry and phase preference of a lipid. Lipids containing a single aliphatic chain are generally cone shaped and adopt a micellar structure as described previously. Lipids with a single sterol or two aliphatic chains can form bilayer or inverted micellar structures depending on the relative size of the head group. Saturated aliphatic chains, which generally contain 6-22 carbons, tend to pack tightly into a hydrophobic core, and generally form cylindrical lipids that prefer the bilayer phase. Unsaturated aliphatic chains, including oleic, linoleic, and elaidic acid, contain at least one carbon-carbon double bond, and are characterized by looser packing and lower melting temperatures than their saturated counterparts.[48] Lipids with unsaturated aliphatic tails and large head groups, like PC and PG, are cylindrical in shape and readily adopt bilayer structures. However, lipids with smaller head groups, including PE and PS, tend to adopt an inverted cone shape and prefer the H_{II} phase under certain environmental conditions [2,19]. Similarly, branched chain lipid tails, such as phytanoic acid or squalenoic acid, have differing phase preferences depending on the size of the head group.

Additionally, the structure of the hydrophobic region dictates fluidity or stability of the bilayer, which is critical to the drug release behavior of bilayer forming lipids. Long aliphatic chains pack into a more ordered, stable bilayer than shorter or unsaturated chains. This is illustrated by the effect of chain length and unsaturation on the solid-liquid crystal transition temperature of a lipid. Increasing chain length or increasing saturation results in an increase in the transition temperature and increased bilayer stability. Generally, more stable bilayers will show slower drug release kinetics, therefore lipids containing longer (C_{20} or C_{18}) saturated chains, show the slowest drug release kinetics. Incorporating shorter (C_{12}-C_{16}) or

unsaturated ($C_{18:1}$) chains increases the fluidity of the bilayer. Substituting polar functional groups into these chains reduces stability[3,10,15].

Another mechanism for altering the fluidity of the bilayer is through the addition of sterols or sterol containing lipids. These rigid, planar hydrophobic groups disrupt aliphatic chain interactions while increasing the rigidity of the bilayer. The addition of sterols can effectively eliminate the phase transition of the bilayer and reduce the rate of liposomal contents leakage, offering another way to control the biophysical properties of the drug delivery system [2,16,17,19,48]. However, free sterols rapidly transfer between lipid bilayers, altering the properties of the drug carrier upon systemic injection. One way to avoid this is by directly conjugating sterols to the lipid backbone in place of one or more acyl chains.[3,16,18] The resulting sterol-modified lipids impart the same properties as free cholesterol and are much more stably incorporated into the liposomal membrane.

1.4 Lipid Nanocarriers for Drug, Gene, and siRNA Delivery

In 1964, Dr. Alec Bangham showed that phospholipids in aqueous environments form closed bilayer structures.[49] Since this discovery, significant advances have been made to understand the chemical, biophysical, pharmacological, and physiological properties of liposomes, and translate these systems into effective drug carriers. Liposomes are capable of encapsulating drugs at high concentrations, promote long circulation and drug persistence *in vivo,* and have tunable properties dictated by the lipids used in the drug formulation. Additionally, the size and composition of the liposome impact its pharmacokinetic profile as well as drug release rates, and can be fine tuned for a given application. These properties have made liposomes excellent candidates for drug delivery applications, and over the past

two decades, 10 liposomal drugs have gained clinical approval worldwide for the treatment of cancer, fungal infections, age related macular degeneration, and pain, with several others currently being evaluated for similar indications. [28]

Drug delivery systems are used to alter the distribution, pharmacokinetics, and toxicity profiles of drugs to increase their therapeutic efficacy.[50] Many drugs are characterized by a short serum half-life, requiring high doses to achieve therapeutic concentrations. However, higher doses increase the likelihood of adverse side effects due to drug related toxicity.[11] The large size of liposomes (> 50 nm in diameter) prevents drug clearance by renal filtration, and hinders extravasation through epithelial layers. Therefore, encapsulation of drugs in liposomes can overcome the limitations of a drug by extending its half-life and limiting drug distribution to potential sites of toxicity (i.e. skin, heart, muscle).[51] Additionally, liposomes are known to accumulate in tumors and sites of inflammation due to more permeable vasculature and compromised lymphatics. This phenomenon, known as the enhanced permeation and retention effect (EPR), makes nanoparticle based drug delivery systems attractive for the treatment of solid tumors because they promote high drug concentrations at the disease site. All of these properties combine to make liposomes an attractive option for drug candidates that could be improved by altering their pharmacokinetic profiles.

1.3.1 Liposomes for small molecule drug delivery

An effective liposomal system for small molecule delivery should have high drug loading, exhibit long circulation times, retain and protect the drug while in circulation, and accumulate at the target site. All of these criteria are dictated by the characteristics of the

liposome, including the size, charge, and lipid composition.[50] Because small molecule drugs generally pass through lipid bilayers, the stability of the lipid nanocarrier is essential to developing a successful delivery system. Release rates depend on the drug properties (size, charge, lipophilicity, etc.), as well as the carrier properties. As such, development of lipid-based carriers for small molecule drugs is often done on a case-by-case basis, with liposomal formulation tailored to optimize the efficacy of the drug based on its pharmacology. These systems are generally comprised of naturally occurring saturated phospholipids, cholesterol, and a PEG-lipid to prevent protein opsonization and increase circulation times.[50]

1.3.2 Liposomes for large molecule drug delivery

Unlike small molecules, macromolecular drugs such as proteins, peptides, DNA, and siRNA are unable to cross cellular membranes due to their large size and charge density.[5] Therefore, these molecules require active, carrier-promoted delivery from compartments along the endocytic pathway into the cytosol.[6] Liposomal encapsulation allows for cellular internalization via endocytosis (Figure 1.1, D), and appropriately designed liposomal carriers can mediate productive delivery to the cytosol by disrupting or fusing with membranes along the endocytic pathway. [5,6,29] Due to this requirement, these systems tend to be more complex than small molecule delivery systems, and often require the development of novel lipids with appropriate biophysical properties to form stable nanocarriers that promote internalization and cytosolic delivery. Here, we will focus specifically on lipid systems for the delivery of siRNA.

siRNA are oligonucleotides (~13 kDa) that catalyze the degradation of complementary cellular mRNA following cellular uptake and processing by the RNA-

induced silencing complex (RISC).[52] siRNA therapeutics are attractive due to their ability to specifically target an almost infinite number of genetic sequences, allowing for the robust regulation of nearly any protein.[53] Since RISC is located in the cytosol, it is imperative that functional synthetic siRNA be delivered to this compartment for RNA interference to occur. Several transfection systems, including viruses, polymers, peptides, and lipids, have been explored, and several excellent candidates exist for *in vitro* delivery across most cell types.[5] However, the development of efficient, well-defined, and well-tolerated *in vivo* delivery systems remains the major hurdle to the successful development of siRNA therapeutics.[6] To date, lipid-based systems are the most promising siRNA delivery technology for clinical applications, with several clinical trials underway for diseases of the liver. However, applications in solid tumors and other organs are still limited due to the lack of a robust delivery system.[6,52]

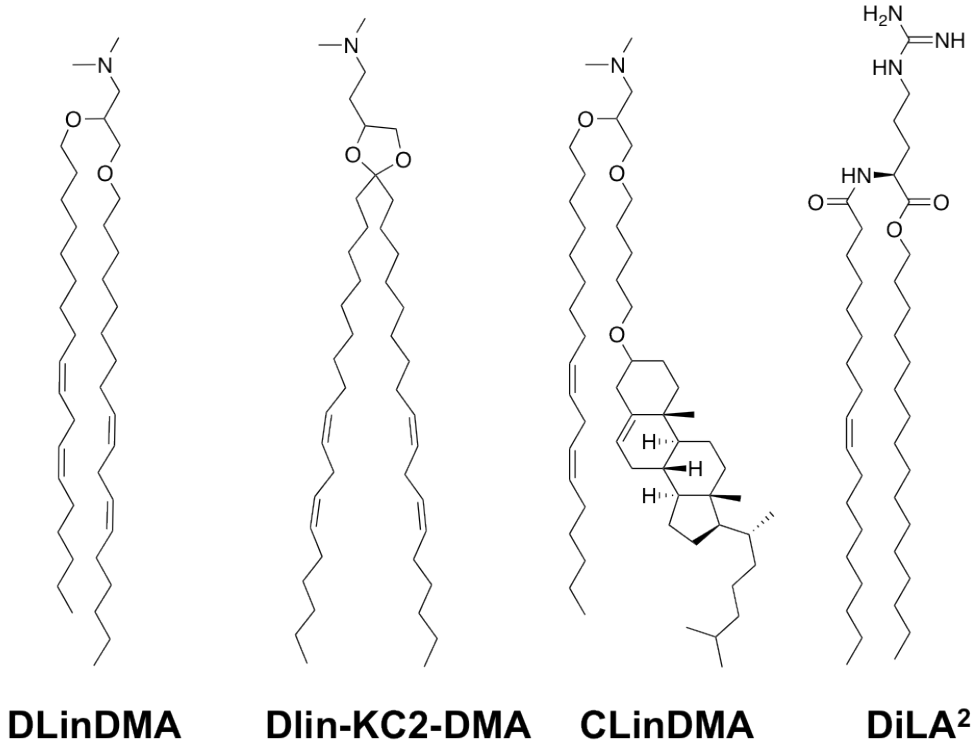

Figure 1.6: Representative examples of synthetic cationic or ionizable lipids for siRNA delivery.[54-56]

Significant literature exists on the development of cationic lipid systems for DNA delivery.[5] Though these systems are excellent *in vitro* transfection reagents, they are generally not suitable for *in vivo* applications due to their immunogenicity and toxicity. However, recent work in the area of synthetic lipid chemistry has resulted in a number of new ionizable aminolipids for siRNA delivery (Figure 1.6), and several have shown promising *in vivo* results.[6,54-56] Additionally, the development of structure activity relationships have provided insight into the specific lipid, and liposomal, characteristics that are required for successful siRNA delivery.[6] In general, these systems contain ionizable, amine containing head groups that are protonated at low-pH, and large, unsaturated hydrophobic regions. Both of these structural aspects are believed to play a role in their *in vivo* efficacy. The amino head group is important for several reasons. First, cationic lipids promote electrostatic interactions with anionic siRNA, allowing for the efficient encapsulation of high concentrations of siRNA in lipid nanoparticles.[57] Second, electrostatic interactions between the cationic carrier lipids and anionic serum proteins leads to protein opsonization and rapid distribution into the liver, where the liposomes are internalized by hepatocytes and macrophages. Following internalization, the cationic lipids ion-pair with anionic lipids along the endocytic pathway, forming a cone-shaped structure where the cross-section of the combined head groups is much smaller than the combined hydrophobic tail area. These cone shaped structures promotes the formation of inverse-hexagonal (H_{II}) phase, which is known to cause membrane disruption, fusion, and liposomal contents release (Figure 1.7).[54,58]

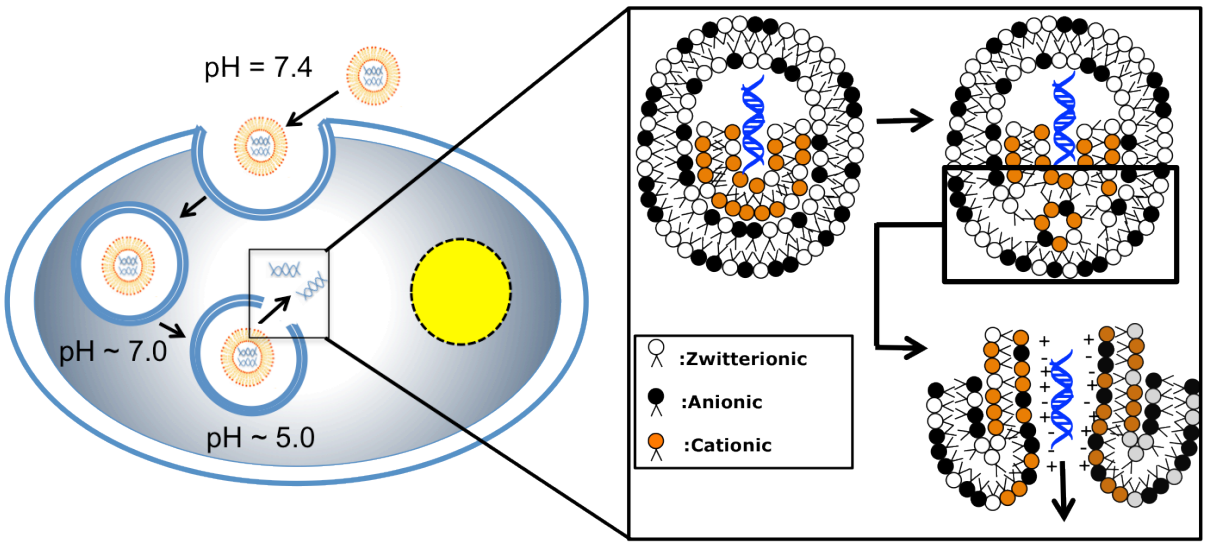

Figure 1.7: Left: Schematic representation of liposomal trafficking through the endocytic pathway. Inset: Once internalized, ion pairing events between cationic carrier lipids and anionic endosomal lipids results in the formation of unstable H_{II} phase structures, which eventually lead to membrane disruption and cytosolic delivery of liposomal contents.

Ionizable systems are preferable to formally cationic systems because at physiological pH, nanoparticles containing these lipids have a lower net positive surface charge than those containing formally cationic lipids.[41] Following internalization, ionizable lipids become cationic in the low-pH environment along the endocytic pathway, thereby selectively promoting electrostatic interactions and membrane disruption. This reduces the immunostimulatory effects of these systems compared to cationic liposomes, however inflammatory immune responses are still observed in these systems, making chronic dosing difficult without pre-dosing with anti-inflammatory medications.[55]

Though ionizable lipids have shown promise for siRNA delivery, there are limitations to the current systems, and the development of novel lipids that overcome these issues is important. Cationic lipids are generally immunostimulatory, making chronic dosing a major concern.[55] Additionally, long circulating cationic systems are difficult to develop due to rapid opsonization of serum proteins, reducing their ability to target solid tumors and other organs

due to the short serum half-life of the carrier. The inclusion of helper lipids, particularly PEG-lipids, which stabilize the particles and prevent protein opsonization has been shown to improve their efficacy.[59] However, reducing the cationic nature of these particles limits their efficacy as transfection reagents, making it particularly difficult to extend the utility of these systems beyond hepatocellular targets. The solution to this problem likely lies in the development of more sophisticated synthetic lipids, targeting moieties, and nanoparticle formulations that can overcome the physiological barriers required to develop a broad range of effective siRNA-based therapeutics.

1.6 Conclusions

The structure, phase preference, and biophysical behavior of lipids in a drug or gene delivery system has a profound impact on the stability and behavior of the nanocarrier. Bilayer phase lipids are generally more suitable for small molecule drug release because they form stable liposomes that slowly release their contents. Due to their membrane disruption properties, lipids that prefer the inverse hexagonal phase are often more appropriate for the delivery of large, charged molecules like DNA, RNA, and proteins that cannot pass through the lipid membrane. Significant synthetic efforts have lead to the development of several interesting aminolipids for the delivery of siRNA to hepatocellular targets *in vivo*. Despite their promising results, poor biodistribution and immunostimulatory effects limits the utility of these systems for systemic delivery of siRNA to tumors and other organs. However, advances in our understanding of the structure-activity relationships for lipid-based siRNA delivery systems are guiding new synthetic efforts that may eventually lead to new materials that overcome these hurdles, allowing siRNA therapeutics to reach their full potential.

1.7 References

1. Huang, Z., Li, W., Mackay, J. & Szoka, F. Thiocholesterol-based lipids for ordered assembly of bioresponsive gene carriers. *Mol Ther* **11**, 409–417 (2005).
2. Hafez, I. & Cullis, P. Roles of lipid polymorphism in intracellular delivery. *Advanced Drug Delivery Reviews* (2001).
3. Silver, B. *The physical chemistry of membranes*. 396 (Unwin Hyman: 1985).
4. Israelachvili, J., Mitchell, D. & Ninham, B. Theory of self-assembly of hydrocarbon amphiphiles into micelles and bilayers. *Journal of the Chemical Society, Faraday Transactions 2* **72**, 1525–1568 (1976).
5. Li, W. & Szoka, F. C. Lipid-based Nanoparticles for Nucleic Acid Delivery. *Pharm Res* **24**, 438–449 (2007).
6. Stanton, M. G. & Colletti, S. L. Medicinal chemistry of siRNA delivery. *J Med Chem* **53**, 7887–7901 (2010).
7. Gissot, A., Camplo, M., Grinstaff, M. W. & Barthélémy, P. Nucleoside, nucleotide and oligonucleotide based amphiphiles: a successful marriage of nucleic acids with lipids. *Org Biomol Chem* **6**, 1324–1333 (2008).
8. Piomelli, D., Astarita, G. & Rapaka, R. A neuroscientist's guide to lipidomics. *Nat Rev Neurosci* **8**, 743–754 (2007).
9. Puri, A., Loomis, K., Smith, B. & Lee, J. Lipid-based nanoparticles as pharmaceutical drug carriers: from concepts to clinic. *Crit Rev Ther Drug Carrier Syst* (2009).
10. Cullis, P. R. & de Kruijff, B. Lipid polymorphism and the functional roles of lipids in biological membranes. *Biochim Biophys Acta* **559**, 399–420 (1979).
11. Peer, D., Karp, J., Hong, S. & Farokhzad, O. Nanocarriers as an emerging platform for cancer therapy. *Nature* (2007).
12. Weselake, R. & Harwood, J. Lipid Library - Lipid Chemistry, Biology, Technology and Analysis. *lipidlibrary.aocs.org* at <http://lipidlibrary.aocs.org/index.html>
13. Drescher, S., Graf, G., Hause, G. & Dobner, B. Amino-functionalized single-chain bolalipids: Synthesis and aggregation behavior of new basic building blocks. *Biophysical chemistry* (2010).
14. Helical nanofibers of self-assembled bipolar phospholipids as template for gold nanoparticles. **112**, 4506–4511 (2008).
15. Cho, W. & Stahelin, R. Membrane-protein interactions in cell signaling and membrane trafficking. *Annu Rev Biophys Biomol Struct* **34**, 119–151 (2005).
16. Huang, Z. & Szoka, F. C., Jr Sterol-Modified Phospholipids: Cholesterol and Phospholipid Chimeras with Improved Biomembrane Properties. *J. Am. Chem. Soc* (2008).doi:10.1021/ja8065557
17. Mukherjee, S. & Maxfield, F. Role of membrane organization and membrane domains in endocytic lipid trafficking. *Traffic* **1**, 203–211 (2000).
18. Zhang, J., Fan, H., Levorse, D. A. & Crocker, L. S. Ionization Behavior of Amino Lipids for siRNA Delivery: Determination of Ionization Constants, SAR, and the Impact of Lipid p Kaon Cationic Lipid−Biomembrane Interactions. *Langmuir* **27**, 1907–1914 (2011).
19. Epand, R. M., Cullis, P. R. & Bailey, A. L. *Lipid polymorphism and membrane properties*. 568 (Academic Pr: 1997).
20. Bildstein, L., Dubernet, C. & Couvreur, P. Prodrug-based intracellular delivery of

anticancer agents. *Advanced Drug Delivery Reviews* 1–21 (2011).doi:10.1016/j.addr.2010.12.005
21. Ganta, S., Devalapally, H., Shahiwala, A. & Amiji, M. A review of stimuli-responsive nanocarriers for drug and gene delivery. *Journal of Controlled Release* **126**, 187–204 (2008).
22. Kohli, A. G., Walsh, C. L. & Szoka, F. C. Synthesis and characterization of betaine-like diacyl lipids: zwitterionic lipids with the cationic amine at the bilayer interface. *Chemistry and Physics of Lipids* **165**, 252–259 (2012).
23. Perttu, E. K., Kohli, A. G. & Szoka, F. C. Inverse-phosphocholine lipids: a remix of a common phospholipid. *Journal of the American Chemical Society* **134**, 4485–4488 (2012).
24. Perttu, E. K. & Szoka, F. C. Zwitterionic sulfobetaine lipids that form vesicles with salt-dependent thermotropic properties. *Chemical Communications* **47**, 12613–12615 (2011).
25. Lv, H., Zhang, S., Wang, B., Cui, S. & Yan, J. Toxicity of cationic lipids and cationic polymers in gene delivery. *Journal of Controlled Release* **114**, 100–109 (2006).
26. Reddy, L. Lipid-Based Anticancer Prodrugs. *Macromolecular Anticancer Therapeutics* (2010).
27. Tan, Y. & Huang, L. Overcoming the inflammatory toxicity of cationic gene vectors. *J Drug Target* **10**, 153–160 (2002).
28. Duncan, R. & Gaspar, R. Nanomedicine(s) under the Microscope. *Mol Pharm* **8**, 2101–2141 (2011).
29. Nguyen, J. & Szoka, F. C. Nucleic Acid Delivery: The Missing Pieces of the Puzzle? *Acc Chem Res* (2012).doi:10.1021/ar3000162
30. Sagnella, S. M. *et al.* Nanostructured nanoparticles of self-assembled lipid pro-drugs as a route to improved chemotherapeutic agents. *Nanoscale* 1–6 (2011).doi:10.1039/c0nr00781a
31. Xu, Y. & Szoka, F. C. Mechanism of DNA release from cationic liposome/DNA complexes used in cell transfection. *Biochemistry* **35**, 5616–5623 (1996).
32. Boggs, J. M. Lipid intermolecular hydrogen bonding: influence on structural organization and membrane function. *Biochim Biophys Acta* **906**, 353–404 (1987).
33. Couvreur, P. *et al.* Squalenoyl Nanomedicines as Potential Therapeutics. *Nano Lett.* **6**, 2544–2548 (2006).
34. Platt, V. *et al.* Influence of Multivalent Nitrilotriacetic Acid Lipid-Ligand Affinity on the Circulation Half-Life in Mice of a Liposome-Attached His(6)-Protein. *Bioconjugate Chemistry* (2010).doi:10.1021/bc900448f
35. Reddy, L. H. *et al.* A new nanomedicine of gemcitabine displays enhanced anticancer activity in sensitive and resistant leukemia types. *Journal of controlled release : official journal of the Controlled Release Society* **124**, 20–27 (2007).
36. Papahadjopoulos, D. *et al.* Sterically Stabilized Liposomes - Improvements in Pharmacokinetics and Antitumor Therapeutic Efficacy. *Proc Natl Acad Sci USA* **88**, 11460–11464 (1991).
37. Schulze, H., Kolter, T. & Sandhoff, K. Principles of lysosomal membrane degradation Cellular topology and biochemistry of lysosomal lipid degradation. *Biochim Biophys Acta* **1793**, 674–683 (2009).
38. Reddy, L. H. *et al.* Anticancer efficacy of squalenoyl gemcitabine nanomedicine on 60

human tumor cell panel and on experimental tumor. *Mol Pharm* **6**, 1526–1535 (2009).
39. Pedersen, P. J. *et al.* Liposomal formulation of retinoids designed for enzyme triggered release. *J Med Chem* **53**, 3782–3792 (2010).
40. Christensen, M. S., Pedersen, P. J., Andresen, T. L., Madsen, R. & Clausen, M. H. Isomerization of all-(E)-Retinoic Acid Mediated by Carbodiimide Activation - Synthesis of ATRA Ether Lipid Conjugates. *Eur. J. Org. Chem.* **2010**, 719–724 (2010).
41. Heyes, J., Palmer, L., Bremner, K. & Maclachlan, I. Cationic Lipid Saturation Influences Intracellular Delivery Of Encapsulated Nucleic Acids. *Journal Of Controlled Release* **107**, 276–287 (2005).
42. Bildstein, L. *Et Al.* Transmembrane Diffusion Of Gemcitabine By A Nanoparticulate Squalenoyl Prodrug: An Original Drug Delivery Pathway. *Journal Of Controlled Release* **147**, 163–170 (2010).
43. Leventis, R. & Silvius, J. R. Interactions Of Mammalian Cells With Lipid Dispersions Containing Novel Metabolizable Cationic Amphiphiles. *Biochim Biophys Acta* **1023**, 124–132 (1990).
44. Friend, D. S., Papahadjopoulos, D. & Debs, R. J. Endocytosis And Intracellular Processing Accompanying Transfection Mediated By Cationic Liposomes. *Biochim Biophys Acta* **1278**, 41–50 (1996).
45. Dosio, F. *Et Al.* Novel Nanoassemblies Composed Of Squalenoyl−Paclitaxel Derivatives: Synthesis, Characterization, And Biological Evaluation. *Bioconjugate Chemistry* **21**, 1349–1361 (2010).
46. Zhu, L., Lu, Y., Miller, D. D. & Mahato, R. I. Structural and Formulation Factors Influencing Pyridinium Lipid-Based Gene Transfer. *Bioconjugate Chemistry* **19**, 2499–2512 (2008).
47. Mahato, R. Water insoluble and soluble lipids for gene delivery. *Advanced Drug Delivery Reviews* **57**, 699–712 (2005).
48. New, R. *Liposomes: a practical approach*. 301 (Oxford University Press, USA: 1990).
49. Bangham, A. D. & Horne, R. W. Negative Staining Of Phospholipids And Their Structural Modification By Surface-Active Agents As Observed In The Electron Microscope. *J. Mol. Biol.* **8**, 660–668 (1964).
50. Drummond, D. C., Noble, C. O., Hayes, M. E., Park, J. W. & Kirpotin, D. B. Pharmacokinetics and in vivo drug release rates in liposomal nanocarrier development. *Journal of pharmaceutical sciences* **97**, 4696–4740 (2008).
51. Gabizon, A., Shmeeda, H. & Barenholz, Y. Pharmacokinetics of pegylated liposomal Doxorubicin: review of animal and human studies. *Clin Pharmacokinet* **42**, 419–436 (2003).
52. Pecot, C. V., Calin, G. A., Coleman, R. L., Lopez-Berestein, G. & Sood, A. K. RNA interference in the clinic: challenges and future directions. *Nature Reviews Cancer* **11**, 59–67 (2010).
53. Castanotto, D. & Rossi, J. J. The promises and pitfalls of RNA-interference-based therapeutics. *Nature* **457**, 426–433 (2009).
54. Semple, S. C. *et al.* Rational design of cationic lipids for siRNA delivery. *Nature Biotechnology* **28**, 172–176 (2010).
55. Abrams, M. T. *et al.* Evaluation of Efficacy, Biodistribution, and Inflammation for a Potent siRNA Nanoparticle: Effect of Dexamethasone Co-treatment. *Mol Ther* **18**, 171–180 (2010).

56. Adami, R. C. *et al.* An Amino Acid-based Amphoteric Liposomal Delivery System for Systemic Administration of siRNA. *Mol Ther* **19**, 1141–1151 (2011).
57. Jeffs, L. B. *et al.* A scalable, extrusion-free method for efficient liposomal encapsulation of plasmid DNA. *Pharm Res* **22**, 362–372 (2005).
58. Zelphati, O. & Szoka, F. C. Mechanism of oligonucleotide release from cationic liposomes. *Proc Natl Acad Sci USA* **93**, 11493–11498 (1996).
59. Ambegia, E. *et al.* Stabilized plasmid-lipid particles containing PEG-diacylglycerols exhibit extended circulation lifetimes and tumor selective gene expression. *Biochim Biophys Acta* **1669**, 155–163 (2005).

Chapter 2: Synthesis and Characterization of Novel Zwitterionic Lipids with pH-Responsive Biophysical Properties

2.1 Abstract

We report the synthesis and biophysical characterization of a novel class of zwitterionic lipids (ZL) with head groups containing a 3° or 4° cationic amine and anionic carboxylate linked by carbon spacers of varying structure. Four distinct head group structures were used to create a focused library of seven ZL. These ZL form stable liposomes that exhibit pH-dependent surface charges ranging from anionic (3° amine) or neutral (4° amine) at physiological pH to cationic at low pH. Varying the structure of the region linking the amine and carboxylate can modulate the pH range where this transition occurs; however we found that linkers greater than a single carbon long have only a small impact on the ionization behavior of the lipid. Increasing the mole percent of ZL increases the maximum and minimum zeta potentials of the liposomes; however the pH-dependent trends remain consistent across all formulations. Results from lipid mixing and membrane lysis assays reveal that when cationic, ZL containing liposomes interact with and disrupt anionic vesicles. ZL with different structures exhibit different membrane lysis behavior. We found that ZL efficiently encapsulate charged molecules, such as siRNA, into small (<100 nm), monodispersed liposomes that have a neutral or slightly negative zeta potential at physiological pH. These systems are not capable of siRNA mediated gene silencing *in vitro* or *in vivo*, likely because they are not effectively protonated in the endosome. However, ZL liposomes are generally well tolerated across several liposomal formulations, and did not induce inflammatory cytokines *in vivo*. This novel class of lipids may be suitable components

for inclusion in various delivery systems due to their ease of synthesis, low toxicity, and unique pH-dependent biophysical properties.

2.2 Introduction

Lipid-based nanoparticles have long been used to deliver biologically active molecules including drugs, DNA, and more recently siRNA *in vivo*. Liposomes and lipoplexes alter the pharmacokinetics, biodistribution, and uptake pathways of encapsulated or associated molecules.[1] Depending on the therapeutic application and drug properties, lipids with specific biophysical characteristics are required to develop an effective delivery system.[1-4] Due to their anionic charge and large size, siRNA are not able to passively cross cellular membranes to reach their site of action.[5,6] Because of these properties, siRNA delivery systems are generally cationic[7-11] or ionizable[2,12,12-15] to allow for high efficiency siRNA encapsulation and promote intracellular membrane fusion.[4] There have been extensive synthetic efforts to develop novel lipids with biophysical properties that can be exploited to promote efficient siRNA delivery while maintaining low cytotoxicity and immunogenicity.[2] Additionally, significant work has been done to understand the structure-activity relationships of these novel lipids to develop a method for the rational design of lipids capable of effectively delivering siRNA to target tissues.[12,14,16] In contrast to cationic lipids, zwitterionic lipids such as phosphatidylcholine (PC) or phosphatidylethanolamine (PE) show low *in vivo* cytotoxicity and immunogenicity.[17] However, their neutral surface charge and pH-independent biophysical properties can limit their ability to efficiently encapsulate and deliver charged, high molecular weight drugs. Here, we describe the design, synthesis, and biophysical characterization of a novel class of zwitterionic lipids (ZL) with

pH-responsive properties. These ZL consist of a 3-amino-1,2-propanediol backbone, ester-linked oleic acid tails, and an anionic carboxylic acid head group linked to the amine through a carbon spacer. The length and structure of the spacer was varied to determine its effect on the biophysical properties of the lipid. We hypothesize that, at physiological pH, ZL are either anionic (3° amine) or neutral (4° amine), and become cationic due to lipid protonation as the pH is decreased (Figure 2.1). The zwitterionic system described here may be advantageous to formally cationic lipids because at physiological pH, delivery systems containing ZL will remain neutral or anionic, limiting their toxicity and immunogenicity while allowing for reduced opsonization of serum proteins and increased circulation times.[18] Once internalized, the low-pH environment will protonate ZL containing liposomes if endocytic pH is less than lipid pKa. This allows for interactions between the transiently cationic ZL and anionic membrane lipids.

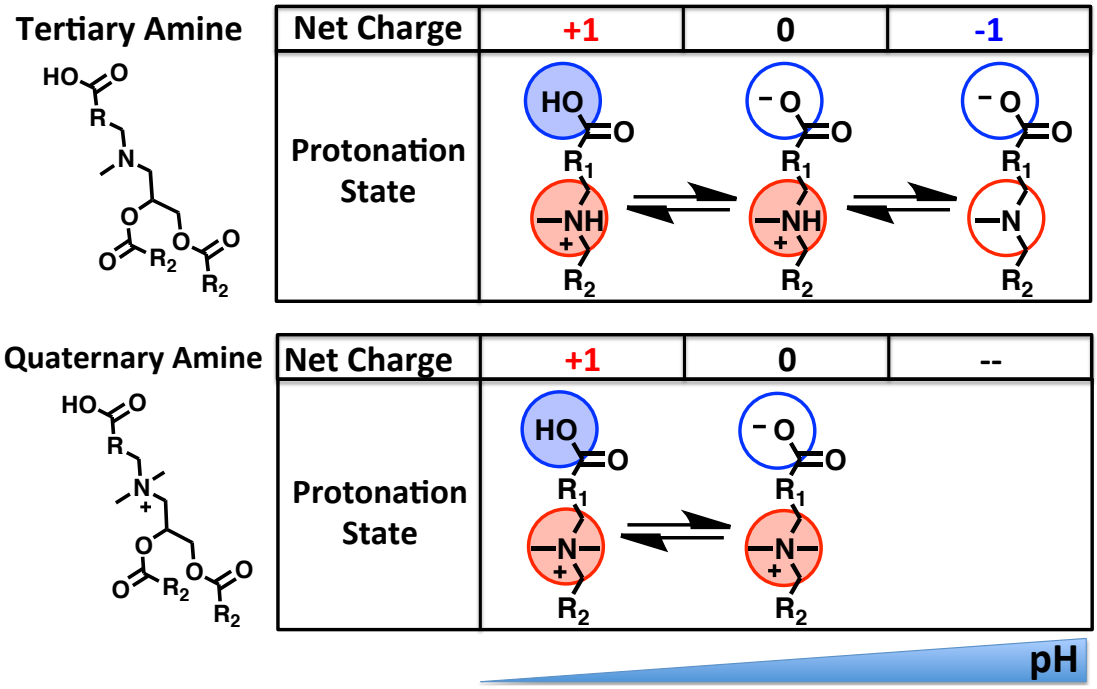

Figure 2.1: Schematic diagram and theoretical ionization behavior of 3° and 4° ZL

Additionally, these lipids may be advantageous to other zwitterionic lipids, such as phosphatidylcholine (PC), used in drug delivery systems. Like PC, ZL are designed to be neutral or slightly anionic at physiological pH, to reduce *in vivo* cytotoxicity and immunogenicity. However, the presence of a carboxylic acid (pKa~4.5) instead of a phosphate group (pKa~2.0) will allow for protonation of ZL at a higher pH than PC or PE lipids This may provide a useful platform for the efficient encapsulation of anionic molecules in a pH range that is unlikely to damage or degrade either the lipids or molecules for encapsulation. Additionally, we hypothesize that ZL containing a 3° amine will be anionic at elevated pH, potentially allowing for the efficient encapsulation of cationic molecules. This ability to modulate interactions between lipid and drug with slight alterations to the pH of the system could prove extremely useful for the encapsulation and delivery of molecules that have traditionally been difficult to load into liposomes.

Understanding the pH-dependent biophysical characteristics of these lipids will help to determine whether they may be useful tools for the delivery of siRNA, charged small molecule drugs, or both. The ionization behavior of multiple ZL containing liposomal formulations was determined by studying their zeta potential from pH=3.0-8.5. Additionally, the ability of ZL containing liposomes to interact with anionic membrane mimicking liposomes as a function of pH was determined using a FRET based lipid-mixing assay. The capacity of fusogenic ZL containing liposomes to disrupt anionic cell membranes when cationic or neutral was tested using a membrane lysis assay. Finally, we investigated whether ZL were capable of forming small liposomes that efficiently encapsulate negatively charged molecules, such as siRNA, using a controlled nucleation method. Our results confirm that we have developed a novel class of pH-responsive lipids with interesting

biophysical properties, and devised methods to systematically test their biophysical behavior and membrane activity as a function of pH.

2.3 Materials and Methods

2.3.1 Materials

1,2-dioleoyl-sn-glycero-3-phosphocholine (DOPC), 1,2-dioleoyl-sn-glycero-3-phosphoethanolamine (DOPE), 1,2-dioleoyl-sn-glycero-3-phospho-(1'-rac-glycerol) (DOPG), 1,2-dioleoyl-3-trimethylamonium-propane (DOTAP), and cholesterol (Chol) were purchased from Avanti Polar Lipids (Alabaster, AL). t-butyl p-(bromomethyl) benzoate was purchased from Cayman Chemical (Ann Arbor, MI). All other reagents were purchased from Sigma-Aldrich (Milwaukee, WI). Solvents were purchased from VWR (Radnor, PA), and used without further purification. TLC analyses were performed on 0.25 mm silica gel F_{254} plates using the described solvent systems. High-performance flash chromatography (HPFC) was performed on a Grace (Deerfield, IL) Reveleris HPFC system with pre-packed Reveleris silica gel columns (70 Å, 40 μm). ^{1}H NMR spectra were acquired using a Bruker 300 Avance MHz instrument. Chemical shifts are expressed as parts per million, and tetramethylsilane was used as an internal standard. MALDI-TOF spectra were acquired using an Applied Biosystems (Foster City, CA) Voyager-DE workstation. The detailed synthetic schemes are described below.

2.3.2 Synthesis of DOBAT and DOBAQ

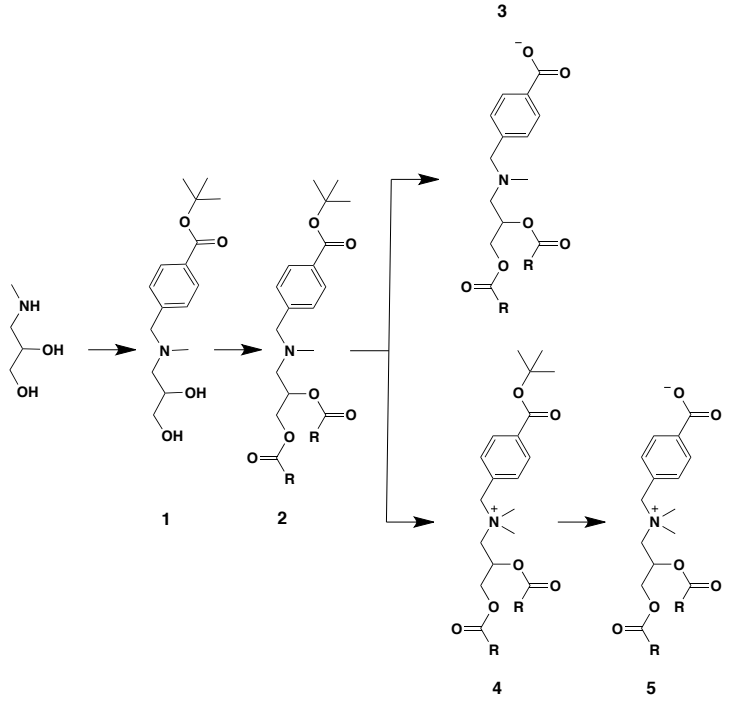

Scheme 2.1: DOBAT and DOBAQ Synthesis

0.6 g (18 mmol) K_2CO_3 was suspended in 35 ml of a 1:1 methanol:THF solution. To the suspension was added 1g (3.7 mmol) t-butyl-p-bromobenzoate and 0.6 g (5.5 mmol) 3-methylamino-1,2-propanediol. The mixture was stirred at 35 C for 16 hrs. The solid K_2CO_3 was filtered off, and the resulting mixture was concentrated in vacuo, resuspended in minimal DCM, and purified by HPFC using a 0-10% methanol in chloroform gradient, which provided 0.65 g (60% yield) of **1** as clear oil. TLC: R_f = 0.5 (eluent 9:1 $CHCl_3$:MeOH). ^{1}H NMR ($CDCl_3$): δ 1.55 (s, 9H); δ 2.40 (s, 3H) δ 2.60 (m, 2H); δ 3.55 (m, 2H); δ 3.70 (m, 2H); δ 3.90 (m, 1H); δ 7.40 (m, 2H); δ 7.90 (m, 2H). MALDI-MS $[M+H]^+$ - calculated 295.18, found 295.8.

A mixture of 0.6 g (2.2 mmol) **1**, 1.3 g (4.8 mmol) oleic acid, 1.05 g (5.5 mmol) DCC, and 0.27 g (2.2 mmol) DMAP in dry DCM (25 ml) was stirred at room temperature for 16 hr.

Precipitated DCU salt was removed by filtration. An additional 75 ml of DCM was added, and the organic phase was washed with 1M HCl (2 x 25 ml), water (2 x 25 ml), and brine (30 ml). The organic was then dried over anhydrous Na_2SO_4 and concentrated by evaporation under reduced pressure to yield a yellow oil as the crude product. This oil was further purified by HPFC using a 0-4% methanol in chloroform gradient to yield 1.21 g (72% yield) of **2** as a clear oil. TLC: R_f = 0.4 (99:1 $CHCl_3$:MeOH). ^{1}H NMR ($CDCl_3$): δ 0.90 (t, 6H); δ 1.20-1.50 (m, 40H); δ 1.55 (s, 9H); δ 1.62 (m, 4H); δ 2.04 (m, 8H); δ 2.30 (m, 4H); δ 2.40 (s, 3H); δ 2.75 (m, 2H); δ 3.55 (m, 2H); δ 4.25 (m, 2H); δ 5.30 (m, 4H); δ 5.40 (m, 1H); δ 7.40 (m, 2H); δ 7.90 (m, 2H). MALDI-MS $[M+H]^+$ - calculated 823.67, found 824.3.

2.3.2.1 DOBAT synthesis

0.5 g (0.6 mmol) of **2** was stirred for 1 hr at room temperature in a solution of 5:4:1 DCM:TFA:TIPS (10 ml). Solvent was removed by evaporation at reduced pressure. The product was purified by HPFC using an elution gradient of 0-10% methanol in chloroform, giving 0.44 g (95% yield) of final product **3**. TLC: R_f = 0.1 (99:1 $CHCl_3$:MeOH). ^{1}H NMR ($CDCl_3$): δ 0.90 (t, 6H); δ 1.20-1.50 (m, 40H); δ 1.62 (m, 4H); δ 2.04 (m, 8H); δ 2.30 (m, 4H); δ 2.40 (s, 3H); δ 2.75 (m, 2H); δ 3.55 (m, 2H); δ 4.25 (m, 2H); δ 5.30 (m, 4H); δ 5.40 (m, 1H); δ 7.40 (m, 2H); δ 7.90 (m, 2H). MALDI-MS $[M+H]^+$ - calculated 768.61, found 768.2.

2.3.2.2 DOBAQ synthesis

To a solution of 0.85 g (1 mmol) **2** dissolved in 10 ml acetone stirring at 0 C, 0.5 ml (5 mmol) was added dropwise, and the reaction was allowed to slowly warm to room temperature, then stirred at room temperature for 16 hr. Solvent was removed by evaporation

in vacuo, the crude oil was solubilized in 50 ml DCM, washed with water (2 x 15 ml) and brine (20 ml), and dried over Na_2SO_4. The crude product was purified by HPLC using a 0-20% methanol in chloroform gradient to yield 0.52 g (60% yield) of **4**. TLC: R_f = 0.2 (95:5 $CHCl_3$:MeOH). ^{1}H NMR ($CDCl_3$): δ 0.90 (t, 6H); δ 1.20-1.50 (m, 40H); δ 1.55 (s, 9H); δ 1.62 (m, 4H); δ 2.04 (m, 8H); δ 2.30 (m, 4H); δ 3.20 (s, 3H); δ 3.3 (s, 3H); δ 3.90 (m, 2H); δ 4.30 (m, 2H); δ 4.80 (m, 2H); δ 5.30 (m, 4H); δ 5.50 (m, 1H); δ 7.70 (m, 2H); δ 8.10 (m, 2H). MALDI-MS $[M+H]^+$ - calculated 838.69, found 839.7.

0.5 g (0.6 mmol) of **4** was stirred for 1 hr at room temperature in a solution of 5:4:1 DCM:TFA:TIPS (10 ml). Solvent was removed by evaporation at reduced pressure. The product was purified by HPFC using an elution gradient of 0-30% methanol in chloroform, giving 0.41 g (87% yield) of final product **5**. TLC: R_f = 0.75 (65:25:4 $CHCl_3$:MeOH:NH_3OH). ^{1}H NMR ($CDCl_3$): δ 0.90 (t, 6H); δ 1.20-1.50 (m, 40H); δ 1.62 (m, 4H); δ 2.04 (m, 8H); δ 2.30 (m, 4H); δ 3.20 (s, 3H); δ 3.3 (s, 3H); δ 3.90 (m, 2H); δ 4.30 (m, 2H); δ 4.80 (m, 2H); δ 5.30 (m, 4H); δ 5.60 (m, 1H); δ 7.70 (m, 2H); δ 8.10 (m, 2H). MALDI-MS $[M+H]^+$ - calculated 782.63, found 783.2.

2.3.3 Synthesis of DOPAT and DOPAQ

1 g (9.5 mmol) of 3-methylamino-1,2-propanediol and 1.34 g (10.5 mmol) t-butyl acrylate were stirred neat at 75 C for 16 hr. Product (**6**) was moved forward without purification due to nearly quantitative yield (2.30 g). TLC: R_f = 0.66 (90:10:1 $CHCl_3$:MeOH:NH_3OH). ^{1}H NMR ($CDCl_3$): δ 1.50 (s, 9H); δ 2.30 (s, 3H); δ 2.40 (m, 2H); δ 2.65 (m, 2H); δ 2.85 (m, 2H); δ 3.5 (m, 1H); δ 3.8 (m, 2H). MALDI-MS $[M+H]^+$ - calculated 233.16, found 233.8.

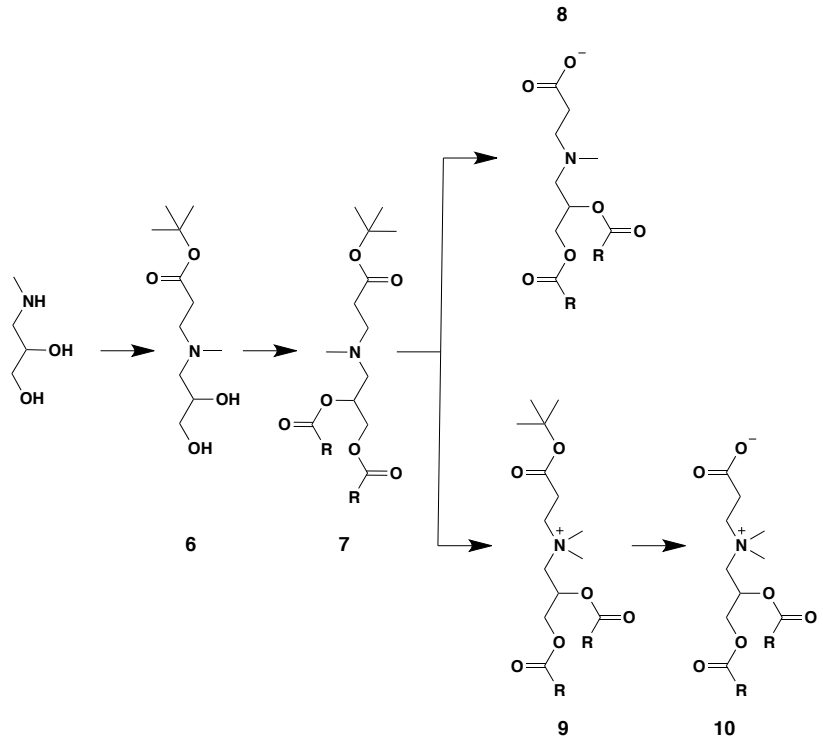

Scheme 2.2: DOPAT and DOPAQ Synthesis

A mixture of 0.8 g (3.4 mmol) **6**, 2.1 g (7.5 mmol) oleic acid, 1.75 g (8.5 mmol) DCC, and 0.42 g (3.4 mmol) DMAP in dry DCM (35 ml) was stirred at room temperature for 16 hr. Precipitated DCU salt was removed by filtration. An additional 75 ml of DCM was added, and the organic phase was washed with 1M HCl (2 x 25 ml), water (2 x 25 ml), and brine (30 ml). The organic was then dried over anhydrous Na_2SO_4 and concentrated by evaporation under reduced pressure to yield a yellow oil as the crude product. This oil was further purified by HPFC using a 0-5% methanol in chloroform gradient to yield 2.1 g (80% yield) of **7** as a clear oil. TLC: R_f = 0.66 (95:5 $CHCl_3$:MeOH). ^{1}H NMR ($CDCl_3$): δ 0. 90 (t, 6H); δ 1.20-1.50 (m, 40H); δ 1.50 (s, 9H); δ 1.65 (m, 4H); δ 2.04 (m, 8H); δ 2.30 (m, 4H); δ 2.40 (s, 3H); δ 2.45 (m, 2H); δ 2.50 (m, 2H); δ 2.80 (m, 2H); δ 4.30 (m, 2H); δ 5.30 (m, 4H); δ 5.40 (m, 1H). MALDI-MS $[M+H]^+$ - calculated 761.65, found 762.8.

2.3.3.1 DOPAT synthesis

0.75 g (1 mmol) of **7** was stirred for 1 hr at room temperature in a solution of 5:4:1 DCM:TFA:TIPS (10 ml). Solvent was removed by evaporation at reduced pressure. The product was purified by HPFC using an elution gradient of 0-10% methanol in chloroform, giving 0.65 g (93% yield) of final product **8**. TLC: R_f = 0.1 (95:5 $CHCl_3$:MeOH). ^{1}H NMR ($CDCl_3$): δ 0. 90 (t, 6H); δ 1.20-1.50 (m, 40H); δ 1.65 (m, 4H); δ 2.04 (m, 8H); δ 2.30 (m, 4H); δ 2.40 (s, 3H); δ 2.45 (m, 2H); δ 2.50 (m, 2H); δ 2.80 (m, 2H); δ 4.30 (m, 2H); δ 5.30 (m, 4H); δ 5.40 (m, 1H). MALDI-MS $[M+H]^+$ - calculated 706.6, found 706.4.

2.3.3.2 DOPAQ synthesis

To a solution of 1.2 g (1.6 mmol) **7** dissolved in 15 ml acetone stirring at 0 C, 1 ml (10 mmol) was added dropwise, and the reaction was allowed to slowly warm to room temperature, then stirred at room temperature for 16 hr. Solvent was removed by evaporation in vacuo, the crude oil was solubilized in 100 ml DCM, washed with water (2 x 20 ml) and brine (25 ml), and dried over Na_2SO_4. The crude product was purified by HPLC using a 0-20% methanol in chloroform gradient to yield 0.7 g (57% yield) of **9**. TLC: R_f = 0.1 (95:5 $CHCl_3$:MeOH). ^{1}H NMR ($CDCl_3$): δ 0. 90 (t, 6H); δ 1.20-1.50 (m, 40H); δ 1.50 (s, 9H); δ 1.65 (m, 4H); δ 2.04 (m, 8H); δ 2.30 (m, 4H); δ 3.10 (m, 2H); δ 3.20 (s, 3H); δ 3.30 (s, 3H); δ 3.75 (m, 2H); δ 3.95 (m, 2H); δ 4.30 (m, 2H); δ 5.30 (m, 4H); δ 5.40 (m, 1H). MALDI-MS $[M+H]^+$ - calculated 776.68, found 777.8.

0.7 g (0.9 mmol) of **9** was stirred for 1 hr at room temperature in a solution of 5:4:1 DCM:TFA:TIPS (10 ml). Solvent was removed by evaporation at reduced pressure. The product was purified by HPFC using an elution gradient of 0-25% methanol in chloroform,

giving 0.5 g (77% yield) of final product **10**. TLC: R_f = 0.5 (80:20 $CHCl_3$:MeOH). ^{1}H NMR ($CDCl_3$): δ 0. 90 (t, 6H); δ 1.20-1.50 (m, 40H); δ 1.65 (m, 4H); δ 2.04 (m, 8H); δ 2.30 (m, 4H); δ 3.10 (m, 2H); δ 3.20 (s, 3H); δ 3.30 (s, 3H); δ 3.75 (m, 2H); δ 3.95 (m, 2H); δ 4.30 (m, 2H); δ 5.30 (m, 4H); δ 5.60 (m, 1H). MALDI-MS $[M+H]^+$ - calculated 720.61, found 721.6.

2.3.4 Synthesis of DOMPAT and DOMPAQ

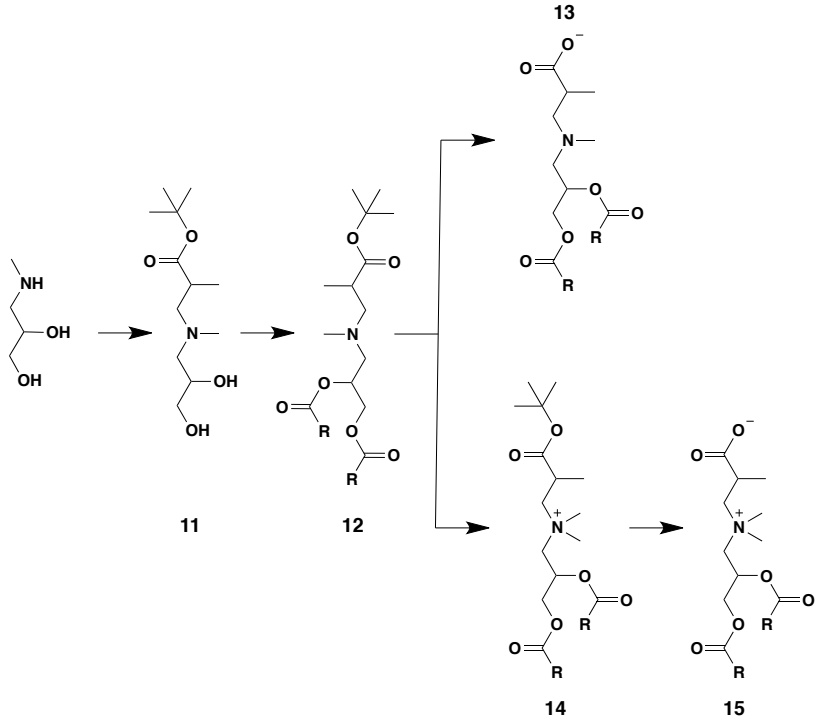

Scheme 2.3: DOMPAT and DOMPAQ Synthesis

1 g (9.5 mmol) of 3-methylamino-1,2-propanediol and 1.49 g (10.5 mmol) t-butyl methacrylate were stirred neat at 75 C for 16 hr. Product (11) was moved forward without purification due to nearly quantitative yield (2.45 g). TLC: R_f = 0.7 (90:10:1 $CHCl_3$:MeOH:NH_3OH). ^{1}H NMR ($CDCl_3$): δ 1.10 (m, 3H); δ 1.50 (s, 9H); δ 2.30 (s, 3H); δ 2.35 (m, 2H); δ 2.40 (m, 1H); δ 2.45 (m, 2H); δ 2.65 (m, 2H); δ 3.75 (m, 1H). MALDI-MS $[M+H]^+$ - calculated 247.18, found 248.4.

A mixture of 1.5 g (6.1 mmol) **11**, 3.77 g (13.4 mmol) oleic acid, 3.1 g (15 mmol) DCC, and 0.74 g (6.1 mmol) DMAP in dry DCM (60 ml) was stirred at room temperature for 16 hr. Precipitated DCU salt was removed by filtration. An additional 75 ml of DCM was added, and the organic phase was washed with 1M HCl (2 x 25 ml), water (2 x 25 ml), and brine (30 ml). The organic was then dried over anhydrous Na_2SO_4 and concentrated by evaporation under reduced pressure to yield a yellow oil as the crude product. This oil was further purified by HPFC using a 0-5% methanol in chloroform gradient to yield 3.6 g (77% yield) of **12** as a clear oil. TLC: R_f = 0.7 (95:5 $CHCl_3$:MeOH). ^{1}H NMR ($CDCl_3$): δ 0.90 (t, 3H); δ 1.10 (m, 3H); δ 1.20-1.50 (m, 40H); δ 1.50 (s, 9H); δ 1.65 (m, 4H); δ 2.04 (m, 8H); δ 2.30 (m, 2H); δ 2.32 (s, 3H); δ 2.35 (m, 4H); δ 2.40 (m, 1H); δ 2.80 (m, 2H); δ 4.30 (m, 2H); δ 5.30 (m, 4H); δ 5.40 (m, 1H). MALDI-MS $[M+H]^+$ - calculated 775.67, found 777.4.

2.3.4.1 DOMPAT synthesis

1.5 g (1.9 mmol) of **12** was stirred for 1 hr at room temperature in a solution of 5:4:1 DCM:TFA:TIPS (20 ml). Solvent was removed by evaporation at reduced pressure. The product was purified by HPFC using an elution gradient of 0-10% methanol in chloroform, giving 1.24 g (90% yield) of final product **13**. TLC: R_f = 0.15 (95:5 $CHCl_3$:MeOH). ^{1}H NMR ($CDCl_3$): δ 0.90 (t, 3H); δ 1.10 (m, 3H); δ 1.20-1.50 (m, 40H); δ 1.65 (m, 4H); δ 2.04 (m, 8H); δ 2.30 (m, 2H); δ 2.32 (s, 3H); δ 2.35 (m, 4H); δ 2.40 (m, 1H); δ 2.80 (m, 2H); δ 4.30 (m, 2H); δ 5.30 (m, 4H); δ 5.40 (m, 1H). MALDI-MS $[M+H]^+$ - calculated 720.61, found 722.8.

2.3.4.2 DOMPAQ synthesis

To a solution of 1 g (1.3 mmol) **12** dissolved in 15 ml acetone stirring at 0 C, 1 ml (10 mmol) was added dropwise, and the reaction was allowed to slowly warm to room temperature, then stirred at room temperature for 16 hr. Solvent was removed by evaporation in vacuo, the crude oil was solubilized in 100 ml DCM, washed with water (2 x 20 ml) and brine (25 ml), and dried over Na_2SO_4. The crude product was purified by HPLC using a 0-20% methanol in chloroform gradient to yield 0.61 g (59% yield) of **14**. TLC: R_f = 0.2 (90:10:1 $CHCl_3$:MeOH:NH_3OH). ^{1}H NMR ($CDCl_3$): δ 0.90 (t, 3H); δ 1.20-1.50 (m, 40H); δ 1.30 (m, 3H); δ 1.50 (s, 9H); δ 1.65 (m, 4H); δ 2.04 (m, 8H); δ 2.35 (m, 4H); δ 3.15 (m, 1H); δ 3.20 (s, 3H); δ 3.30 (s, 3H); δ 3.80 (m, 2H); δ 3.90 (m, 2H); δ 4.30 (m, 2H); δ 5.30 (m, 4H); δ 5.40 (m, 1H). MALDI-MS $[M+H]^+$ - calculated 790.69, found 792.8.

0.61 g (0.8 mmol) of **14** was stirred for 1 hr at room temperature in a solution of 5:4:1 DCM:TFA:TIPS (10 ml). Solvent was removed by evaporation at reduced pressure. The product was purified by HPFC using an elution gradient of 0-25% methanol in chloroform, giving 0.44 g (74% yield) of final product **15**. TLC: R_f = 0.2 (90:10:1 $CHCl_3$:MeOH:NH_3OH). ^{1}H NMR ($CDCl_3$): δ 0.90 (t, 3H); δ 1.20-1.50 (m, 40H); δ 1.30 (m, 3H); δ 1.65 (m, 4H); δ 2.04 (m, 8H); δ 2.35 (m, 4H); δ 3.15 (m, 1H); δ 3.20 (s, 3H); δ 3.30 (s, 3H); δ 3.80 (m, 2H); δ 3.90 (m, 2H); δ 4.30 (m, 2H); δ 5.30 (m, 4H); δ 5.40 (m, 1H). MALDI-MS $[M+H]^+$ - calculated 734.63, found 736.7.

2.3.5 Synthesis of DOAAQ

A mixture of 0.5 g (4.2 mmol) 3-(dimethylamino)-1,2-propanediol, 2.61 g (9.25 mmol) oleic acid, 2.2 g (10.5 mmol) DCC, and 0.51 g (4.2 mmol) DMAP in dry DCM (40

ml) was stirred at room temperature for 16 hr. Precipitated DCU salt was removed by filtration. An additional 60 ml of DCM was added, and the organic phase was washed with 1M HCl (2 x 25 ml), water (2 x 25 ml), and brine (30 ml). The organic was then dried over anhydrous Na_2SO_4 and concentrated by evaporation under reduced pressure to yield a yellow oil as the crude product. The crude product was purified by HPFC using an elution gradient of 0-5% methanol in chloroform, giving 2.47 g (91% yield) of **16** as a yellow oil. TLC: R_f = 0.7 (95:5 $CHCl_3$:MeOH). ^{1}H NMR ($CDCl_3$): δ 0.90 (t, 3H); δ 1.20-1.50 (m, 40H); δ 1.65 (m, 4H); δ 2.04 (m, 8H); δ 2.30 (s, 6H); δ 2.35 (m, 4H); δ 2.60 (m, 2H); δ 4.30 (m, 2H); δ 5.30 (m, 4H); δ 5.60 (m, 1H). MALDI-MS $[M+H]^+$ - calculated 647.59, found 649.8.

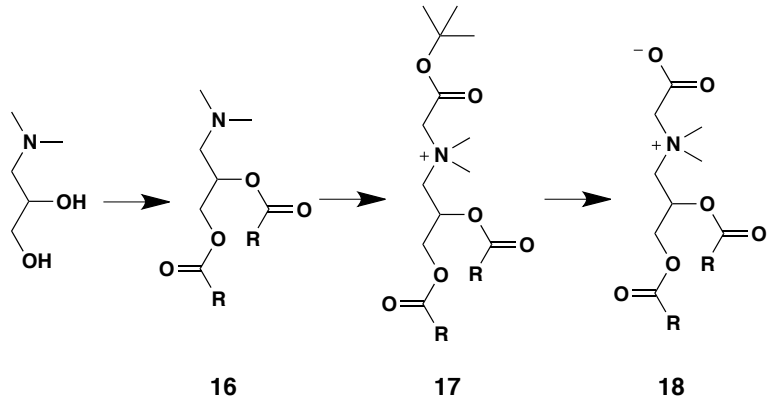

Scheme 2.4: DOAAQ Synthesis

1.5 g (2.3 mmol) of **16** in THF (30 ml) was stirred at 40 C with 0.7 g (3.45 mmol) t-butyl bromoacetate and 0.6 g (4.6 mmol) Hunig's base for 48 hrs. Solvent was removed by evaporation under reduced pressure, and the crude oil was resuspended in 50 ml DCM and washed with water (2 X 15 ml) and brine (15 ml). The organic was dried over anhydrous Na2SO4 and concentrated by evaporation under reduced pressure to yield a yellow oil as the crude product. The product was purified by HPFC using an elution gradient of 0-10% methanol in chloroform, giving 0.8 g (45% yield) of **17** as a yellow oil. TLC: R_f = 0.15 (95:5

$CHCl_3$:MeOH). ^1H NMR ($CDCl_3$): δ 0.90 (t, 3H); δ 1.20-1.50 (m, 40H); δ 1.50 (s, 9H); δ 1.65 (m, 4H); δ 2.04 (m, 8H); δ 2.35 (m, 4H); δ 3.50 (s, 3H); δ 3.60 (s, 3H); δ 3.90 (m, 2H); δ 4.30 (m, 2H); δ 4.35 (m, 2H); δ 5.30 (m, 4H); δ 5.60 (m, 1H). MALDI-MS $[M+H]^+$ - calculated 762.66, found 763.2.

0.8 g (1 mmol) of **17** was stirred for 1 hr at room temperature in a solution of 5:4:1 DCM:TFA:TIPS (20 ml). Solvent was removed by evaporation at reduced pressure. The product was purified by HPFC using an elution gradient of 0-20% methanol in chloroform, giving 0.65 g (88% yield) of final product **18**. TLC: R_f = 0.1 (90:10:1 $CHCl_3$:MeOH:NH_3OH). ^1H NMR ($CDCl_3$): δ 0.90 (t, 3H); δ 1.20-1.50 (m, 40H); δ 1.65 (m, 4H); δ 2.04 (m, 8H); δ 2.35 (m, 4H); δ 3.50 (s, 3H); δ 3.60 (s, 3H); δ 3.90 (m, 2H); δ 4.30 (m, 2H); δ 4.35 (m, 2H); δ 5.30 (m, 4H); δ 5.60 (m, 1H). MALDI-MS $[M+H]^+$ - calculated 706.60, found 708.4.

2.3.6 Buffers

Unless otherwise stated, isosmotic buffers containing 10 mM buffering agent and 50 mM NaCl were used for all experiments. Buffers from pH=3.0-8.5 in 0.5 pH increments were used. The buffering agent used was dependent on the desired pH of the buffer. Sodium acetate was used for pH=3.0-5.5; 2-(*N*-morpholino)ethanesulfonic acid (MES) was used for pH=6.0-7.0; tris(hydroxymethyl)aminomethane (TRIS-HCl) was used for pH=7.5-8.5.

2.3.7 Size and zeta potential measurements

The mean diameter of liposomes for all experiments was determined by dynamic light scattering using a Zetasizer NanoZS (Malvern, Westborough MA). 10 uL of liposome

solution (10 mM) was diluted into 740 uL of 10 mM Tris-HCl, 50 mM NaCl (pH=7.4) for size measurements.

Zeta potential measurements of liposomal formulations containing betaine-like lipids were performed at various pH values using a Zetasizer NanoZS (Malvern, Westborough MA). 10 μL of 10 mM liposomal solution was diluted into 740 μl of isosmotic buffer in a dip cell cuvette for zeta potential measurements

2.3.8 Zeta potential of ZL:DOPC formulations

Dry lipid films of the desired ZL:DOPC lipid ratios (5 μmol total lipid) were hydrated in 0.5 ml of buffer (pH=8.5), sonicated two minutes to disperse the lipid film, then extruded 11 times through a 200 nm polycarbonate membrane (Whatman International, Kent, UK) using a handheld extruder (Avestin, Ottawa, ON, Canada) extruder at room temperature. Zeta potential was measured as a function of pH from pH=3.0-8.5 in 0.5 pH intervals. Measurements were taken four times per sample and averaged to give the final value and standard deviation.

2.3.9 Determination of fusogenic potential through lipid mixing assay

Dry lipid films 43:30:25:1:1 DOPC:ZL:DOPE:Rho-PE:NBD-PE were rehydrated at a lipid concentration of 10 mM in buffer (pH=8.5), sonicated 2 minutes to disperse the lipid film, then extruded 11 times through 100 nm polycarbonate membrane at room temperature. Dry lipid films containing 45:20:20:15 DOPC:DOPE:DOPG:Chol (acceptor composition) were rehydrated at a lipid concentration of 10 mM in buffer (pH=8.5), sonicated two minutes

to disperse the lipid film, then extruded 11 times through 100 nm polycarbonate membrane at room temperature.

Lipid mixing between ZL containing liposomes and anionic liposomes was investigated using fluorescence resonance energy transfer (FRET) to determine the fusogenic potential of ZL.[19] The DOPE-conjugated FRET probes lissamine rhodamine B (Rho-PE) and 7-nitrobenzo-2-oxa-1,3-diazole (NBD-PE) were combined into a single liposomal formulation, resulting in attenuated NBD fluorescence due to FRET with Rho. Upon lipid mixing with a probe-free acceptor vesicle, NBD signal increases due to an increase in average distance between the two probes as they redistribute across the two membranes. For mixing experiments, 2 μL of donor vesicles (10 mM) were added to 1980 μL of buffer and the baseline fluorescence was measured (F_{min}). 18 μL of acceptor liposomes (10 mM) were injected, and fluorescence was measured after 5 minutes at 37 °C (F). 30 μL of 15% $C_{12}E_{10}$ were then added, and the fluorescence was measured after 30 seconds (F_{max}). % lipid mixing was defined as $(F-F_{min})/(F_{max}-F_{min})*100$, and was reported as the average of triplicate measurements. All fluorescence measurements were made on a Spex Fluorolog fluorimeter (Horiba Jobin Yvon, Edison NJ) at Ex/Em = 465/520 nm.

2.3.10 Lysis of biomembrane mimicking vesicles

Dry lipid films of anionic biomembrane mimicking vesicles (BMV) containing 45:20:20:15 DOPC:DOPE:DOPG:Chol[14] were hydrated at a lipid concentration of 10 mM in a solution containing 12.5 mM ANTS, 42.5 mM DPX, 10 mM Tris-HCl, 20 mM NaCl (pH=7.4), and sonicated 10 minutes at 25° C to form a homogeneous dispersion.[20] Unencapsulated ANTS/DPX was removed by column purification on a Sephadex G-25 (PD-10) desalting column using an isosmotic buffer (pH=7.4) to a final concentration of 5 mM.

Dry lipid films of ZL vesicles containing 45:30:25 DOPE:ZL:DOPC were hydrated at a lipid concentration of 5 mM in buffer containing 10 mM Tris-HCl and 150 mM NaCl (pH= 7.4), sonicated 2 minutes to disperse the lipid film, then extruded 11 times through 100 nm polycarbonate membrane at room temperature.

10 μL of purified ANTS/DPX containing liposomes diluted into 1 ml of buffer (final concentration of 50 μM) containing 10 mM Tris-HCl and 150 mM NaCl (pH=7.4) or 10 mM sodium acetate and 150 mM NaCl (pH=4.0). 20 μL of ZL containing vesicles were added (final concentration 100 μM), and the ANTS fluorescence (Ex/Em = 360nm/530nm) was measured at t = 0 min (F_0) and t = 30 min (F_{30}). 5 μL of a 15% $C_{12}E_{10}$ solution was added to lyse all vesicles, and the max fluorescence (F_{max}) was measured. The percentage of free ANTS at t = 30 min should correlate with membrane lysis, and is reported as % lysis = $(F_{30}-F_0)/(F_{max}-F_0)*100$. The data reported are the average of triplicate measurements, and all fluorescence measurements were made on a Spex Fluorolog fluorimeter (Horiba Jobin Yvon, Edison NJ).

2.3.11 Encapsulation of siRNA in ZL liposomes

ZL lipid nanoparticles were prepared using a batch mixing process at 25°C. 2 mg total lipid was dissolved in 250 μL of ethanol and sonicated at 25°C for 5 min. The lipid/ethanol solution was subsequently injected into a magnetically stirred 2.5 ml vial, which contained 100 μg of siRNA dissolved in 250 μL of 50 mM citric acid buffer, pH 4. For reproducible injection speed, a KD Scientific pump holding a syringe with a 22 G x 1 1/2 needle was used to inject the methanol lipid solution into the aqueous phase. The injection rate was 5 mL/min. The lipid suspension was stirred for 10 min and then extruded through 80

nm polycarbonate membranes 5 times at room temperature. Ethanol was removed by dialysis against PBS (pH 7.4) without Ca^{2+} and Mg^{2+} for 24h. Encaspulation efficiency of siRNA was quantified by measuring the fluorescence signal upon addition of Ribogreen to aliquots of lipid nanoparticle formulations in the presence or absence of 0.4% Triton-X. Fluorescence was measured using the Fluostar fluorescence plate reader (BMG Labtech, Cary, NC) (Ex/Em = 485/520 nm). siRNA was quantified by a calibration curve ranging from 50 ng/ml to 1μg/ml siRNA. Liposome size and zeta potential were measured 3 times per sample on a Zetasizer NanoZS (Malvern, Westborough MA) and averaged.

2.3.12 in vitro knockdown in Hela-Luc cells

Stably transfected HeLa-Luc cells were cultured in MEM Eagles's with Earle's BSS Medium supplemented with 10% heat-inactivated FCS. Twenty-four hours before transfection, cells were seeded in 96-well plates at a density of 8,000/well. Liposomal formulations (65:35:1 DOBAQ:DOPE:PEG-DMG) correlating to 90 or 180 nM siRNA were added to cells in medium supplemented with 10% fetal calf serum. Weight/weight (ZL/siRNA) ratios of 15 and 30 were used. After 24 h incubation, medium was replaced, and the cells were analyzed for luciferase gene silencing. In addition to anti-luc siRNA, non-specific siRNA was used to assay for gene silencing by cytotoxic or off-target effects. Luciferase gene silencing activity was measured according to the protocol provided by Promega (Madison, WI, USA). Briefly, luciferase light units were quantified by adding 100 μL of Steady-Glo (Promega, Madison, WI, USA) to the cells containing 100 μL of media per well. The relative light units (RLU) were measured with a 1450 MicroBeta Trilux, Liquid Scintillation and Luminescence Counter (Perkin Elmer, Waltham, MA). Data were expressed

as percentage of control (untreated cells). Luciferase expression of untreated non-transfected cells was set as 100%. All experiments were performed in quadruplicate.

2.3.13 in vivo Factor VII assay

Six to eight week old, female CD-1 mice (Charles River Laboratories) were administered ZL-siRNA formulations via tail vein injection at an siRNA concentration of 5mg/kg (15:1 w:w ratio of ZL:siRNA) in a total volume of 200 µl. Control mice received an injection of 200 ul PBS. 48h after administration, animals were anesthetized with isoflurane. Blood was collected by submandibular cheek bleeding. Serum samples were obtained by allowing the blood to clot for 30 min and then centrifuging for 15 min at 15,000 rpm at 4°C. The supernatant was collected and analyzed for serum levels of Factor VII protein using the Biophen VII colorimetric assay (Aniara, Mason, OH) according to manufacturer's instructions.[12] A standard curve was generated using serially diluted concentrations of PBS-treated animals. Serum levels of mice treated with siRNA-ZL formulations were expressed as percentage of PBS-control. Each group consisted of n=3 mice. DLinDMA served as a positive control.

ZL Liposomal Formulations Tested:

1. DOBAQ:Chol:DSPC:PEG-DMG (55:25:10:10)
2. DOBAQ:DOPE:PEG-DMG:Lactosylceramide (60:30:7:3)
3. DOBAQ:CHEMS:PEG-DMG (60/30/10)
4. DOBAQ:DOPE:PEG-DMG:Lactosylceramide (60/30/7/3)

Lactosylceramide was chosen as a hepatocyte targeting ligand that interacts with the asialoglycoprotein receptor. When incorporated in liposomes, lactosylceramide is known to promote liposomal accumulation in hepatocytes.[21]

2.3.14 in vivo cytokine induction by DOBAQ liposomes

Six-to eight-week-old, female CD-1 mice (Charles River Laboratories) were administered DOBAQ/Chol/DSPC/PEG-DMG (40/40/10/10) formulation via tail vein injection at an siRNA concentration of 5mg/kg ((15:1 w:w ratio of ZL:siRNA) in a total volume of 200 μl. Control mice received an injection of 200 ul PBS. 48h after administration, animals were anesthetized with isoflurane. Blood was collected by submandibular cheek bleeding. Serum samples were obtained by allowing the blood to clot for 30 min and then centrifuging for 15 min at 15,000 RPM at 4C. The supernatant was collected and frozen at -80C. Serum samples were analyzed by Eve Technologies (Calgary, Alberta, Canada) using the Mouse 32-Plex Cytokine / Chemokine Panel.

2.3.15 siRNA Sequences

Lowercase = 2'-fluoro modified nucleotides

Asterisk = phosphorothioate linkage

Anti-Luciferase

Sense: 5' –GCUACAUUCUGGAGAGAUAdTdT-3'

Antisense: 5'-UAUGUCUCCAGAAUGUAGCdTdT-3'

Non-specific control provided by Pfizer

Factor VII

Sense: 5'-GGAucAucucAAGucuuAcT*T-3'

Antisense: 5'-GuAAGAcuuGAGAuGAuccT*T-3'

Non-specific: siGenome Non-Targeting siRNA #5 (Dharmacon, Lafeyette, CO)

2.4 Results and Discussion

2.4.1 Chemistry and structure of ZL

The goal of this work was to develop novel zwitterionic lipids that show pH-dependent surface charges ranging from anionic (3° amine) or neutral (4° amine) at physiological pH to cationic at low pH. We hypothesize that due to their pH-sensitive characteristics, ZL are able to promote membrane destabilization at lower pH and at the same time have potential utility for efficiently encapsulating charged drugs in small, neutral particles. To this end, we created a focused library of betaine-like lipids (ZL) with head groups containing a cationic amine, anionic carboxylate, and a linker region with varying molecular structures. The structures synthesized were chosen to test the impact of the length, hydrophobicity, and structure of the region linking the amine and the carboxylate on the biophysical behavior of the lipid at various pH. We hypothesized that differences in linker structure could impact the protonation behavior of ZL, their ability to form stable liposomes, or their membrane interactions. Additionally, we studied the impact of amine substitution (3° vs. 4°) on lipid behavior across a range of pH.

The synthesized library consisted of seven ZL structures containing a 3-amino-1,2-propanediol backbone, ester-linked oleic acid tails, and one of four different carboxylic acid containing headgroups (Figure 2.2). ZL were colloquially named as follows: DOPAQ and DOPAT contain a Propionic Acid head group and a Quaternary or Tertiary amine, respectively; DOMPAQ and DOMPAT contain a MethylPropionic Acid head group and a Quaternary or Tertiary amine, respectively; DOBAQ and DOBAT contain a Benzoic Acid head group and a Quaternary or Tertiary amine, respectively. The seventh lipid, DOAAQ,

contains an Acetic Acid head group, and was synthesized with only a Quaternary amine. The head group in DOAAQ was not protonated in the tested pH range, indicating that this structure was not a suitable candidate for further development. Therefore, an analogous tertiary DOAAT lipid was not synthesized.

Synthesis of the DOPA, DOMPA, and DOBA compounds was achieved using two similar schemes. The headgroup was assembled by either Michael-type conjugate addition of t-butyl protected acrylates (DOPA, DOMPA)[22] or S_N2 addition of t-butyl protected bromobenzylacetate (DOBA) to a 3-methylamino-1,2-propanediol. Oleic acid was conjugated to the 1° and 2° hydroxyl via DCC coupling to yield a dioleyl amphiphile. At this step, the molecule was either deprotected to yield the 3° ZL, or methylated then deprotected to yield the 4° ZL. DOPAQ was found to degrade rapidly following purification, likely due to a retro-Michael reaction, yielding 1,2-dioleoyloxy-3-dimethylamino propane and acrylic acid (data not shown). Due to this instability, biophysical characterization was not carried out for this molecule.

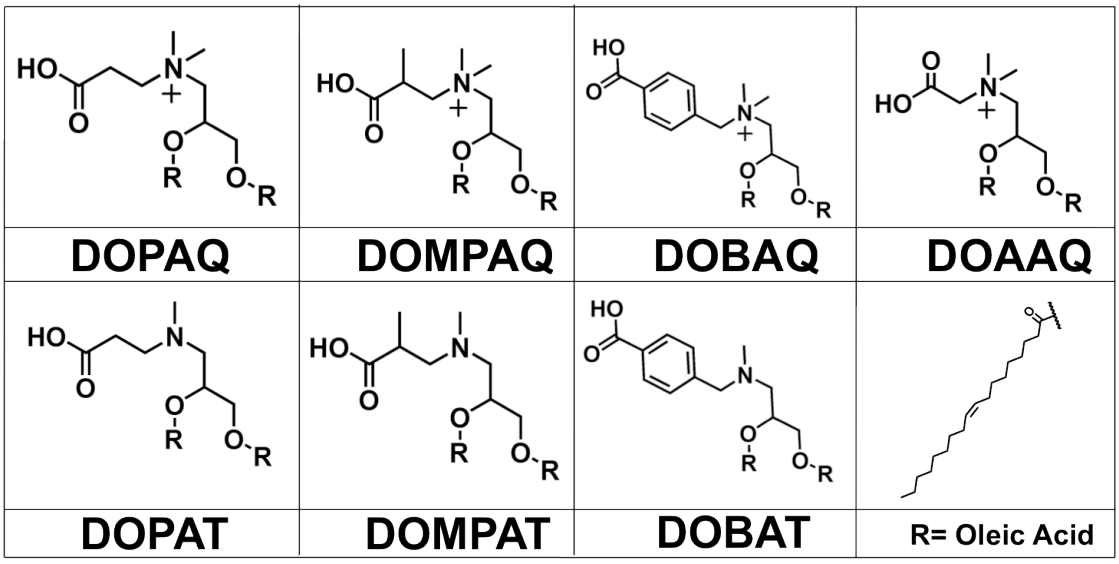

Figure 2.2: Schematic structures of the synthesized zwitterionic lipids

The DOAAQ compound was synthesized by coupling oleic acid tails to the 1° and 2° hydroxyls of 3-dimethylamino-1,2-propanediol, followed by the S_N2 addition of a t-butylbromoacetate and subsequent acid deprotection. This scheme was used to avoid disubstitution of the protected bromoacetate, which reacted much faster than the benzylbromoacetate. Additionally, this scheme eliminates the need for methylation, thereby reducing the total number of synthetic steps.

2.4.2 Vesicle formation

Both 3° and 4° ZL generally form stable liposomes as pure component systems (data not shown). However, DOBAT and DOBAQ ZL, which contain a benzene ring in the linker region, were less stable than the remaining non-aromatic ZL, and did aggregate over time. This is likely due to the presence of a rigid, hydrophobic region in the hydrophilic head group. The addition of helper lipids, including DOPC, cholesterol, and PEG-DMG allowed for formulation of stable, monodisperse ZL containing liposomes. Multiple formulations were used to test the biophysical characteristics of ZL containing liposomes, depending on the requirements of the individual experiment.

2.4.3 Zeta potential of ZL containing liposomes

Understanding the ionization behavior of ZL in liposomes is important to characterize their overall biophysical behavior. Direct measurement of lipid pKa is difficult because the molecule is insoluble in water. In a liposome, the ionizable molecule is located at a hydrophobic/hydrophilic interface with zwitterionic, polyelectrolyte characteristics. The effect of the interfacial environment on lipid pKa is not well understood, however it is expected that as the pH approaches the lipid pKa, the liposomal zeta potential will increase.

The zeta potential of ZL:DOPC liposomes was measured across a range of pH to determine the impact of environmental pH on their surface charge. Three formulations, containing 1:9, 1:3, and 1:1 ZL:DOPC, were tested in half pH unit intervals from pH=3.0 to pH=8.5, and these data were used to study the ionization behavior of these liposomes.

2.4.3.1 Impact of amine substitution on zeta potential

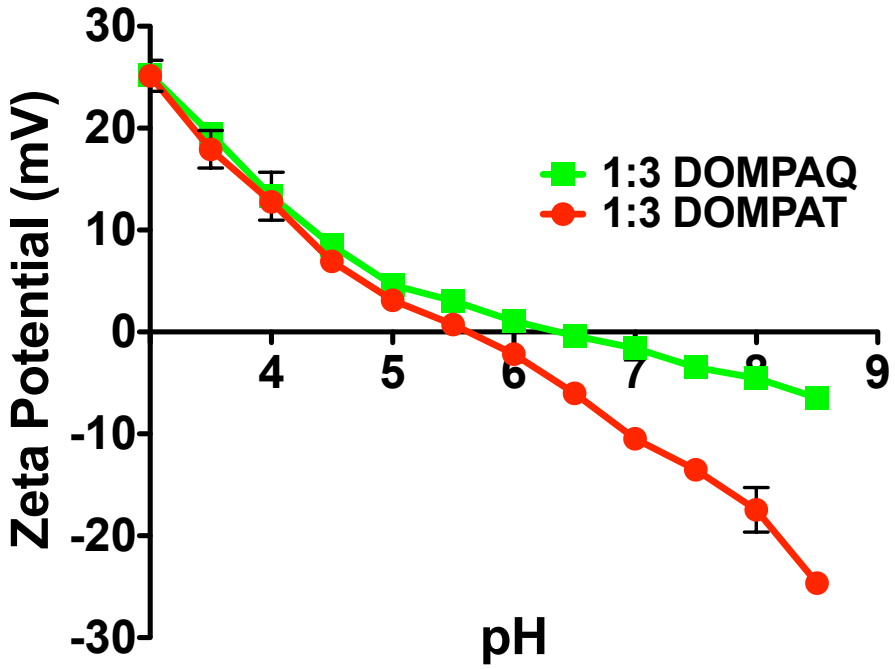

Figure 2.3: Zeta potential vs. pH data for DOMPAT and DOMPAQ liposomes

Comparing the pH responsive zeta potential data of analogous tertiary (DOMPAT) and quaternary (DOMPAQ) ZL reveals the similarities and differences in their behavior (Figure 2.3). At low pH, formulations containing equal amounts of DOMPAT and DOMPAQ have nearly identical zeta potentials. As the pH increases, formulations containing DOMPAT become neutral and eventually anionic, while those containing DOMPAQ remain neutral. This behavior is consistent for all ZL and all formulations (Table

2.1). At low pH, the tertiary amine is likely fully protonated, and the limiting step in these vesicles becoming cationic is the protonation of the carboxylate. The different behavior of tertiary and quaternary ZL at physiological pH allows for the tailoring of vesicle properties based on the desired liposomal properties. Additionally, tertiary ZL have fewer synthetic steps, potentially making them more attractive for use in drug delivery systems.

2.4.3.2 Impact of liposomal formulation on zeta potential

The liposomal formulation has a significant impact on the magnitude of the surface charge of ZL containing vesicles (Figure 2.4). As expected, the maximum zeta potential for all formulations occurred at the lowest pH tested (pH=3.0), and the minimum zeta potential occurred at the highest pH tested (pH=8.5) (Table 2.1). Increasing the ratio of ZL:DOPC increases the number of ionizable head groups in the formulation, thereby increasing the magnitude of the surface charge of the vesicle in pH ranges where those groups are protonated. DOAAQ containing vesicles remained approximately neutral (0 ± 10 mV) across the entire pH range tested, indicating they are ionized below pH=3.0. All other ZL show pH-dependent zeta potentials, with DOBAQ showing the highest maximum zeta potential, and DOBAT showing the lowest minimum zeta potential across all formulations. These data also show that the minimum zeta potential of all quaternary formulations are approximately neutral, while the tertiary formulations all become anionic. Changing the helper lipid from DOPC to DOPE does not impact the zeta potential of the resulting liposome, confirming that the pH-responsive zeta potential behavior is due to the presence of ZL (data not shown).

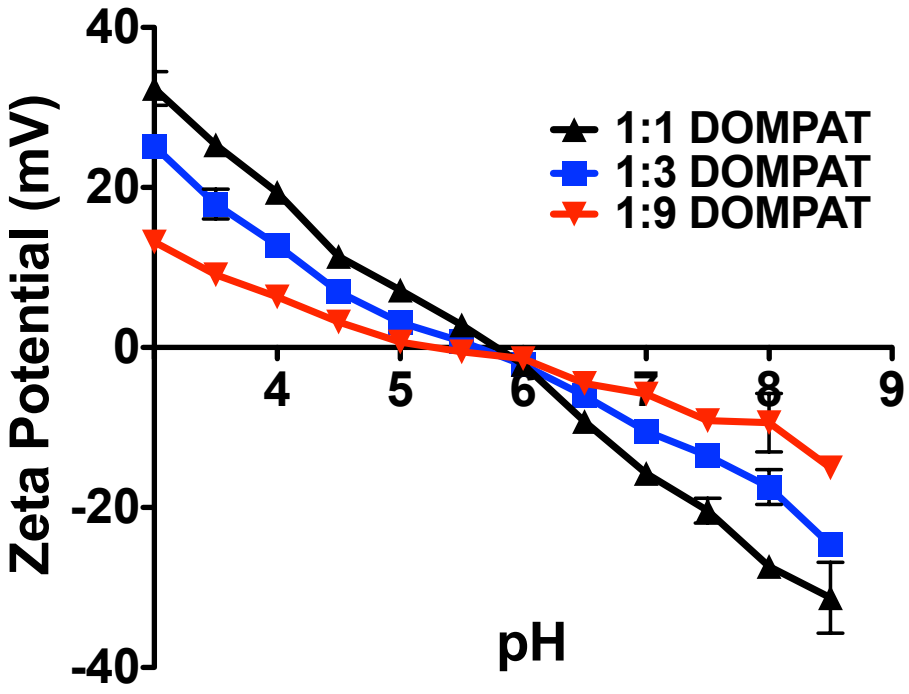

Figure 2.4: Impact of formulation on the zeta potential of DOMPAT liposomes

BLL	Ratio	Max Value (mV)	Min Value (mV)
DOMPAT	1:1	32.38 ± 2.11	-31.28 ± 4.42
	1:3	25.15 ± 1.52	-24.65 ± 0.95
	1:9	13.20 ± 0.98	-15.03 ± 1.30
DOPAT	1:1	38.90 ± 0.59	-43.85 ± 0.68
	1:3	30.00 ± 1.06	-29.18 ± 1.06
	1:9	13.40 ± 0.71	-16.00 ± 0.71
DOBAT	1:1	36.30 ± 2.30	-52.13 ± 1.25
	1:3	29.63 ± 1.34	-38.88 ± 1.60
	1:9	16.53 ± 0.46	-21.75 ± 0.64
DOMPAQ	1:1	32.75 ± 0.37	-10.80 ± 0.59
	1:3	25.25 ± 1.08	-6.47 ± 0.63
	1:9	12.48 ± 1.07	-6.26 ± 1.28
DOBAQ	1:1	35.48 ±1.91	-11.18 ± 1.10
	1:3	35.28 ± 0.64	-6.82 ± 0.68
	1:9	18.60 ± 1.13	-6.36 ± 0.66
DOAAQ	1:1	N.D.	N.D.
	1:3	1.13 ± 1.95	-6.78 ± 0.71
	1:9	N.D.	N.D.

Table 2.1: Zeta potential behavior of ZL formulations

2.4.3.3 Zeta potential of 1:3 ZL:DOPC liposomes

In an effort to determine the effect of structural differences in ZL head groups on their biophysical behavior, the pH-dependent zeta potential behavior of liposomes containing 1:3 ZL:DOPC was studied for all synthesized lipids (Figure 2.5). We hypothesized that the length and structure of the region linking the carboxylate and amine could affect the pKa of the lipid head group, thereby modulating the zeta potential behavior of the vesicles. The predicted pKa of the synthesized ZL are shown in Table 2.2. The predicted values indicate that DOAAQ, which contains a single carbon linker between the carboxylate and amine, should not be protonated in the pH range tested, and therefore should remain neutral. DOAAQ is not ionized because the close proximity of the electron withdrawing quaternary amine prevents protonation of the carboxylate. As the amine is moved farther from the carboxylate, its impact on carboxylate protonation decreases, resulting in a higher pKa. This is seen for the remaining tertiary (DOMPAT, DOPAT, DOBAT) and quaternary (DOMPAQ, DOBAQ) ZL, which contain longer linker regions, and have similar predicted pKa. However, slight differences in the pKa of both the amine and carboxylate are predicted due to variations in the head group structure. This may result in slight differences in the ionization behavior of these lipids. Figure 2.5 shows that, as expected, DOAAQ liposomes are not ionized in this pH-range, and therefore remain neutral across all pH. All other tertiary or quaternary ZL show trends similar to those seen in Figure 2.3: at low pH, tertiary and quaternary ZL are cationic, but at high pH, tertiary ZL become anionic while quaternary ZL remain neutral. These results indicate that modulating the linker region can indeed alter the lipid pKa, as predicted in Table 2.2.

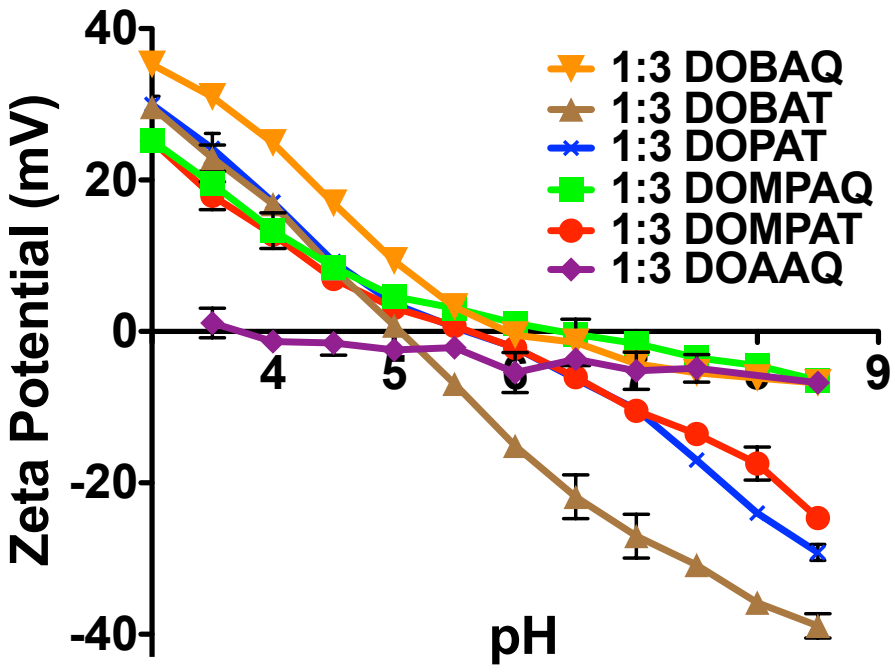

Figure 2.5: Zeta potential vs. pH for 1:3 ZL:DOPC formulations

However, differences in the absolute zeta potential behavior are seen in these formulations. DOBAT liposomes become anionic at a much lower pH than those containing DOMPAT or DOPAT, however the maximum zeta potential of all three formulations is nearly identical. The 3° amine in DOBAT was predicted to have a lower pKa than the other tertiary amines tested (Table 2.2), possibly explaining the discrepancies in zeta potential behavior. Also, DOBAQ liposomes show a consistently higher zeta potential than all other formulations at pH<5.0, indicating they may become membrane active at higher pH than other formulations tested. Interestingly, both ZL containing aromatic linkers show behavior that differs from non-aromatic ZL. It is possible that the aromatic ring in the linker region of DOBAT and DOBAQ is altering the ionization behavior of the amine and/or carboxylate when assembled in a lipid bilayer. The carboxylate of DOBAQ appears to be more easily protonatable than the other ZL tested, resulting in higher zeta potentials at low pH.

Alternatively, the 3° amine in DOBAT appears to be more difficult to protonate, therefore decreasing the pH at which these vesicles cross the origin. This could be due to lipid orientation or molecular interactions in the bilayer, however it is difficult to accurately determine why this occurs due to the complexity of the system.

BLL	pKa (Carboxylate)	pKa (Amine)
DOMPAT	3.7 ± 0.3	8.3 ± 0.5
DOPAT	3.6 ± 0.2	7.8 ± 0.5
DOBAT	4.0 ± 0.1	7.1 ± 0.5
DOMPAQ	3.7 ± 0.3	NA
DOBAQ	3.8 ± 0.1	NA
DOAAQ	1.7 ± 0.3	NA

Table 2.2: Predicted pKa of ionizable groups on ZL. Values predicted using ACD Laboratories software

The results of these experiments show that altering the length or structure of the ZL linker region can impact the ionization behavior of the lipid, as predicted by the pKa estimations shown in Table 2.2. This also confirms that, as expected, lipid pKa directly affects the pH-dependent ionization behavior of ZL in liposomes. We find that, in general, the pH-dependent zeta potential behavior of all tertiary and quaternary ZL exhibit similar trends. However, we also find that structural differences between ZL can impact their ionization behavior, likely due to the complex inter and intramolecular interactions that occur at the liposomal surface.

2.4.4 Determination of ZL fusogenic potential using a lipid mixing assay

In order to determine the fusogenic potential of ZL as a function of pH, their ability to interact with anionic membranes was assayed using a FRET based lipid-mixing assay[19]. Vesicles containing 43:30:25:1:1 DOPC:DOPE:ZL:Rho-PE:NBD-PE were used as donor

vesicles for all experiments. Biomembrane mimicking anionic vesicles containing 45:20:20:15 DOPC:DOPE:DOPG:Chol were used as acceptors. Lipid mixing between the donor and acceptor vesicles result in a dilution of the FRET pair and a change in the fluorescence profile. The extent of mixing is directly correlated to the increase in fluorescence intensity of the NBD probe.[19]

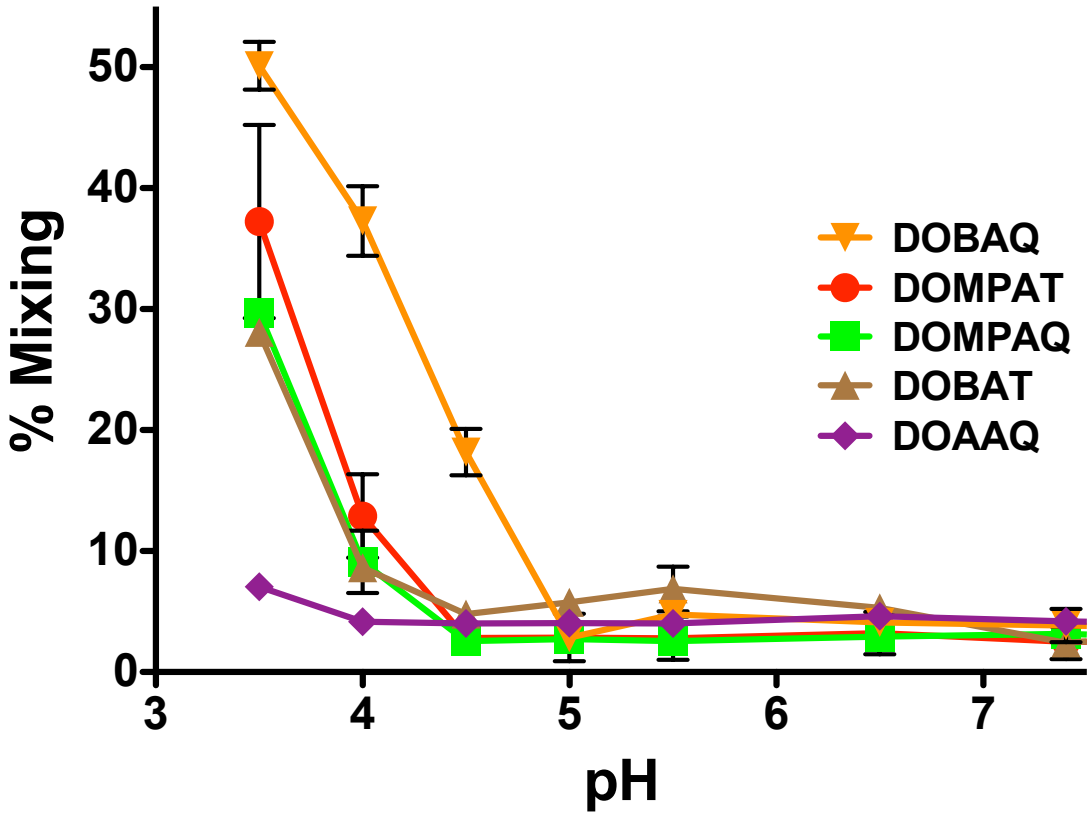

Figure 2.6: pH-dependent lipid mixing of ZL containing liposomes

Figure 2.6 shows that all liposomal formulations show no mixing at pH> 5.0. As the pH decreases below pH=4.5, lipid mixing increases for all active formulations; maximum lipid mixing for all formulations is achieved at pH=3.5, the lowest pH tested in this experiment. DOBAQ liposomes, which had the highest zeta potential at all pH< 5.0, show the highest levels of lipid mixing across all pH. DOAAQ, which is not protonated in the

range tested, shows baseline levels of lipid mixing across all tested pH values. These results indicate that, as expected, electrostatics drive membrane interactions in this system.

Comparing the data from Figure 2.3 and Figure 2.5, we see that the pH at which lipid mixing begins does not correlate exactly with a liposomal zeta potential of 0 mV. This indicates that there is a threshold zeta potential value required to induce membrane interactions between the cationic and anionic vesicles. According to these data, that threshold appears to be approximately +10 mV. This result agrees with previous reports, which indicate that the threshold where nanoparticle surface charge is great enough to promote electrostatic interactions is approximately ±10 mV.[23,24] This threshold is crossed by DOBAQ containing vesicles at pH=4.5 and by all other active ZL at pH=4.0; this correlates precisely with an increase in lipid mixing from baseline levels.

2.4.5 Lysis of biomembrane mimicking vesicles

It is hypothesized that the charge state of ionizable lipids impacts their ability to disrupt anionic biomembranes along the endocytic pathway and deliver contents to the cytosol.[2,12,14] When cationic, these lipids can ion-pair with naturally occurring anionic lipids, inducing a phase transition from the stable L_α to the unstable H_{II} phase, promoting endosomal escape.[25,26] The efficiency of this process is key to the effective delivery of liposomal contents to the cytosol.[2,4,16,25] Though ZL are protonated at the low end or below the range found along the endocytic pathway (pH~7.4-5.0)[27], we were nonetheless interested in understanding whether lipids with this general structure were capable of disrupting anionic membranes when cationic.

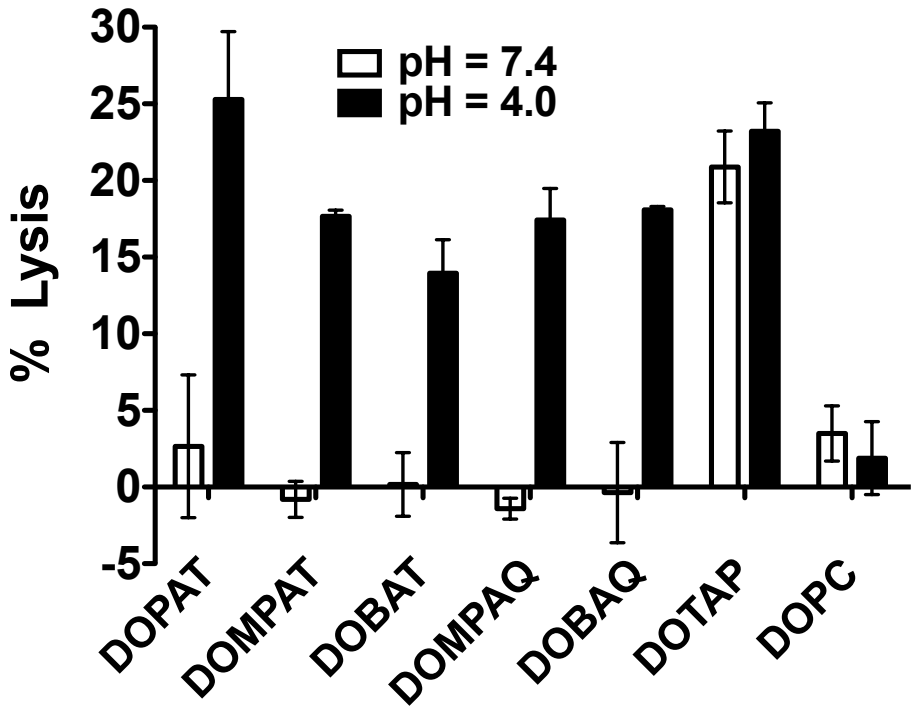

Figure 2.7: ZL mediated membrane lysis as a function of pH

We investigated the capacity of ZL containing liposomes to lyse biomembrane mimicking vesicles (BMV) encapsulating the fluorophore/quencher ANTS/DPX as a function of pH. BMV consisted of 45:20:20:15 DOPC:DOPE:DOPG:cholesterol.[28] A fusogenic ZL formulation containing 45:30:25 DOPE:ZL:DOPC was used to promote membrane mixing when cationic. pH=4.0 and 7.4 were chosen because previous zeta potential and lipid mixing experiments confirmed that liposomes containing 25-30% ZL were cationic and membrane active at pH=4.0 and neutral (4° ZL) or anionic (3° ZL) at pH=7.4 (previously discussed). The dye/quencher ANTS/DPX was used because carboxyfluorescein rapidly transfers out of the bilayer at pH=4.0 due to protonation of the phenol and carboxylic acid (data not shown). We hypothesized that at low pH, ZL liposomes would induce contents leakage from BMV due to membrane fusion or destabilization following ion pairing.[14]

Our results show that all ZL liposomes are capable of lysing BMV at pH=4.0, but cause no lysis at pH=7.4 (Figure 2.7). These results indicate that, as expected, ZL containing lipids disrupt anionic membranes, and ionization of the ZL head group is essential for this to occur. Additionally, these liposomes do not interact with membranes when they are not charged; an essential characteristic of long-circulating, non-toxic liposomal drug delivery systems, and a significant shortcoming of formally cationic lipids such as DOTAP.

These data show that there is variability in the ability of ZL liposomes to induce membrane lysis. Interestingly, these results do not correlate precisely with the observed zeta potential behavior of ZL liposomes, possibly indicating that ZL structure may impact their membrane lysis properties. Our results show that DOPAT exhibits the highest levels of membrane lysis at 25.3%, and DOBAT shows the lowest level at 14.0%. Interestingly, DOBAQ, which showed higher zeta potential and membrane mixing at pH = 4.0, induced 18.1% leakage, which was significantly lower than that of DOPAT. These results indicate that the aromatic spacer may be less effective at permeating the inner leaflet and promoting contents release as compared to the non-aromatic ZL. This may be due to the rigid, hydrophobic nature of these head groups, compared to the smaller, more flexible linear or branched spacers present in the other ZL.

2.4.6 Low-pH encapsulation of siRNA in ZL liposomes

We hypothesized that ionized ZL could encapsulate anionic molecules such as siRNA more efficiently than other zwitterionic lipids by exploiting their cationic charge at low pH. Liposomes were formed using a batch mixing process, where equal volumes of siRNA in aqueous buffer (pH=3.0) and lipids dissolved in methanol were mixed, extruded, then

dialyzed against PBS (pH=7.4) to remove all methanol and return the system to pH=7.4. Electrostatic interactions between the ionized lipids and the anionic siRNA was expected to result in high encapsulation efficiencies, as shown previously with similar systems.[16,29] ZL that are protonated at pH=3.0 (DOBAQ, DOMPAQ, DOPAT) all exhibit encapsulation efficiencies above 65%, with both DOBAQ and DOPAT encapsulating more than 80% of the siRNA. DOPC and DOAAQ, which are not protonated at pH=3.0, show less than 5% encapsulation, indicating that ionized ZL can indeed mediate higher encapsulation of anionic molecules than neutral lipids. Following dialysis, the liposomes formed using this method are smaller than 100 nm and have a neutral or slightly anionic zeta potential, both of which are essential characteristics of long circulating liposomes. This proof of concept experiment illustrates the potential utility of the pH-sensitive characteristics of ZL for encapsulating charged drugs in small, neutral particles by modulating the pH of the system during encapsulation.

Formulation	Encapsulation efficiency (%)	Hydrodynamic diameter (nm)	Zeta potential (mV)
DOBAQ/DOPE/PEG-DMG (60/30/10)	83 ± 4%	75 ± 15 nm	- 3.1 ± 3 mV
DOMPAQ/DOPE/ PEG-DMG (60/30/10)	65 ± 8%	80 ± 9 nm	- 1.5 ± 2 mV
DOPAT/DOPE/PEG-DMG (60/30/10)	91 ± 9%	91 ± 12 nm	- 5.7 ± 2 mV
DOAAQ/DOPE/PEG-DMG (60/30/10)	2 ± 2%	86 ± 8 nm	-4.2 ± 4 mV
DOPC/DOPE/PEG-DMG (60/30/10)	5 ± 3 %	79 ± 10 nm	-5.0 ± 1 mV

Table 2.3: Low-pH siRNA encapsulation and liposomal characterization data

2.4.7 siRNA mediated knockdown of luciferase in vitro with DOBAQ liposomes

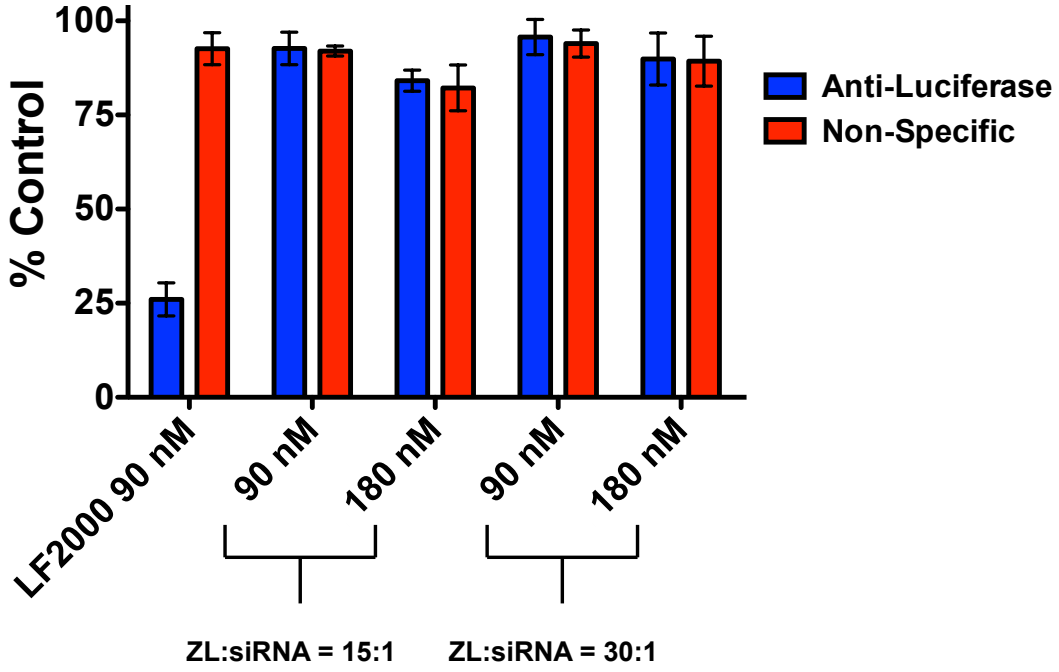

Figure 2.8: siRNA knockdown in HeLa-Luc cells using ZL liposomes (65:34:1, DOBAQ:DOPE:PEG-DMG)

We investigated ZL liposomes as siRNA delivery systems in a stably transfected HeLa-Luc cell line.[13] DOBAQ was chosen as a representative ZL due to its ionization behavior and enhanced membrane interactions. Anti-luciferase and non-specific siRNA was encapsulated in DOBAQ liposomes (65:34:1 DOBAQ:DOPE:PEG-DMG) at an ZL:siRNA (w:w) ratios of 15 and 30 (N:P = 6.66, 13.34 respectively). No siRNA mediated gene silencing was observed at siRNA concentrations of 90 nM or 180 nM following a 24-hour incubation (Figure 2.8). Lipofectamine 2000 (LF2000), a cationic positive control, showed 75% knockdown at 90 nM siRNA. Altering the ZL lipid structure or the liposomal formulation had no impact on transfection efficiency (data not shown). We believe that the inability to transfect is likely because ZL are not effectively protonated at pH levels generally

found in the endosome (pH=5.0-7.0). Therefore, these delivery systems are not becoming cationic in the endosome, and membrane disruption and fusion are not occurring.

2.4.8 siRNA mediated knockdown of FVII in vivo with DOBAQ liposomes

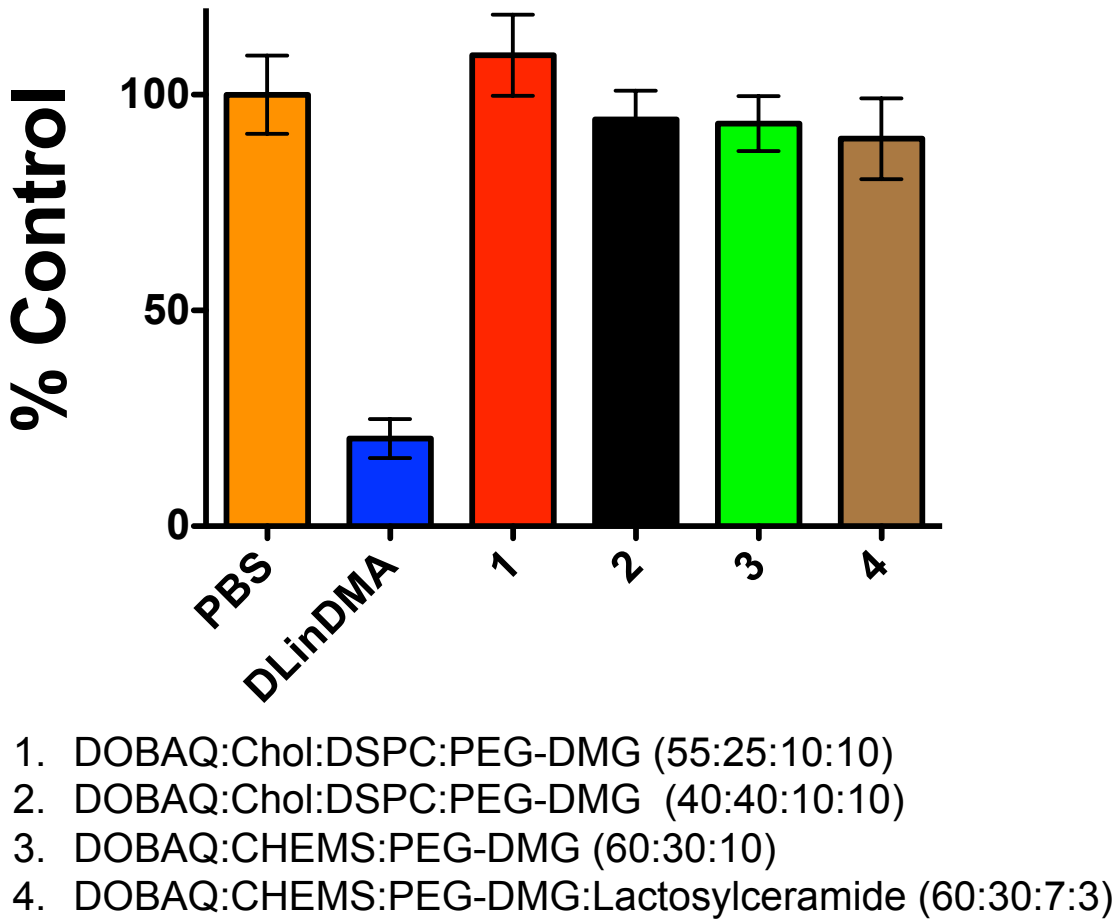

Figure 2.9: siRNA mediated knockdown of Factor VII in CD-1 mice using DOBAQ liposomes. All doses were 5 mg/kg total siRNA.

The mouse Factor VII model was chosen as the primary *in vivo* screen for ZL liposome mediated delivery of siRNA to hepatocytes via systemic injection.[22] DOBAQ was again used as a representative ZL due to its favorable biophysical properties. Four DOBAQ formulations were tested at doses of 5 mg/kg *in vivo*: DOBAQ:Chol:DSPC:PEG-DMG (55:25:10:10); DOBAQ:DOPE:PEG-DMG:Lactosylceramide (60:30:7:3);

DOBAQ:CHEMS:PEG-DMG (60:30:10); DOBAQ:DOPE:PEG-DMG:Lactosylceramide (60:30:7:3). These formulations were chosen to determine if the choice of helper lipid (Chol, DSPC, DOPE, CHEMS) impacted the efficacy of the formulation. Additionally, targeted formulations containing Lactosylceramide, which targets the asialoglycoprotein receptor on hepatocytes, were used to determine whether a targeting ligand can increase hepatocellular uptake and promote knockdown. Our results indicate that DOBAQ liposomes are not capable of siRNA mediated gene regulation regardless of formulation (Figure 2.9). Increasing the total siRNA dose to 10 mg/kg did not induce Factor VII knockdown (data not shown). DLinDMA (Figure 1.6), an ionizable lipid known to transfect hepatocytes *in vivo*, was used as a positive control in a formulation containing DLinDMA:Chol:DSPC:PEG-DMG (40:40:10:10), and resulted in a 90% reduction in Factor VII (Figure 2.9). Again, we hypothesize that ZL are not protonated along the endocytic pathway, and therefore cannot efficiently deliver siRNA to the cytosol through carrier-mediated membrane fusion.

2.4.9 Cytokine induction by DOBAQ liposomes in CD-1 mice

Cationic lipid based siRNA delivery vehicles are currently limited by inflammatory toxicities associated with particle uptake by the mononuclear phagocyte system.[30,31] Interactions between cationic lipids and TLR2 and TLR4 on the cell surface of macrophages, as well as siRNA and TLR3 and TLR7 in endosomes stimulate the production of inflammatory cytokines. Though systemic injection of siRNA containing ZL liposomes did not lead to gene silencing, we were nonetheless interested in whether these particles stimulated an inflammatory immune response similar to that seen in other siRNA delivery systems.[31] We measured cytokine concentration in plasma 6 hours after a 5 mg/kg dose (15:1 ZL:siRNA) of DOBAQ:Chol:DSPC:PEG-DMG (40:40:10:10) (Figure 2.10). No

inflammatory immune response was observed, as no inflammatory cytokines were significantly elevated compared to PBS. This indicates that a zwitterionic system may be able to overcome the inflammatory toxicity seen with cationic or ionizable amino lipid vectors.

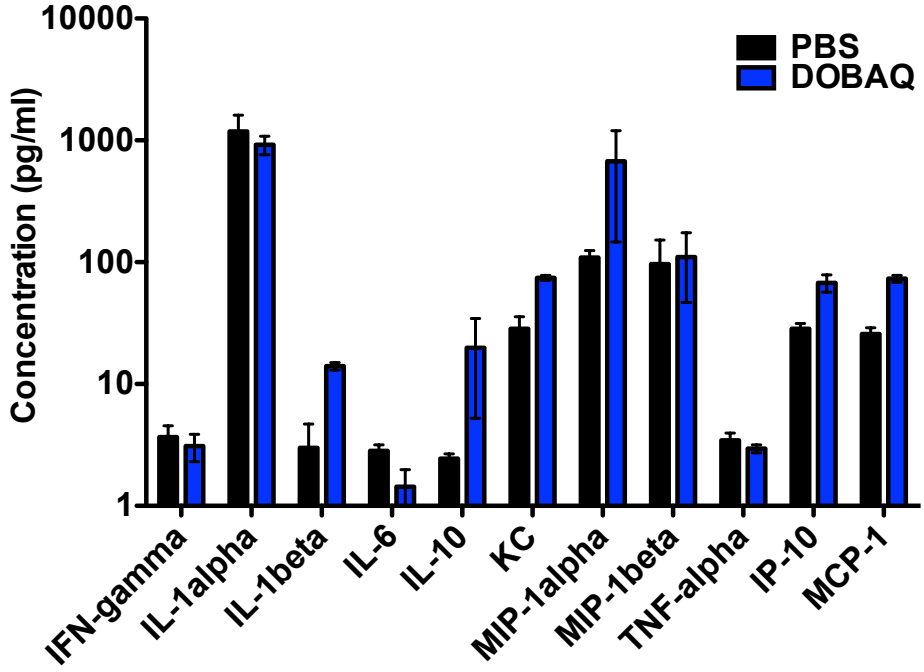

Figure 2.10: Cytokine induction by DOBAQ:Chol:DSPC:PEG-DMG (40:40:10:10) liposomes in CD-1 mice (5 mg/kg siRNA, 15:1 w:w ZL:siRNA).

2.5 Summary and Conclusions

Here we have described the synthesis and pH-dependent biophysical behavior of betaine-like lipids, a novel class of ionizable, zwitterionic lipids containing a cationic amine and anionic carboxylate. Seven ZL with varying structures were synthesized, six of which showed pH-responsive behavior between pH=3.0-8.5. Structural variations in the head group impact the ionization behavior of ZL; however once the carbon spacer is greater than one carbon, all ZL show the same general trends. ZL are capable of forming small, monodisperse liposomes that

efficiently encapsulate siRNA when ionized, and show pH-dependent zeta potentials ranging from anionic (3° ZL) or neutral (4° ZL) at physiological pH to cationic at low pH. At pH < 4.5, active ZL promote lipid mixing with anionic membrane mimicking vesicles, and at pH=4.0, fusogenic vesicles containing ZL induce lysis of biomembrane mimicking vesicles. No membrane disruption (mixing or lysis) was seen with ZL containing liposomes at physiological pH, indicating that ZL are a new class of biocompatible lipids that should be long circulating, non-toxic, and non-immunogenic. Representative studies using the ZL DOBAQ indicate that these lipids are not capable of delivering siRNA *in vitro* or to hepatocytes *in vivo*. However, cytokine induction studies indicate that ZL are non-immunogenic when delivered systemically. These properties make ZL an interesting class of new molecules for use in liposomal drug, gene, or siRNA delivery systems where pH-responsive electrostatic interactions are desired either for drug encapsulation or membrane interactions. Additionally, structural modifications to increase lipid pKa may result in zwitterionic lipid systems that efficiently deliver siRNA while limiting the inflammatory immune response.

2.6 References

1. Puri, A., Loomis, K., Smith, B. & Lee, J. Lipid-Based Nanoparticles As Pharmaceutical Drug Carriers: From Concepts To Clinic. *Crit Rev Ther Drug Carrier Syst* (2009).
2. Stanton, M. G. & Colletti, S. L. Medicinal Chemistry Of siRNA Delivery. *J Med Chem* **53**, 7887–7901 (2010).
3. Whitehead, K. A., Langer, R. & Anderson, D. G. Knocking Down Barriers: Advances In siRNA Delivery. *Nature Reviews Drug Discovery* **8**, 129–138 (2009).
4. Li, W. & Szoka, F. C. Lipid-Based Nanoparticles For Nucleic Acid Delivery. *Pharm Res* **24**, 438–449 (2007).
5. Lu, J. J., Langer, R. & Chen, J. A Novel Mechanism Is Involved In Cationic Lipid-

Mediated Functional siRNA Delivery. *Mol Pharm* **6**, 763–771 (2009).

6. Schroeder, A., Levins, C. G., Cortez, C., Langer, R. & Anderson, D. G. Lipid-Based Nanotherapeutics For siRNA Delivery. *J Intern Med* **267**, 9–21 (2010).
7. Adami, R. C. *Et Al.* An Amino Acid-Based Amphoteric Liposomal Delivery System For Systemic Administration Of siRNA. *Mol Ther* **19**, 1141–1151 (2011).
8. Ceballos, C. *Et Al.* Cationic Nucleoside Lipids Derived From Universal Bases: A Rational Approach For siRNA Transfection. *BIOCONJUGATE CHEMISTRY* 1–8 (2010).
9. Zhang, S., Zhao, B., Jiang, H., Wang, B. & Ma, B. Cationic Lipids And Polymers Mediated Vectors For Delivery Of siRNA. *Journal Of Controlled Release : Official Journal Of The Controlled Release Society* **123**, 1–10 (2007).
10. Yang, H., Yi, J., Bang, E. & Jeon, E. Cationic Nucleolipids As Efficient siRNA Carriers. *Org Biomol Chem* (2010).
11. Gilot, D., Miramon, M., Benvegnu, T. & Ferrieres, V. Cationic Lipids Derived From Glycine Betaine Promote Efficient And Non-Toxic Gene Transfection In …. *J Gene Med* (2002).
12. Semple, S. C. *Et Al.* Rational Design Of Cationic Lipids For siRNA Delivery. *Nature Biotechnology* **28**, 172–176 (2010).
13. Love, K. T. *Et Al.* Lipid-Like Materials For Low-Dose, In Vivo Gene Silencing. *Proceedings Of The National Academy Of Sciences* **107**, 1864–1869 (2010).
14. Zhang, J., Fan, H., Levorse, D. A. & Crocker, L. S. Ionization Behavior Of Amino Lipids For siRNA Delivery: Determination Of Ionization Constants, SAR, And The Impact Of Lipid P Kaon Cationic Lipid−Biomembrane Interactions. *Langmuir* **27**, 1907–1914 (2011).
15. Obata, Y., Tajima, S. & Takeoka, S. Evaluation Of Ph-Responsive Liposomes Containing Amino Acid-Based Zwitterionic Lipids For Improving Intracellular Drug Delivery In Vitro And In Vivo. *Journal Of Controlled Release : Official Journal Of The Controlled Release Society* **142**, 267–276 (2010).
16. Heyes, J., Palmer, L., Bremner, K. & Maclachlan, I. Cationic Lipid Saturation Influences Intracellular Delivery Of Encapsulated Nucleic Acids. *Journal Of Controlled Release* **107**, 276–287 (2005).

17. Fricker, G. *Et Al.* Phospholipids And Lipid-Based Formulations In Oral Drug Delivery. **27**, 1469–1486 (2010).
18. Akinc, A. *Et Al.* Development Of Lipidoid-siRNA Formulations For Systemic Delivery To The Liver. *Mol Ther* **17**, 872–879 (2009).
19. Struck, D., Hoekstra, D. & Pagano, R. Use Of Resonance Energy Transfer To Monitor Membrane Fusion. *Biochemistry* (1981).
20. Ellens, H., Bentz, J. & Szoka, F. Fusion Of Phosphatidylethanolamine-Containing Liposomes And Mechanism Of L. Alpha.-HII Phase …. *Biochemistry* (1986).
21. Frese, J., Jr., Wu, C. H. & Wu, G. Y. Targeting Of Genes To The Liver With Glycoprotein Carriers. *Advanced Drug Delivery Reviews* **14**, 137–152 (1994).
22. Akinc, A. *Et Al.* A Combinatorial Library Of Lipid-Like Materials For Delivery Of Rnai Therapeutics. *Nature Biotechnology* **26**, 561–569 (2008).
23. Duplessis, J., Ramachandran, C., Weiner, N. & Muller, D. The Influence Of Lipid Composition And Lamellarity Of Liposomes On The Physical Stability Of *Liposomes Upon Storage. International Journal of Pharmaceutics* **127**, 273–278 (1996).
24. Clogston, J. D. & Patri, A. K. Zeta Potential Measurement. **697**, 63–70 (2011).
25. Xu, Y. & Szoka, F. C. Mechanism Of DNA Release From Cationic Liposome/DNA Complexes Used In Cell Transfection. *Biochemistry* **35**, 5616–5623 (1996).
26. Hafez, I. M. & Cullis, P. R. Roles Of Lipid Polymorphism In Intracellular Delivery. *Advanced Drug Delivery Reviews* **47**, 139–148 (2001).
27. Mintzer, M. A. & Simanek, E. E. Nonviral Vectors For Gene Delivery. *Chem. Rev.* **109**, 259–302 (2009).
28. Koynova, R. An Intracellular Lamellar-Nonlamellar Phase Transition Rationalizes The Superior Performance Of Some Cationic Lipid Transfection Agents. *Proceedings Of The National Academy Of Sciences* **103**, 14373–14378 (2006).
29. Jeffs, L. B. *Et Al.* A Scalable, Extrusion-Free Method For Efficient Liposomal Encapsulation Of Plasmid DNA. *Pharm Res* **22**, 362–372 (2005).
30. Sakurai, H., Kawabata, K., Sakurai, F., Nakagawa, S. & Mizuguchi, H. Innate Immune Response Induced By Gene Delivery Vectors. *International Journal Of Pharmaceutics* **354**, 9–15 (2008).
31. Abrams, M. T. *Et Al.* Evaluation Of Efficacy, Biodistribution, And Inflammation For A

Potent siRNA Nanoparticle: Effect Of Dexamethasone Co-Treatment. *Mol Ther* **18**, 171–180 (2010).

Chapter 3: Synthesis and Characterization of Betaine-like Diacyl Lipids: Zwitterionic Lipids with the Cationic Group at the Bilayer Interface

3.1 Abstract

We synthesized and characterized a series of zwitterionic, acetate-terminated, quaternized amine diacyl lipids (AQ). These lipids have an inverted headgroup orientation as compared to naturally occurring phosphatidylcholine (PC) lipids; the cationic group is anchored at the membrane interface, while the anionic group extends into the aqueous phase. AQ lipids preferentially interact with highly polarizable anions (ClO_4^-) over less polarizable ions (Cl^-), in accord with the Hofmeister series, as measured by the change in zeta potential of AQ liposomes. Conversely, AQ lipids have a weaker association with calcium than do PC lipids. The transition temperatures (Tm) of the AQ lipids are similar to the Tm observed with phosphatidylethanolamine (PE) lipids of the same chain length. AQ lipids form large lipid sheets after heating and sonication; however, in the presence of cholesterol (Chol) these lipids form stable liposomes that encapsulate carboxyfluorescein. The AQ:Chol liposomes retain their contents in the presence of serum at 37 °C, and when injected intravenously into mice, their organ biodistribution is similar to that observed with PC:Chol liposomes. AQ lipids demonstrate that modulating the headgroup charge orientation significantly alters the biophysical properties of liposomes. For the drug carrier field, these new materials provide a non-phosphate containing zwitterionic lipid for the production of lipid vesicles.

3.2 Introduction

An increasingly diverse toolbox of lipid headgroups, linkers and hydrophobic domains is being populated by the systematic study of natural lipid components and surfactants. This lipid collection has elucidated the influence of headgroup properties such as hydrogen bonding capability, size, and charge on superstructure formation and molecular interactions.[1,2] For instance, zwitterionic surfactants interact with ions with higher affinity than do surfactants with a nonionic headgroup.[3] However, there are a number of lipid headgroup architectures that have not been well characterized. In particular, modifications to the phosphocholine headgroup have been investigated less than other classes of lipids, despite their important role in biological membranes. As a result, less is known about the effects of zwitterionic headgroup structure and charge orientation on superstructure formation and lipid interactions.

Naturally occurring zwitterionic headgroups are oriented with an anion proximal to, and a cation distal to the membrane interface. Inverting this charge orientation in single chain surfactants by placing the cation proximal to the interface has yielded insight into the charge interactions of zwitterionic micelles.[4] Zwitterionic sulfobetaine micelles and lecithin liposomes can specifically interact with anions; this interaction follows the Hofmeister series and Pearson's hard—soft classification.[5,6] "Soft" bases with low charge densities and high polarizability, such as ClO_4^-, bind these micelles more effectively than "hard" bases with high charge densities and low polarizability, such as F^-.

Recently, our group has synthesized zwitterionic sulfobetaine diacyllipids and zwitterionic choline phosphate diacyl lipids with interesting salt-dependent thermotropic properties.[7] These diacyl lipids have a cationic amine adjacent to the membrane interface and an anionic group (sulfonate, phosphate or ethylphosphate) that extends away from the

membrane. The nature of the anionic counterion influences the sulfobetaine lipid thermal transition. In high salt solutions, these lipids exhibit transition temperatures (Tm) similar to that of PC lipids of the same chain length. Conversely, at low salt concentrations, these lipids exhibit elevated Tm similar to those observed in phosphatidylethanolamine (PE) lipids of the same chain length. We propose that the change in Tm is driven by interactions of anions with the cationic amine at the membrane interface.[7]

Here, we expand on this work by synthesizing a class of inverse zwitterionic lipids that have an anionic acetic acid group extending into the aqueous phase and a cationic quaternized amine adjacent to the bilayer interface (Figure 1A). These Acetate Quaternized amine (AQ) lipid vesicles bind to anions and have interesting phase transition temperatures. To our knowledge, this is the first example of the synthesis of diacyl AQ headgroup lipids and of the characterization of the supramolecular assemblies and biophysical properties of such lipids.

3.3 Materials and Methods

3.3.1 Materials

1,2-dimyristoyl-*sn*-glycero-3-phosphocholine (DMPC), 1,2-dipalmitoyl-*sn*-glycero-3-phosphocholine (DPPC), 1,2-distearoyl-*sn*-glycero-3-phosphocholine (DSPC), and cholesterol were obtained from Avanti Polar Lipids (Alabaster, AL). Trifluoroacetic acid was obtained from AK Scientific (Union City, CA); all other solvents were obtained from VWR Scientific (Radnor, PA). PD-10 sephadex columns were obtained from GE Healthcare (San Francisco, CA). All other reagents were purchased from Sigma Aldrich (St. Louis, MO).

Buffers were prepared using Milli-Q deionized water. GraceResolv Silica thin layer chromatography plates were obtained from Grace Davison Discovery Sciences (Deerfield, IL).

3.3.2 Instruments

NMR measurements were taken on a Bruker (Billerica, MA) 300 MHz Avance system and analyzed using TopSpin software. Chemical shifts are expressed as parts per million using tetramethylsilane as an internal standard. ^{13}C NMR measurements were composed of 10,000 scans while ^{1}H measurements were composed of 32 scans. ^{13}C experiments were performed in $CDCl_3$ with 10% MEOD. ^{1}H experiments were performed in $CDCl_3$ or deuterated DMSO. MALDI-TOF measurements were taken on PerSeptive Biosystems Voyager-DE from Applied Biosystems (Carlsbad CA). High performance flash chromatography (HPFC) was carried out using a Grace Reveleris Flash System (Columbia, MD) with pre-packed silica gel columns. Zeta potential and size measurements were carried out using a Nano-ZS Dynamic Light Scattering Instrument from Malvern (Westborough, MA). Differential Scanning Calorimetry (DSC) measurements were obtained using a high-temperature MC-DSC 4100 calorimeter from Calorimetry Sciences Corp. (Lindonk, UT). Fluorescence measurements were made on a FLUOstar plate reader from BMG Labtech (Durham, NC) with excitation at 485 nm and emission at 518 nm.

3.3.3 Synthesis of AQ lipids

The AQ lipid library was synthesized from a 3-(dimethylamino)-1,2-propanediol core (2) via a three-step synthesis (Scheme 3.1). The synthesis is straightforward and provides a high yield of the title compounds.

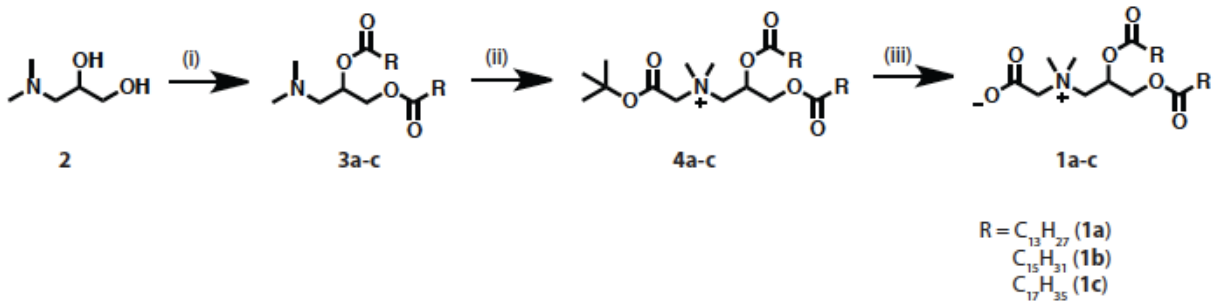

Scheme 3.1: (i) Dichloromethane, 4-dimethylaminopyridine, N,N′-dicyclohexylcarbodiimide, RT, 16h (ii) dichloromethane, N,N-diisopropylethylamine, 40◦C, 16h (iii) dichloromethane, trifluoroacetic acid, RT, 1 h.

1 molar equivalent (6.3 mmol, 0.75 g) of 3-(dimethylamino)-1,2-propanediol was solubilized in 10 mL dichloromethane (DCM). 2.2 molar equivalents of the alkyl acid chain (myristic acid (3a), palmitic acid (3b), or stearic acid (3c)) were added and the reaction was diluted to a final concentration of 0.1 M with DCM. Next, 0.5 molar equivalents of dimethylaminopyridine (DMAP) and 2.5 equivalents of *N,N'*-Dicyclohexanecarbodiimide (DCC) were added to the reaction. The reaction proceeded overnight at room temperature and was monitored by thin layer chromatography (solvent: 10-20% methanol in DCM, visualized by bromocresol green and iodine vapor) and MALDI-TOF. If necessary, DCC was added to drive the reaction toward completion. In order to purify the product (3a-c), the remaining DCC was converted to DCU by addition of 2 mL glacial acetic acid. The produced DCU was removed by vacuum filtration through 55 mm filter paper. To remove residual DCU, the reaction was diluted with 50 mL DCM, washed twice with 10 mL 1 M HCl. The DCM solution was dried over Na_2SO_4. Solvent was removed by rotary evaporation and then by vacuum. The product was purified using HPFC (0-10% methanol in chloroform); this step had 70-80% yield. The compound structure was confirmed using TLC, MALDI-TOF, and ^{1}H NMR.

One molar equivalent (2 g) of 2a-c was solubilized in 30 mL DCM by stirring at room temperature. Next, 3 molar equivalents of Hunig's base were added to the reaction. 2 molar equivalents of tert-butyl bromoacetate were gradually dripped into the reaction in order to avoid excessive heating. The reaction proceeded overnight at 40°C in an oil bath and was monitored by TLC (10-20% methanol in DCM) and MALDI-TOF. An additional 0.5 equivalents of tert-butyl bromoacetate and Hunig's base were added to drive the reaction to near completion. The reaction mixture was diluted with 50 mL DCM, washed twice with 10 mL 1 M HCl to remove residual Hunig's base and tert-butyl bromoacetate, and dried over Na_2SO_4. The quaternized product was purified by precipitation at 0°C in DCM. Solvent was removed by rotary evaporation and high vacuum; this step had 90% yield. 4a-c formation was confirmed by TLC, MALDI-TOF, and ^{1}H NMR.

4a-c was solubilized in 20 mL DCM and 10 mL TFA. 1 mL of triisopropylsilane was added as a scavenger of carbocations. The reaction was allowed to proceed for 1 hour at room temperature and was monitored by TLC (10-20% methanol, visualized by bromocresol green and iodine vapor) and MALDI-TOF. The reaction was diluted with 50 mL DCM, washed twice with 10 mL 1 M $NaHCO_3$ to remove residual TFA, and dried over Na_2SO_4. DMAQ (1a), DPAQ (1b), and DSAQ (1c) were formed in 50-70% overall yield. Product was confirmed by TLC, MALDI-TOF, ^{1}H NMR, ^{13}C NMR and C, H, N elemental analysis.

3a: ^{1}H NMR ($CDCl_3$:MeOD ~10:1): δ .88 (t, 6H); δ 1.26 (m, 40H); δ 1.64 (p, 4H); δ 2.3-2.6 (m, 4H); δ 2.78 (s, 6H); δ 3.1-3.3 (m, 2H); δ 4.15 (m, 1H); δ 4.45 (m, 1H); δ 5.47 (p,1H). MALDI-TOF calculated: 539.49, observed: 541.40.

3b: ^{1}H NMR ($CDCl_3$:MeOD ~10:1): δ .88 (m, 6H); δ 1.26 (m, 48H); δ 1.64 (m, 4H); δ 2.3-2.6(m, 4H); δ 2.78 (m, 6H); δ 3.1-3.3 (m, 2H); δ 4.15 (m, 1H); δ 4.45 (m, 1H); δ 5.45 (m,1H). MALDI-TOF calculated: 595.55, observed 598.37.

3c: ^{1}H NMR ($CDCl_3$:MeOD ~10:1): δ .88 (m, 6H); δ 1.26 (m, 56H); δ 1.64 (m, 4H); δ 2.3-2.6(m, 4H); δ 2.78 (s, 6H); δ 3.1-3.3 (m, 2H); δ 4.15 (m, 1H); δ 4.45 (m, 1H); δ 5.45 (p,1H). MALDI-TOF calculated: 651.62, observed 654.11.

4a: ^{1}H NMR ($CDCl_3$:MeOD ~10:1): δ .88 (t, 6H); δ 1.26 (m, 40H); δ 1.52 (s, 9H); δ 1.64 (m, 4H); δ 2.35 (m, 4H); δ 3.6-3.75 (m, 6H); δ 4.05-4.25(m, 2H); δ 4.5-4.8 (m, 4H); δ 5.58 (m,1H). MALDI-TOF calculated: 654.57, observed: 655.59.

4b: ^{1}H NMR ($CDCl_3$:MeOD ~10:1): δ .88 (m, 6H); δ 1.26 (m, 48H); δ 1.52 (s, 9H); δ 1.64 (m, 4H); δ 2.4 (m, 4H); δ 3.78 (m, 6H); δ 4.05-4.25 (m, 2H); δ 4.5-4.9 (m, 4H); δ 5.6 (m,1H). MALDI-TOF calculated: 710.63, observed 713.49.

4c: ^{1}H NMR ($CDCl_3$:MeOD ~10:1): δ .88 (m, 6H); δ 1.26 (m, 56H); δ 1.52 (s, 9H); δ 1.64 (m, 4H); δ 2.4 (m, 4H); δ 3.78 (m, 6H); δ 4.05-4.25 (m, 2H); δ 4.5-4.9 (m, 4H); δ 5.6 (m,1H). MALDI-TOF calculated: 766.69, observed 768.86.

1a (DMAQ): ^{1}H NMR ($CDCl_3$:MeOD ~10:1): δ .88 (m, 6H); δ 1.26 (m, 40H); δ 1.64 (m, 4H); δ 2.35 (m, 4H); δ 3.35 (m, 6H); δ 4.05-4.25(m, 2H); δ 4.0-4.4(m, 6H); δ 5.55 (m,1H) (Supplementary Figure 1). ^{13}C NMR ($CDCl_3$): δ -0.02, δ 14.10, δ 22.68, δ 24.65, δ 24.74, δ 29.09, δ 29.11, δ 29.25, δ 29.29, δ 29.35, δ 29.56, δ 29.50, δ 29.65, δ 29.68, δ 31.91, δ 33.86, δ 34.20, δ 51.87, δ 52.53, δ 63.26, δ 63.47, δ 65.66, δ 66.61, δ 164.53, δ 172.79, δ 173.09

(Supplementary Figure 2). MALDI-TOF calculated: 597.50, observed: 599.72. Elemental analysis (% expected, % observed): C (70.3, 70.09), H (11.29, 11.05), N (2.34, 2.36)

1b (DPAQ): ^{1}H NMR (DMSO): δ .88 (t, 6H); δ 1.26 (m, 48H); δ 1.55 (m, 4H); δ 2.35 (m, 4H); δ 3.35 (m, 6H); δ 3.8-4.1(m, 4H); δ 4.2-4.4(m, 4H); δ 5.55 (m, 1H) (Supplementary Figure 3). ^{13}C NMR ($CDCl_3$): δ -0.11, δ 14.02, δ 22.63, δ 24.63, δ 29.29, δ 29.62, δ 31.87, δ 33.78, δ 34.09, δ 51.79, δ 52.26, δ 63.20, δ 63.53, δ 165.80, δ 173.39 (Supplementary Figure 4). MALDI-TOF calculated: 653.56, observed: 656.51. Elemental analysis (% expected, % observed): C (71.62, 71.28), H (11.56, 12.08), N (2.14, 2.17)

1c (DSAQ): ^{1}H NMR (DMSO): δ .88 (t, 6H); δ 1.26 (m, 56H); δ 1.55 (m, 4H); δ 2.35 (m, 4H); δ 3.35 (m, 6H); δ 3.8-4.1(m, 4H); δ 4.2-4.4(m, 4H); δ 5.55 (m, 1H). (Supplementary Figure 5). ^{13}C NMR ($CDCl_3$): δ 3.75, δ 17.89, δ 26.53, δ 28.53, δ 33.20, δ 33.54, δ 35.78, δ 37.70, δ 37.99, δ 55.71, δ 56.07, δ 57.16, δ 67.18, δ 69.49, δ 169.98, δ 177.01, δ 177.44 (Supplementary Figure 6). MALDI-TOF calculated: 709.62, observed: 712.66. Elemental analysis (% expected, % observed): C (72.73, 72.33), H (11.78, 11.28), N (1.97, 2.00)

3.3.4 Elemental analysis

5-10 mg of dry lipid was submitted to Microanalytical Laboratory at the University of California, Berkeley for elemental analysis determinations.

3.3.5 Transmission Electron Microscopy (TEM)

TEM images were obtained at the University of California Berkeley Robert D. Ogg Electron Microscope Laboratory. Thin films of DPAQ:Chol formulations were rehydrated in

50 mM HEPES 150 mM NaCl to a final lipid concentration of 20 mM. Preparations were sonicated for 7 minutes at 80 °C. Ten μL of liposome solutions were added to glow discharged copper grids with 400 mesh and Formvar/carbon coatings from Structure Probe, Inc (West Chester, PA). Liposomes were allowed to adsorb on grids for two minutes. Grids were washed three times with distilled water. Liposomes were negatively stained with 1% uranyl acetate and imaged using an FEI Tecnai 12 TEM (FEI, Hillsboro, OR).

3.3.6 Liposome formation in buffers with various anions

Thin lipid films were hydrated in a range of buffers to a final concentration of 20 mM. Preparations were heated at 80 °C for 10 minutes and then sonicated for 7 minutes at 80 °C. After allowing samples to stabilize at room temperature, zeta potential and diameter were measured on a Malvern Nano-ZS. Zeta potential was fit using the Smoluchowski model, while Mark-Houwink parameters were used to determine diameter. All samples were run in triplicate.

3.3.7 Effect of $[Ca^{2+}]$ on vesicle zeta potential and size

Liposomes were prepared as outlined above. Liposome suspensions were spiked into a solution containing between 0 and 10 mM $CaCl_2$ and made isotonic with NaCl. Zeta potential and size measurements were obtained using the Malvern Nanosizer. All samples were run in triplicate.

3.3.10 Carboxyfluorescein (CF) release from DMAQ and DMPC vesicles

The carboxyfluorescein encapsulating protocol was adapted from Weinstein *et al.*[8] 10 μmol lipid film was rehydrated in 10 mM Tris, 100 mM carboxyfluorescein (CF), pH 7.4 to a final concentration of 20 mM lipid. Each sample was heated at 80 °C for 10 minutes and subsequently sonicated at 80 °C for 10 minutes. Liposomes were then extruded 13 times through a 100 nm polycarbonate membrane. Free CF was removed by size exclusion chromatography with a PD-10 sephadex column. Two concentrations of liposomes (5 or 20 μL) were incubated in 200 μL of 105 mM NaCl, 10 mM HEPES pH 7.4 with or without 30% (v/v) fetal bovine serum, .02% sodium azide at 37 °C for one week. Leakage was measured with a FLUOstar plate reader with excitation at 485 nm and emission at 518 nm. Percent leakage values were obtained by normalization to the fluorescence of the samples after lysis of liposomes using 0.5% $C_{12}E_{10}$. Leakage measurements were run in triplicate.

3.3.11 Differential scanning calorimetry (DSC)

DSC experiments were based upon a protocol described in [9] DSC was performed with three reusable Hastelloy sample ampoules and a reference ampoule. Data were collected over a range of 5-90 °C at 1°C/min with the relevant buffer as the reference. The CpCalc 2.1 software package was used to convert the raw data into a molar heat capacity. The data was then exported and plotted in Matlab. Liposomes for DSC measurements were prepared as outlined above and loaded into the ampule using a glass syringe (250 μL per sample). Samples were scanned through a heat-cool-heat cycle and data was collected from the second heating cycle.

3.3.12 Cell viability assay

C26 murine colon carcinoma cells were seeded at 10^4 cells per well in 100 μL media in a cell culture treated 96-well plate (Costar). After 24 hours, liposomes were added in 100 μL at varying concentrations. Two lipid formulations with similar transition temperatures were investigated: DPAQ liposomes: DPAQ:Cholesterol:DPPG (60:40:5 mol ratio) and DSPC liposomes: DSPC:Cholesterol:DSPG (60:40:5: mol ratio). Cells were incubated with liposomes for 72 hours. Cells were washed with Dulbecco's phosphate-buffered saline (PBS) without calcium and magnesium and fresh media was added. Ten μL of 12 mM (3-(4,5-Dimethylthiazol-2-yl)-2,5-diphenyltetrazolium bromide (MTT) was added to each well and cells were incubated for 4 hours at 37 °C. All but 25 μL of the media was removed and 50 μL of DMSO was added to each well. After a 10-minute incubation at 37 °C, absorbance was read at 540 nm using a OptiMax Microplate Reader from Molecular Devices (Sunnyvale, CA).

3.3.13 Liposome distribution and pharmacokinetics in vivo

All animal experiments were performed in compliance with the NIH guidelines for animal research under a protocol approved by the Committee on Animal Research at the University of California, San Francisco. Thirty μmol of total lipid was rehydrated in HEPES buffered saline. For liposome stability and liposome fluorescence, 1,2-dipalmitoyl-*sn*-glycero-3-phospho-(1'-*rac*-glycerol) (DPPG) and 1,1'-dioctadecyl-3,3,3',3'-tetramethylindodicarbocyanine (DiD) were incorporated in liposome formulations, respectively. Two lipid formulations with similar transition temperatures were investigated: DPAQ liposomes: DPAQ:Cholesterol:DPPG:DiD (60:40:5:0.2 mol ratio) and DSPC

liposomes: DSPC:Cholesterol:DSPG:DiD (60:40:5:0.2 mol ratio). Lipid formulations with cholesterol showed no transition temperature. To prepare liposomes, the lipids were sonicated at 80 °C for 20 minutes and extruded 9-15 times through 100 nm polycarbonate membranes. Samples were then dialyzed overnight against Hepes buffered saline (10 mM Hepes, 50 mM NaCl) and filtered through a 200-micron membrane. Two hundred μL of each liposome preparation was injected into the tail vain of BALB/C mice tumored with C26 murine carcinoma cells. Relative lipid concentrations were measured using the DiD signal. The mice were divided into two cohorts. Cohort 1 (n=3 mice per formulation) was bled at 10 minutes, 30 minutes, and 300 minutes post injection. Cohort 2 (n=3 mice per formulation) was bled at 90 minutes, 24 hours and 48 hours post injection. Both cohorts were sacrificed after the last bleeding. Standard DiD curves were constructed for the relevant organs and the plasma by spiking known quantities of DiD into organ and plasma samples. DiD concentration was then measured according to these curves. In order to calculate pharmacokinetic parameters, data was fit to a two-compartment model using MATLAB.

3.4 Results

3.4.1 AQ lipid synthesis

A straightforward three-step synthetic route was employed to synthesize the AQ lipids (Scheme 3.1). The starting compound, 3-(dimethylamino)-1,2-propanediol (2), was linked to myristic acid (C_{14}), palmitic acid (C_{16}), or stearic acid (C_{18}) by DCC coupling (i). After purification via HPFC, the disubstituted product (3a-c) was obtained in high yield (70-80%). Next, the amine was quaternized by S_N2 addition of tert-butyl bromoacetate (4a-c, ii). Finally, the carboxylic acid was deprotected under acidic conditions to give the final product (1a-c, iii). Column purification was not necessary after the second or third step, as the

quaternized compounds readily precipitated out of dichloromethane (DCM). The yields for the last two synthetic steps were effectively quantitative and the overall yield for the synthesis was 50-70% from starting material. The lipids were named using the following acronym: Di-Myristoyl/Palmitoyl/Stearoyl Acetate Quaternized-amine (DMAQ, DPAQ, and DSAQ respectively) (Figure 1A). Lipid products were confirmed by MALDI-TOF mass spectrometry, ^{1}H NMR, ^{13}C NMR and C, H, N elemental analysis (Supplementary Figures 3.1-3.6).

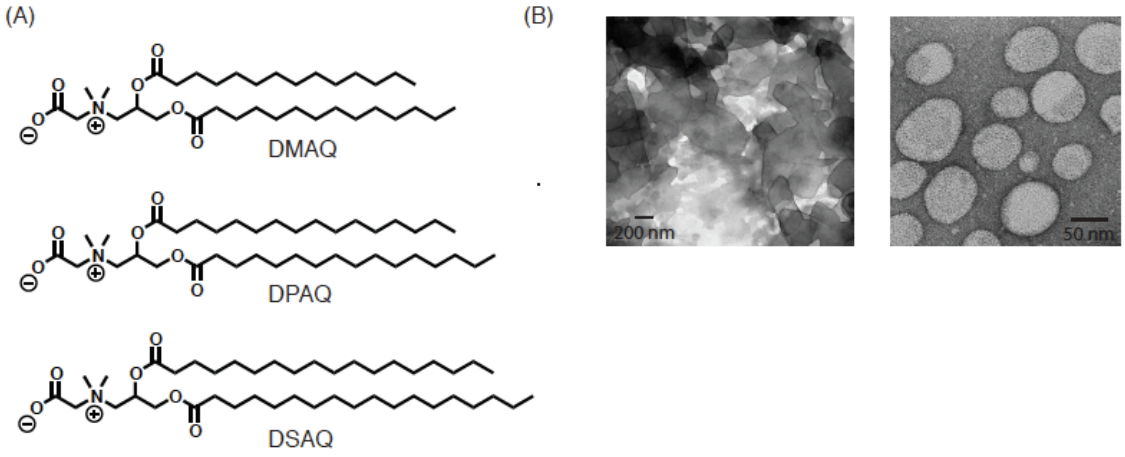

(C)

	Diameter (nm)	Polydispersity Index	Zeta potential (mV)	Standard deviation (mV)
DMAQ:Cholesterol	56.6	0.21	0.773	7.69
DPAQ:Cholesterol	64.8	0.27	-2.39	4.21
DSAQ:Cholesterol	120.0	0.30	-1.97	8.05

Figure 3.1: AQ lipid structure and vesicle formation. (A) The structures of the synthesized AQ lipids are shown. (B) TEM images of (right) DMAQ lipids after heating and sonication and (left) of DPAQ:Chol liposomes. (C) Size and zeta potential measurements for AQ:Chol liposomes. Formulations composed of 60% AQ lipids and 40% cholesterol form stable vesicles with neutral zeta potential.

3.4.2 Vesicle formation and characterization

The ability of AQ lipids to form superstructures was investigated. Single component AQ lipid formulations formed large aggregated vesicles and planar lipid bilayer sheets after

heating and sonication as visualized by negative stain transmission electron microscopy (TEM) (Figure 3.1B, left). Directly after sonication, optically clear suspensions were observed. After 5 minutes at room temperature, these dispersions reorganized into viscous hydrogels or large lipid aggregates. These formulations did not form stable vesicles regardless of saturated chain length or the pH and salt concentration of the hydration buffer. However, addition of 40 mole percent cholesterol to AQ composition allowed for the formation of vesicles. Small diameter uniform vesicular-like structures are observed by TEM (Figure 3.1B, right). The TEM images corroborated the size distribution data obtained by dynamic light scattering (DLS) (Figure 3.1C). DMAQ formulations including more than 50% molar DPPC formed vesicles at a temperature above the phase transition temperature. However, when the temperature was reduced below the Tm of DMAQ, the vesicles aggregated and their contents released (data not shown).

3.4.3 Anions bind to DMAQ liposomes according to the Hofmeister series

Zwitterionic sulfobetaine liposomes[7] bind to anions in aqueous solutions to a greater extent than do phosphatidylcholines. To investigate if this binding preference is a general phenomenon associated with the inverted headgroup, we measured the zeta potential of DMAQ:Chol liposomes in the presence of various anions and compared it to the zeta potential of DMPC:Chol liposomes measured under the same conditions. DMAQ:Chol liposomes demonstrate more negative zeta potentials than DMPC:Chol liposomes for each anion investigated (Figure 3.2A). This result indicates that anions bind DMAQ:Chol liposomes more effectively than DMPC:Chol liposomes. DMAQ:Chol liposomes sequester anions with high polarizability (ClO_4^-, I^-) more than those with low polarizability (Cl^-) (Figure 3.2A), and this preference parallels the Hofmeister series.[10] Fluoride, which is less

polarizable than Cl^- in the Hofmeister series, demonstrated similar interactions with AQ:Chol liposomes as did Cl^-. DMPC:Chol liposomes also bind ions according to the Hofmeister series; however, the magnitude of the change in zeta potential is reduced as compared to DMAQ:Chol liposomes (Figure 3.2A).

3.4.4 Interaction of calcium with AQ liposomes

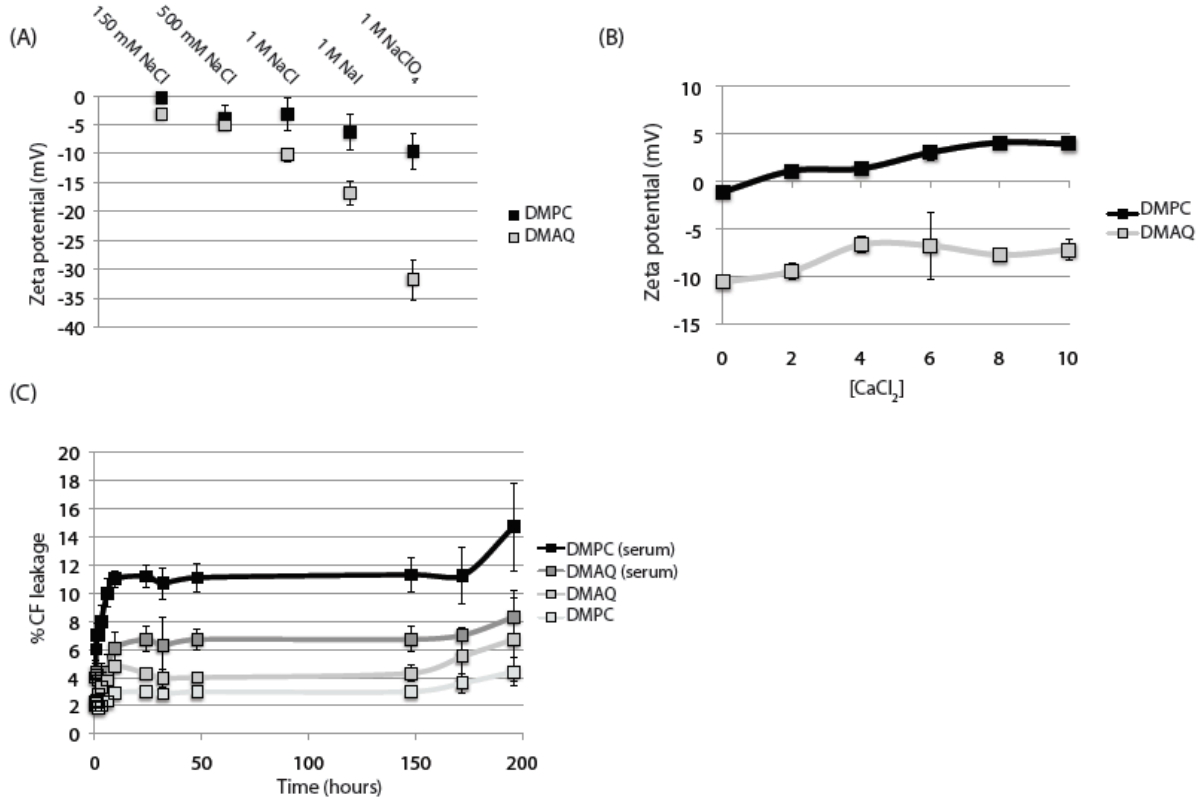

Figure 3.2: Ionic interactions and stability of AQ vesicles. (A) Zeta potential measurements of anionic interactions of DMPC:Chol and DMAQ:Chol vesicles. Anions with low charge density decrease the zeta potential more than those with a high charge density. (B) Calcium interactions of DMAQ:Chol and DMPC:Chol liposomes. Both formulations become increasingly positive in the presence of increasing [Ca2+]. DMAQ:Chol vesicles remain negatively charged at 10 mM [Ca2+] while DMPC:Chol liposomes adopt a positive charge. (C) DMAQ:Chol vesicles show comparable stability to DMPC:Chol vesicles at 37◦C in 30% serum over one week. For (A)–(C), samples were run in triplicate and error bars represent ± standard deviation.

We investigated the interaction of calcium with the DMAQ:Chol and DMPC:Chol liposome compositions using the zeta potential as a surrogate for direct calcium binding (Figure 3.2B). The surface potential of the DMPC:Chol vesicles becomes more positive as

the Ca^{2+} concentration increases. While the zeta potential for the DMAQ:Chol vesicles increases along with Ca^{2+} concentration, the rate of change is less than observed in DMPC:Chol vesicles and the surface potential remains negative at 10 mM [Ca^{2+}] (Figure 3.2B). Conversely, DMPC:Chol vesicles adopt a positive charge at 10mM [Ca^{2+}].

In vivo, divalent cations are known to interact with lipid headgroups to induce aggregation and fusion of vesicles.[11] As such, we measured the impact of increasing Ca^{2+} concentrations on the aggregation of DMAQ:Chol and DMPC:Chol vesicles. In the presence of 10 mM Ca^{2+} neither formulation showed aggregation (data not shown). .

3.4.5 Permeability of AQ liposome to an encapsulated water-soluble anion

The charge at the membrane interface is believed to influence the permeation of charged molecules through the membrane.[12] Naturally occurring phospholipids have an anionic phosphate group positioned at the membrane interface, while the AQ lipids have a cationic group adjacent to the interface. To better understand the role of this inverted orientation on the permeability of the membrane to water soluble compounds, we measured the leakage rate of carboxyfluorescein (CF), a water soluble anion, from DMAQ:Chol and DMPC:Chol liposomes (Figure 3.2C).[8] In the absence of serum both DMPC:Chol and DMAQ:Chol liposomes showed minimal leakage of CF at 37 °C. In the presence of serum, DMPC:Chol liposomes exhibited slightly more leakage than did the DMAQ:Chol vesicle compositions.

3.4.6 Phase transition temperatures of lipid dispersions prepared from AQ lipids

The phase transition temperature of a lipid formulation can lend insight into the intermolecular forces governing lipid headgroup and hydrophobic domain interactions. The phase transition temperatures for DMAQ, DPAQ, and DSAQ lipids were investigated by differential scanning calorimetry; all three lipids demonstrated transition temperatures significantly greater than analogous di-substituted saturated chain PC lipids but similar to analogous PE lipids (Figure 3.3A).

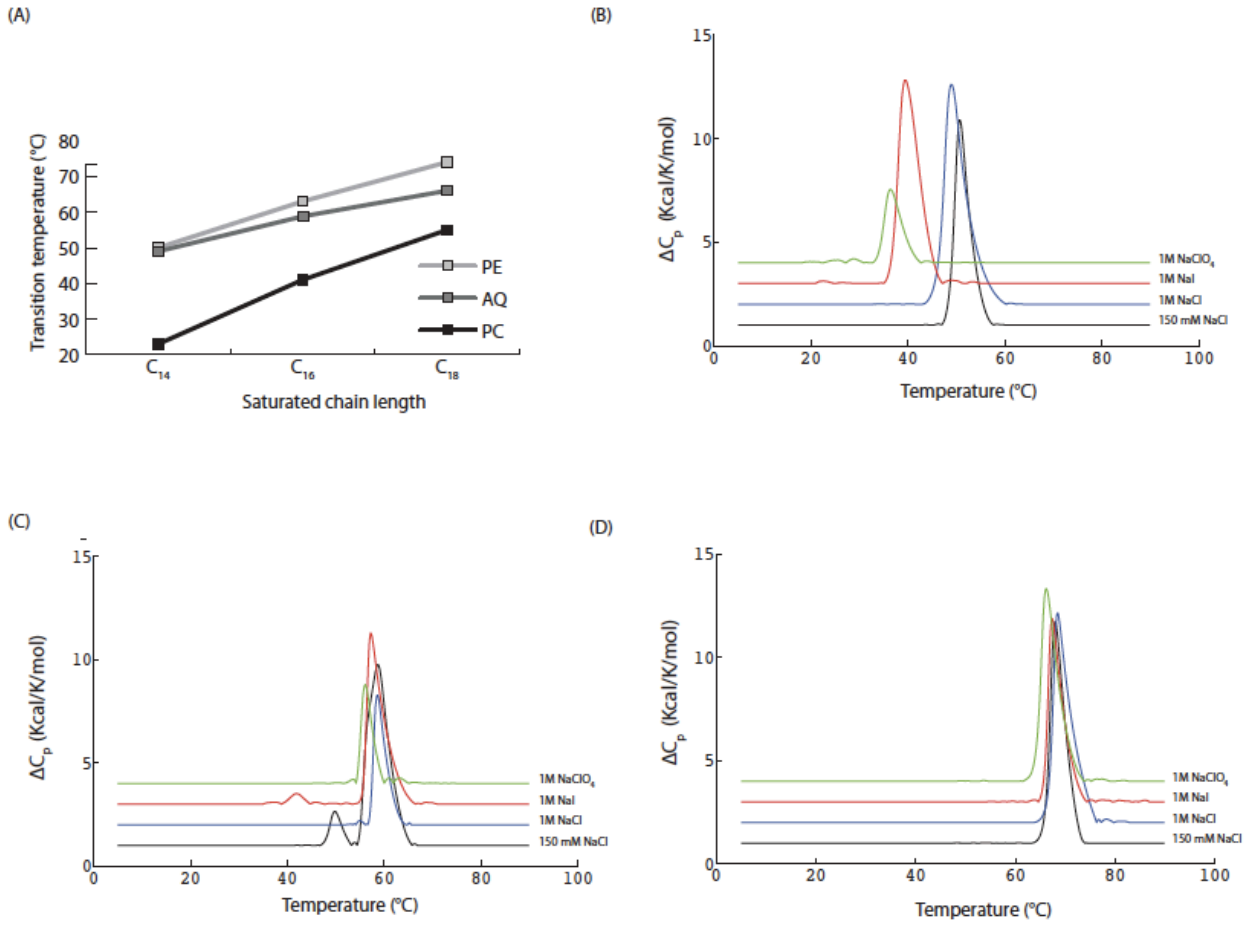

Figure 3.3: AQ lipids show elevated transition temperatures. (A) AQ transition temperatures are plotted alongside those for PC and PE lipids. (DMAQ Tm = 48.8 °C, DPAQ Tm = 58.3 °C, DSAQ Tm = 65.5 °C). (B)–(D) Thermograms of DMAQ, DPAQ, and DSAQ lipid dispersions in various salts.

In the presence of anions with low charge density (ClO_4^-, I^-), DMAQ lipids exhibited a downward shift in transition temperature (Figure 3.3B). A shift in the Tm was not observed in the presence of large cations, such as tert-butyl ammonium or in the presence of F^- (data not shown). DPAQ and DSAQ lipids exhibit no such shift in transition temperatures in the presence of various anions (Figure 3C, 3D). DPAQ lipids exhibit a pre-transition at low salt concentrations that is eliminated at increased ionic strength (Figure 3.3C).

3.4.7 in vitro cytotoxicity of liposomes composed of AQ lipids

To determine if the AQ lipids are tolerated when applied to cells in culture, we compared the viability of C26 colon carcinoma cells exposed to DPAQ:Chol or DSPC:Chol liposomes using an MTT assay. At concentrations that are commonly used in vitro or obtained after in vivo administration, both formulations were well tolerated by cells and demonstrated little toxicity (Figure 3.4A). At millimolar concentrations, the DPAQ liposomes showed a two fold greater reduction in cell viability in culture than did the DSPC liposomes

3.4.8 in vivo properties of AQ lipids

After confirming the *in vitro* stability of liposomes prepared from the AQ lipids and the low *in vitro* cytotoxicity, we investigated their biodistribution and pharmacokinetic parameters in BALB/C mice tumored with C26 murine colon carcinoma cells. To measure the *in vivo* distribution of AQ liposomes we incorporated 1,1'-dioctadecyl-3,3,3',3'-tetramethylindodicarbocyanine (DiD) into the lipid composition as a fluorescent lipid marker. Two lipid formulations were compared: DSPC:Chol:DSPG:DiD (60:40:5:0.2 mol ratio) and DPAQ:Chol:DPPG:DiD (60:40:5:0.2 mol ratio). Small diameter vesicles were prepared form

both lipid compositions (DPAQ: 87 nm, DSPC: 78 nm). It is worth noting that neither formulation contained poly(ethylene glycol)-DSPE. The pharmacokinetic data indicates that the DPAQ liposomes demonstrate an extensive alpha phase and a terminal half-life of 9.5 hours (Figure 3.4B, D). The DSPC have a shorter distribution phase and a terminal half-life of 12.7 hours. Both formulations accumulate in the liver and spleen, with the AQ composition having a greater uptake into the liver and spleen at 48 hours post-administration than the DSPC liposomes (Figure 3.4C). Liposome uptake into the tumor was greater for the DSPC liposome composition than for the AQ composition (Figure 3.4C).

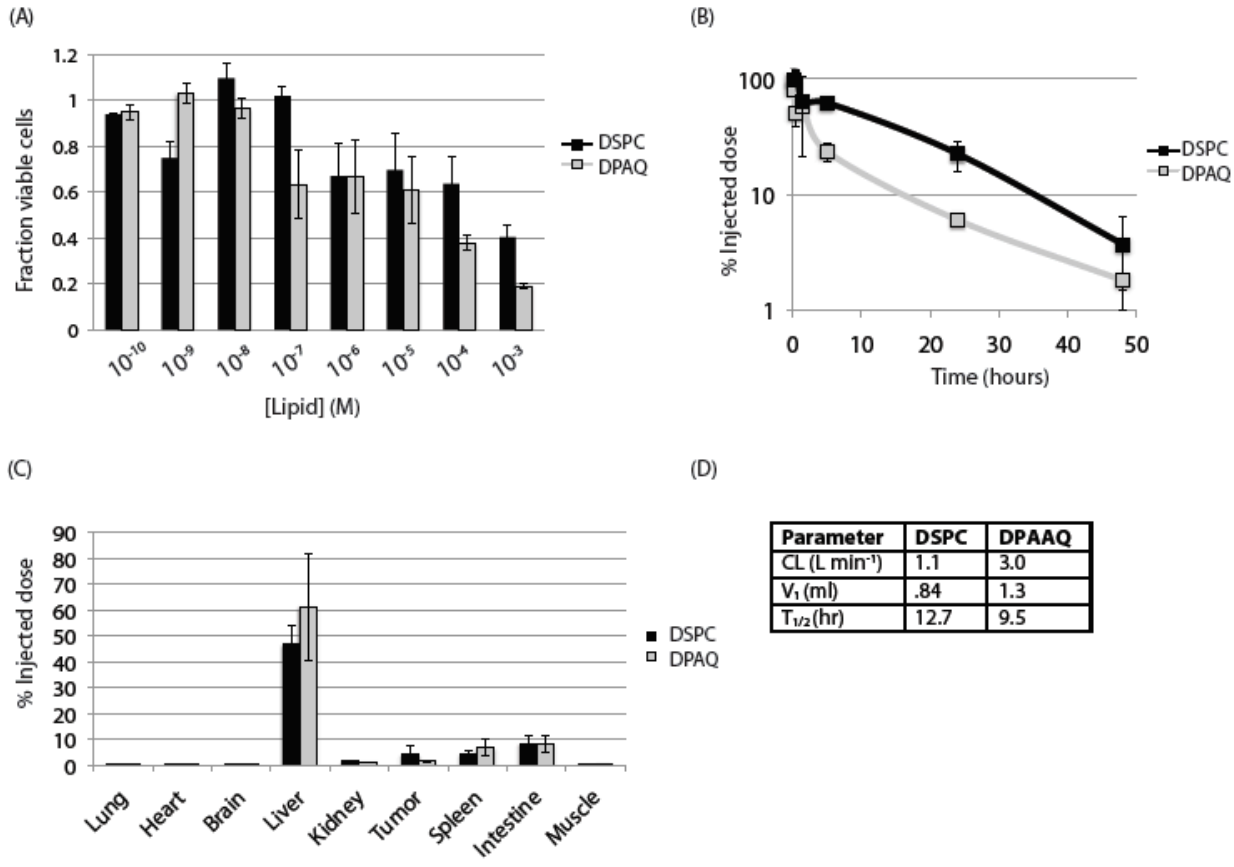

Parameter	DSPC	DPAAQ
CL (L min^{-1})	1.1	3.0
V_1 (ml)	.84	1.3
$T_{1/2}$(hr)	12.7	9.5

Figure 3.4: Cytotoxicity, pharmacokinetics and biodistribution of AQ lipid vesicles. (A) Viability of C26 colon carcinoma cells in the presence of DPAQ:Chol or DSPC:Chol liposomes. Samples were run in triplicate. Error bar represent ± standard error of the mean. (B) Pharmacokinetics and (C) biodistribution of DPAQ and DSPC liposomes. Experiments were run with n = 3 mice per group. (D) Pharmacokinetic parameters of DPAQ and DSPC liposomes. Error bars represent ± standard deviation.

3.5 Discussion

We describe the synthesis of a new class of inverse-zwitterionic lipids with betaine-like headgroups. These lipids form vesicles in formulations that contain cholesterol and interact with anions with a greater affinity than do liposomes prepared from naturally occurring PC lipids.

In the absence of cholesterol, AQ lipids form a turbid dipersion of lipid aggregates. TEM reveals that these formulations form structures resembling planar bilayer sheets. AQ:Chol formulations form a clear solution of small lipid vesicles. Cholesterol will act as a spacer between adjacent AQ lipids and may interfere with extra static interactions between adjacent AQ lipids. It may also allow for a greater membrane curvature necessary to transition from a planar bilayer to spherical vesicles.

Anion binding to AQ lipid vesicles parallels the Hofmeister series, with low charge density anions binding more favorably than those with a high density. The Hofmeister series is a classification of ions according to their ability to salt in or salt out proteins. Ions with high charge densities (F^-,Cl^-) are strongly hydrated. Conversely, ions with a low charge densities (I^-,ClO_4^-) are weakly hydrated. Large anions with low charge density penetrate further into the bilayer of PC liposomes than do small anions.[13] The anion concentration dictates the zeta potential of AQ liposomes according to the Hofmeister series. This result corroborates previous studies that demonstrate that zwitterionic diacyl lipids[7,14] with the cationic group at the membrane interface and zwitterionic micelles with a cationic group proximal to the micelle interface bind anions according to the Hofmeister series.[15] We

hypothesize that the location of the quaternary amine at the bilayer interface is responsible for this behavior.

AQ lipids prepared with cholesterol can stably encapsulate the water-soluble dye carboxyfluorescein. The influence of the headgroup charge orientation on the permeability of the bilayer to charged water-soluble molecules and ions has been the subject of considerable investigation. Recent computational studies suggest that the anchoring of the phosphate at the hydrophobic bilayer interface promotes the partitioning of cations into and out of bilayers.[12] Perttu and coworkers have found that carboxyfluorescein release from sulfobetaine inverse lipids was slow and similar in magnitude to the CF release observed from PC liposomes.[7] Conversely, carboxyfluorescein leakage was significantly faster from liposomes prepared from inverse choline phosphate lipids than from liposomes prepared from analogous PC lipids.[14] The AQ lipids behave similarly to the sulfobetaine lipids with regard to CF leakage. However, considerably more permeability studies across a range of charged substances are required to resolve the influence of headgroup charge orientation on charged solute permeability.

The AQ lipids demonstrate transition temperatures between those of PC and PE lipids with similar saturated chain lengths. The transition temperature profiles of the DMAQ and DPAQ lipids are also affected by anion charge density and concentration (Figure 3B,C). DMAQ lipids exhibit a downward shift in transition temperature in the presence of 1 M ClO_4^- or I^-. We hypothesize that these anions intercalate into the interfacial region of bilayer and disrupt lipid packing, which leads to decreased transition temperatures. The bilayer packing disruption may be relatively more pronounced for DMAQ than for DPAQ or DSAQ lipids because of its shorter acyl chains. Alternatively, the anion binding may disrupt

hydrogen bonding or electrostatic interactions among adjacent lipids. It is thought that PE lipids show greater transition temperatures than PC lipids with matching hydrophobic tails because of the hydrogen-bonding capabilities of PE headgroups.[16] As such, the increased Tm of AQ lipids may be due to an altered headgroup conformation that reduces surface area and increases headgroup packing as compared to PC lipids.

While lipid dispersion prepared from DPAQ lipids do not exhibit a drop in transition temperature in the presence of the polarizable anions, they do exhibit a dampening of the pre-transition with increasing anion polarizability. Generally, PC lipids demonstrate pre-transitions while PE lipids do not. The pre-transition indicates a subtle change in lipid packing conformation. It is not observed in high radius of curvature PC vesicles and can be eliminated by small amounts of lipid impurities such as fatty acids.[17] In the presence of large anions, the DPAQ lipids may adopt a packing configuration similar to PE lipids. This change in packing conformation may be driven by a change in the hydration state of DPAQ lipids in the presence of highly polarizable anions.

The AQ:Chol liposomes demonstrate similar cytotoxicity and biodistribution profiles to PC:Chol liposomes. Both formulations distribute to the liver, spleen and intestine *in vivo*. Although the two compositions have a similar beta phase, the larger alpha phase of the AQ liposomes (Figure 4B**)** requires further investigation. It may indicate that there is a dose dependent interaction of AQ liposomes with blood components when injected into animals.

The altered biophysical properties of AQ liposomes compared to PC liposomes provide a new tool for exploring the role of charge orientations at membrane interfaces on ion trafficking across the bilayer. AQ lipid membranes may also provide insight into function

of charge orientation in regulating interaction soluble protein binding and membrane protein function. Finally, the AQ lipids may have useful properties for preparing liposome-based drug carriers to treat cancer and infectious diseases.

3.6 Supplemental Information

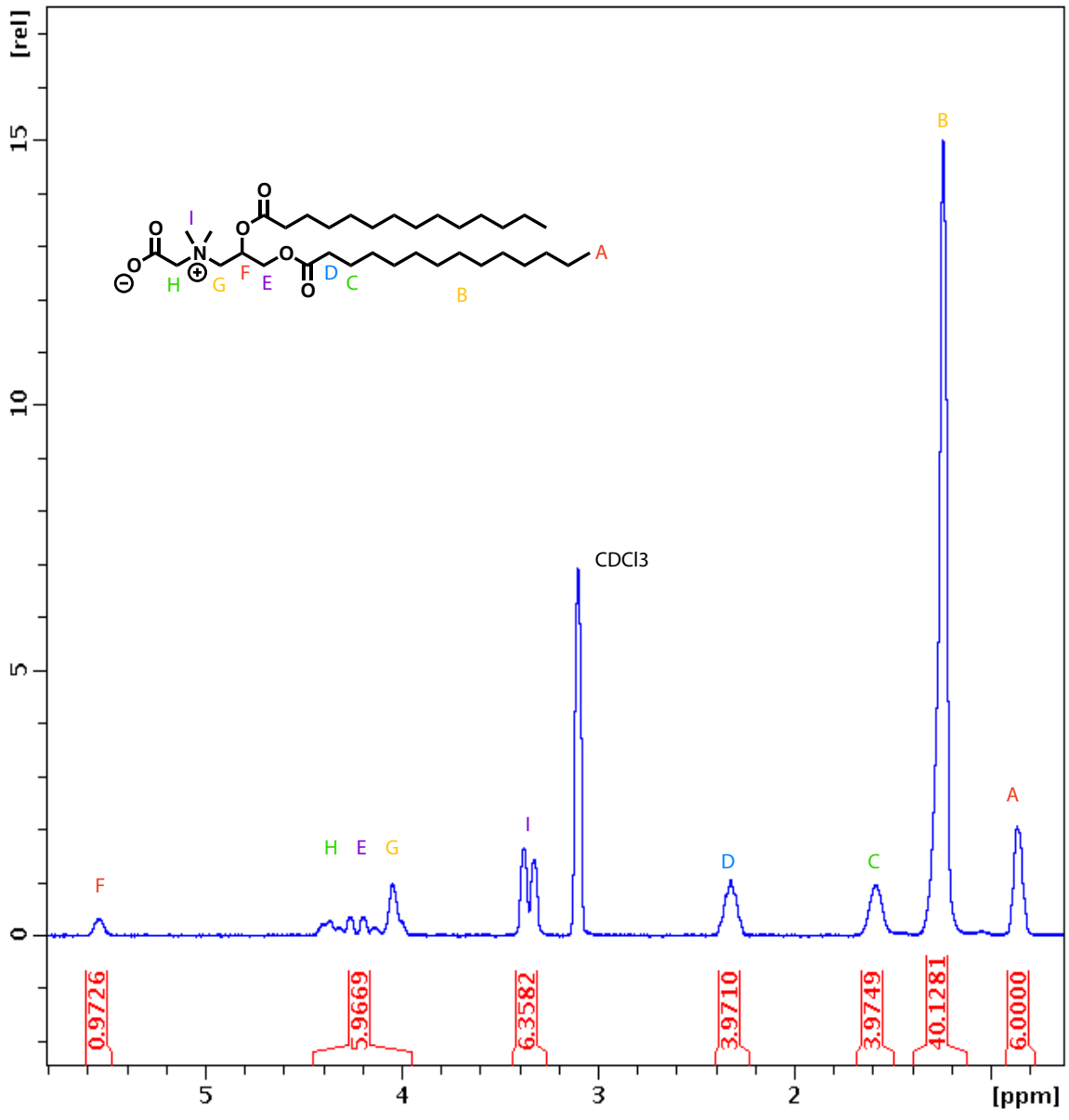

Supplementary Figure 3.1: ^{1}H NMR spectra of DMAQ in CDCl3.

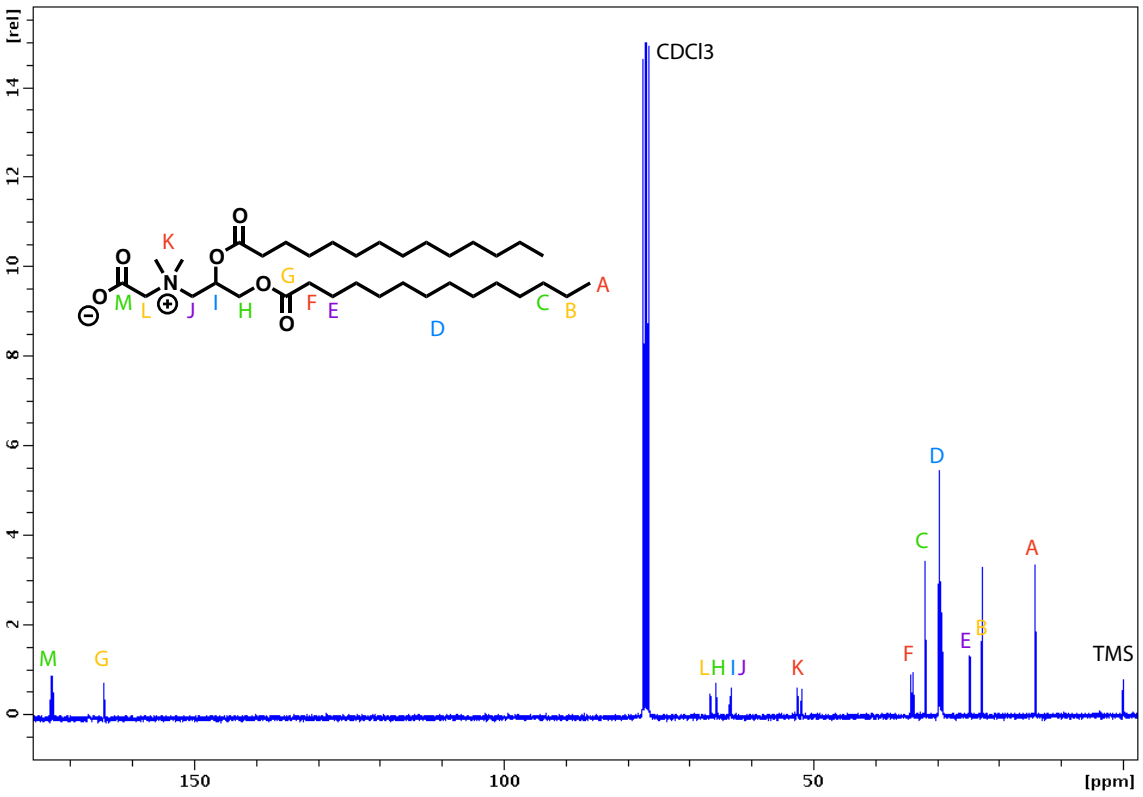

Supplementary Figure 3.2: ^{13}C NMR spectra of DMAQ in CDCl3.

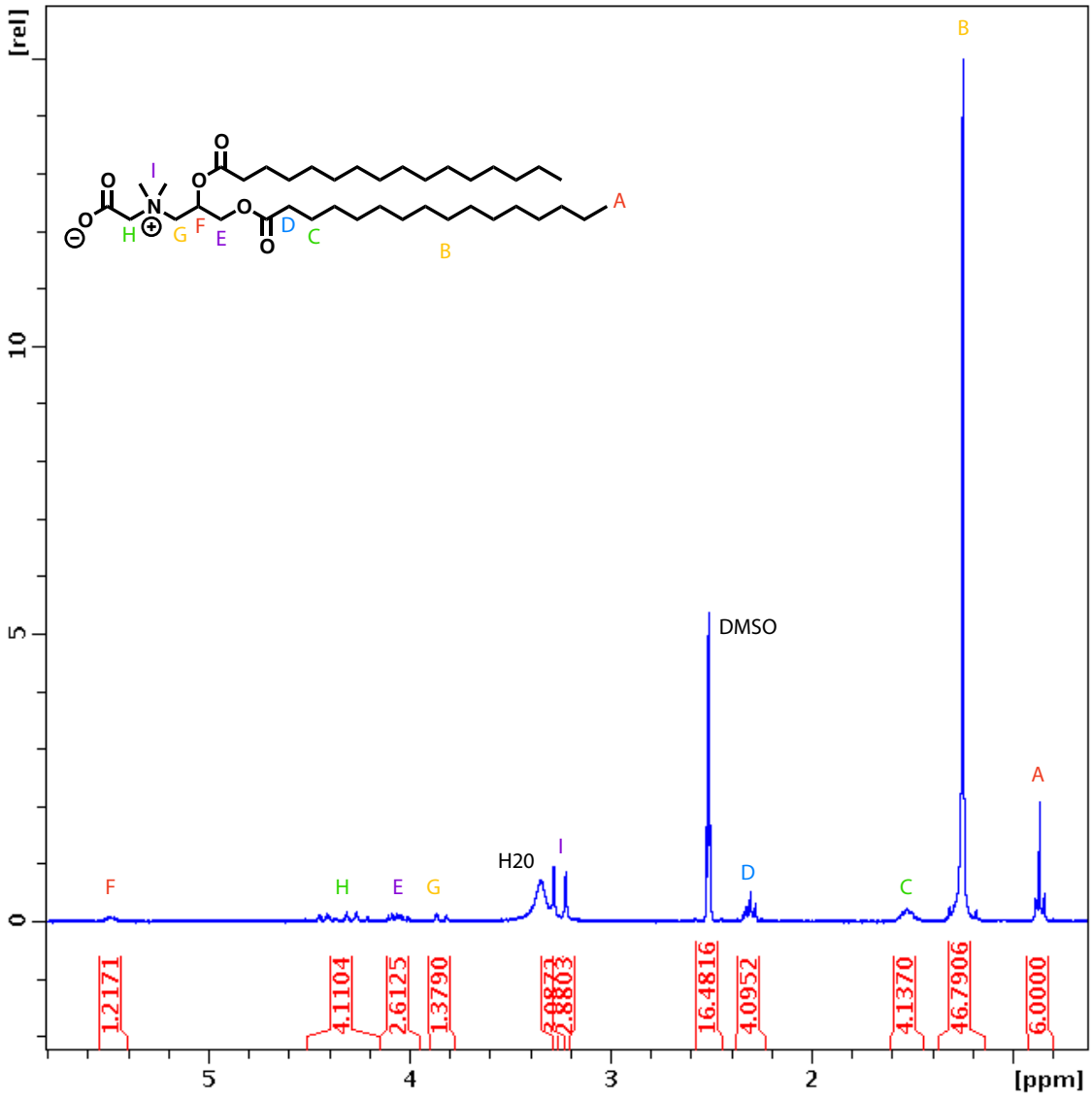

Supplementary Figure 3.3: ^{1}H NMR spectra of DPAQ in DMSO.

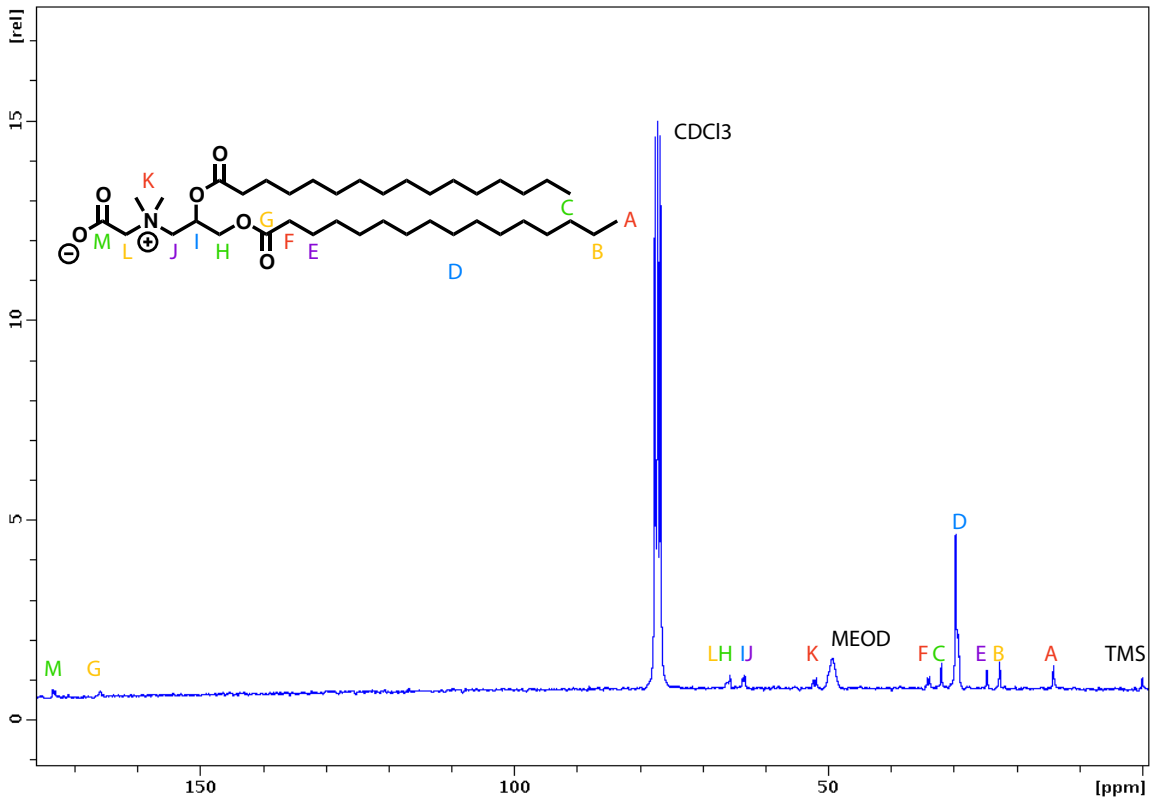

Supplementary Figure 3.4: ^{13}C NMR spectra of DPAQ in CDCl3.

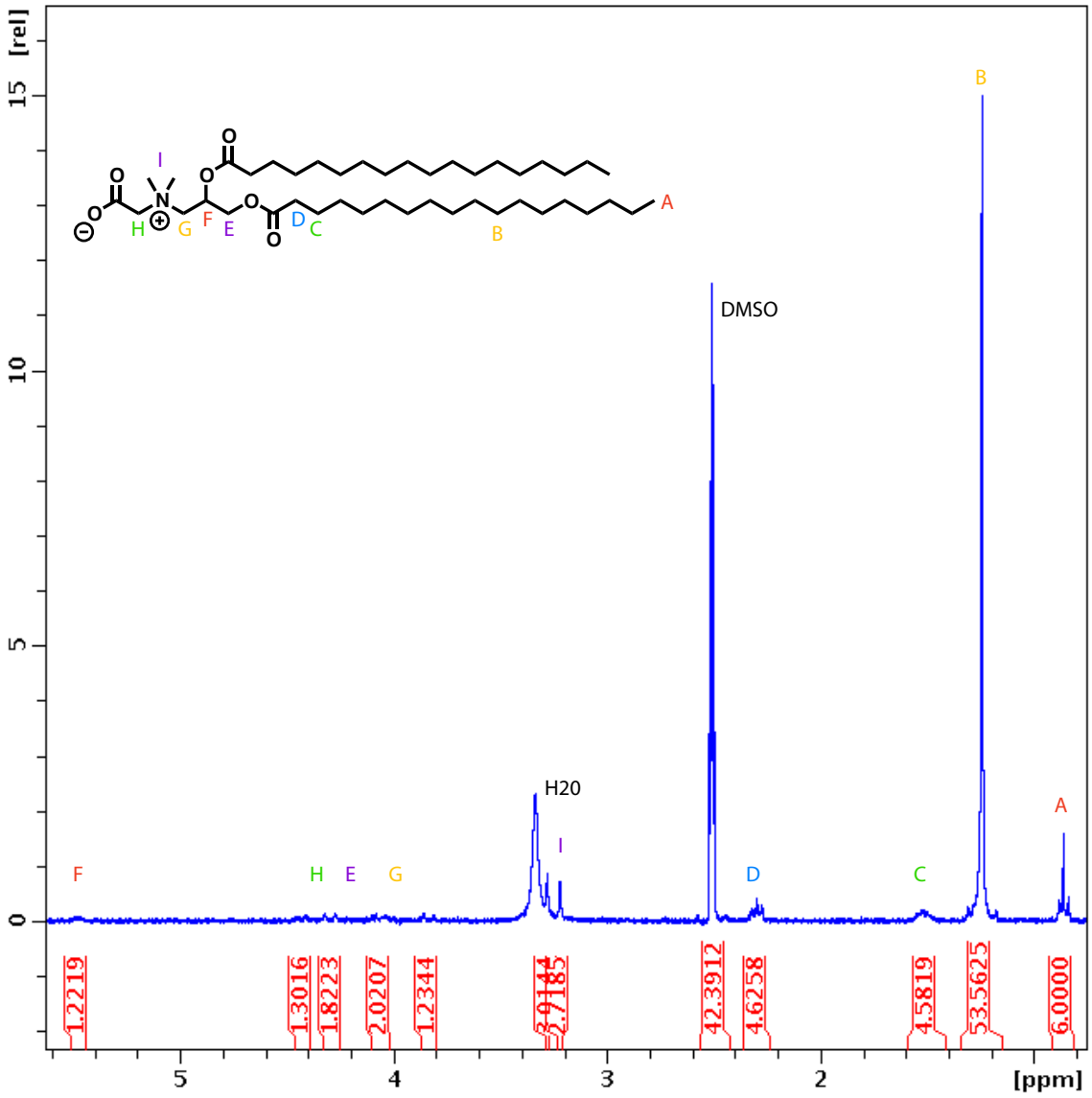

Supplementary Figure 3.5: ^{1}H NMR spectra of DSAQ in DMSO.

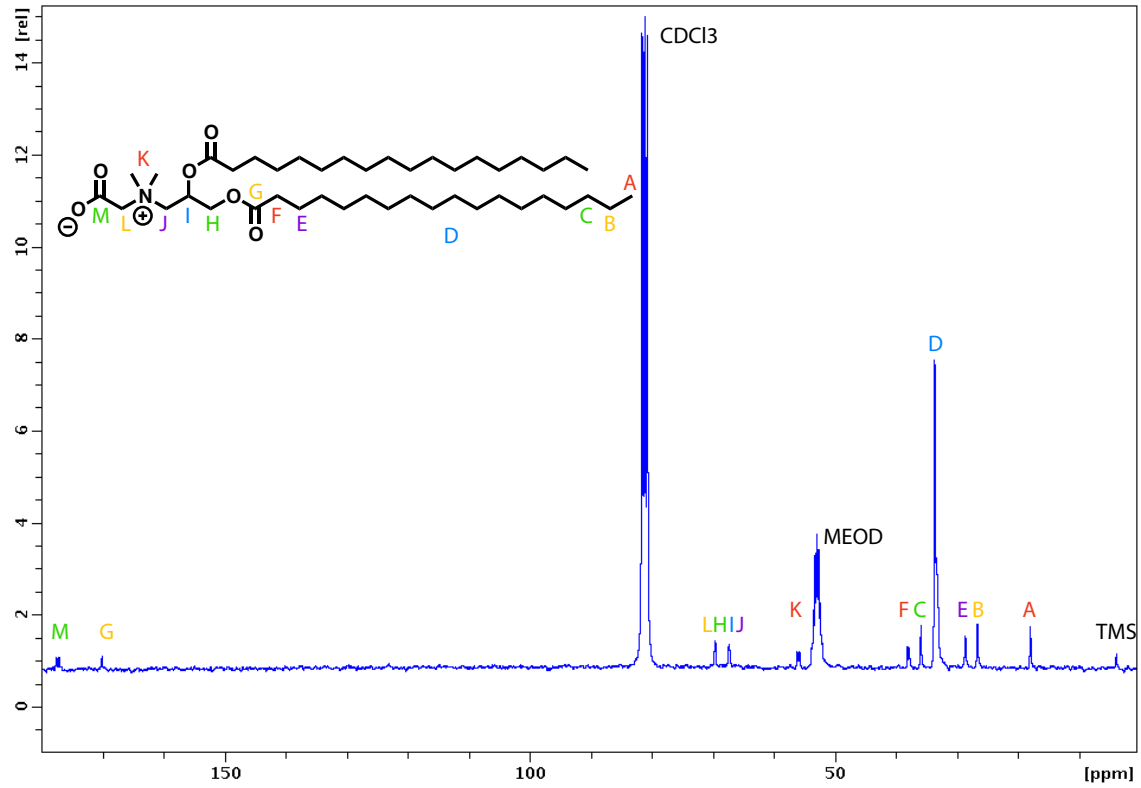

Supplementary Figure 3.6: ^{13}C NMR spectra of DSAQ in CDCl3.

3.7 References

1. Langner, M. & Kubica, K. The electrostatics of lipid surfaces. *Chemistry and Physics of Lipids* **101**, 3–35 (1999).
2. Chemin, C. *et al.* Consequences of ions and pH on the supramolecular organization of sphingomyelin and sphingomyelin/cholesterol bilayers. *Chemistry and Physics of Lipids* **153**, 119–129 (2008).
3. Marte, L. *et al.* Specific anion binding to sulfobetaine micelles and kinetics of nucleophilic reactions. *The journal of physical chemistry B* **111**, 9762–9769 (2007).
4. Tondo, D. W. *et al.* Synthesis of a new zwitterionic surfactant containing an imidazolium ring. Evaluating the chameleon-like behavior of zwitterionic micelles. *Langmuir : the ACS journal of surfaces and colloids* **26**, 15754–15760 (2010).
5. Kamenka, N. & Chevalier, Y. Aqueous solutions of zwitterionic surfactants with varying carbon number of the intercharge group. 1. Micelle aggregation numbers. *Langmuir : the ACS journal of surfaces and colloids* (1995).at <http://pubs.acs.org/doi/abs/10.1021/la00009a015>
6. Minnes, R., Ytzhak, S., Weitman, H. & Ehrenberg, B. The effect of solution electrolytes on the uptake of photosensitizers by liposomal membranes: a salting-out effect. *Chemistry and Physics of Lipids* **155**, 38–42 (2008).
7. Perttu, E. K. & Szoka, F. C. Zwitterionic sulfobetaine lipids that form vesicles with

salt-dependent thermotropic properties. *Chemical Communications* **47**, 12613–12615 (2011).
8. Weinstein, J., Yoshikami, S., Henkart, P., Blumenthal, R. & Hagins, W. Liposome-cell interaction: transfer and intracellular release of a trapped fluorescent marker. *Science* **195**, 489–492 (1977).
9. Huang, Z. & Szoka, F. C., Jr Sterol-Modified Phospholipids: Cholesterol and Phospholipid Chimeras with Improved Biomembrane Properties. *J. Am. Chem. Soc* (2008).doi:10.1021/ja8065557
10. Zhang, Y. & Cremer, P. S. Interactions between macromolecules and ions: The Hofmeister series. *Current opinion in chemical biology* **10**, 658–663 (2006).
11. Needham, D., Anyarambhatla, G., Kong, G. & Dewhirst, M. W. A new temperature-sensitive liposome for use with mild hyperthermia: characterization and testing in a human tumor xenograft model. *Cancer Research* **60**, 1197–1201 (2000).
12. Khavrutskii, I. V., Gorfe, A. A., Lu, B. & McCammon, J. A. Free energy for the permeation of Na(+) and Cl(-) ions and their ion-pair through a zwitterionic dimyristoyl phosphatidylcholine lipid bilayer by umbrella integration with harmonic fourier beads. *Journal of the American Chemical Society* **131**, 1706–1716 (2009).
13. Sachs, J. N. & Woolf, T. B. Understanding the Hofmeister effect in interactions between chaotropic anions and lipid bilayers: molecular dynamics simulations. *Journal of the American Chemical Society* **125**, 8742–8743 (2003).
14. Perttu, E. K., Kohli, A. G. & Szoka, F. C. Inverse-phosphocholine lipids: a remix of a common phospholipid. *Journal of the American Chemical Society* **134**, 4485–4488 (2012).
15. Priebe, J. P. *et al.* The chameleon-like nature of zwitterionic micelles: the intrinsic relationship of anion and cation binding in sulfobetaine micelles. *The journal of physical chemistry B* **112**, 14373–14378 (2008).
16. Mabrey, S. & Sturtevant, J. M. Incorporation of saturated fatty acids into phosphatidylcholine bilayers. *Biochim Biophys Acta* **486**, 444–450 (1977).
17. Knight, C. G. *Liposomes, from physical structure to therapeutic applications*. 497 (Elsevier-North-Holland Biomedical Press: 1981).

Chapter 4: Synthesis, Characterization and Evaluation of Ionizable Lysine-Based Lipids for siRNA Delivery

4.1 Abstract

We report the synthesis and characterization of a series of ionizable lysine-based lipids (ILL), novel lipids containing a lysine head group linked to a long-chain dialkylamine through an amide linkage at the lysine α-amine. These ILLs contain two ionizable amines and a carboxylate, and exhibit pH-dependent lipid ionization that varies with lipid structure. The synthetic scheme employed allows for the simple, orthagonal manipulation of lipids. This provides a method for the development of a compositionally diverse library with varying ionizable headgroups, tail structures, and linker regions. A focused library of four ILLs was synthesized to determine the impact of hydrophobic fluidity, lipid net charge, and lipid pKa on the biophysical and siRNA transfection characteristics of this new class of lipids. We found that manipulation of lipid structure impacts the protonation behavior, electrostatic driven membrane disruption, and ability to promote siRNA mediated knockdown *in vitro.* ILL-siRNA liposomal formulations were tested in a murine Factor VII model, however no significant siRNA-mediated knockdown was observed. These results indicate that ILL may be useful *in vitro* transfection reagents, however further optimization of this new class of lipids is required to develop an effective *in vivo* siRNA delivery system.

4.2 Introduction

Lipid-based nanoparticles have long been used to deliver biologically active molecules including drugs, DNA, and more recently siRNA *in vivo.*[1,2] Liposomes and lipoplexes alter the pharmacokinetics, biodistribution, and uptake pathways of encapsulated

or associated molecules.[3] Depending on the therapeutic application and drug properties, lipids with specific biophysical characteristics are required to develop an effective delivery system.[4] Due to their anionic charge and large size, siRNA are not able to passively cross cellular membranes to reach their site of action in the cytoplasm.[5,6] Therefore, delivery systems that actively promote cellular internalization and endosomal escape are essential.[7,8] Because of these properties, lipid-based siRNA delivery systems are generally cationic or ionizable to allow for high efficiency siRNA encapsulation and to promote intracellular membrane disruption and endosomal escape.[7,9-16] Recent work on the rational design of amino lipids using structure-activity relationships indicates that fusogenic lipids with pKas in the pH=6.0-7.0 range are promising candidates for siRNA delivery *in vivo*.[7,12] Following internalization, the low-pH environment of the endocytic pathway is believed to ionize these lipids, promoting electrostatic interactions between carrier lipids and naturally occurring anionic membrane lipids. These interactions drive the formation of unstable, non-bilayer structures that lead to membrane disruption and contents delivery to the cytoplasm.[17-19] Formulation of nanoparticles using these ionizable lipids at low-pH allows for efficient siRNA encapsulation, and incorporation of helper lipids including phospholipids, sterols, and PEG-lipids alters the size, surface charge, and stability of these formulations, providing some control over the *in vivo* pharmacokinetic properties of these systems.[20,21]

Despite recent advances in the field, ionizable and cationic systems are still limited by their immunostimulatory effects and poor pharmacokinetics.[14] In contrast to cationic lipids, zwitterionic lipids such as phosphatidylcholine (PC) or phosphatidylethanolamine (PE) show low *in vivo* cytotoxicity and immunogenicity.[22] However, their neutral surface charge and pH-independent biophysical properties limit their ability to efficiently encapsulate and

deliver charged, high molecular weight drugs. Previously, we reported a new class of zwitterionic lipids (ZL) with head groups containing a cationic amine and an anionic carboxylate.[23] These lipids are non-immunogenic and non-toxic, and are capable of encapsulating siRNA at low-pH. However, ionization of these head groups occurs at a pH below that found in the endosomes, limiting the utility of ZL as siRNA delivery systems.[23] Building on this work, we describe the design, synthesis, and characterization of ionizable lysine-based lipids (ILL) containing a lysine head group linked to a long-chain dialkylamine through an amide linkage at the lysine α-amine (Figure 4.1). The resulting lipid structure contains a primary and tertiary amine, as well as a single carboxylate, and the overall net charge of the lipid depends upon the ionization state of each protonatable moiety (Figure 4.2). The general ILL structure maintains a zwitterionic head group at the bilayer interface, potentially reducing immunogenicity compared to other cationic systems. However, the addition of a second ionizable amine in the lipid core is expected to increase ILL pKa into a physiologically relevant range to promote membrane destabilization, endosomal escape, and siRNA delivery to the cytoplasm. We hypothesized that varying the structure of ILL would impact their ionization behavior, membrane interactions, and siRNA transfection both *in vitro* and *in vivo*. A focused library of four ILLs with distinct structures was synthesized to determine the impact of hydrophobic fluidity, lipid net charge, and lipid pKa on the biophysical and transfection characteristics of this new class of lipids.

4.3 Materials and Methods

4.3.1 Materials and Chemicals

1,2-dioleoyl-*sn*-glycero-3-phosphocholine (DOPC), 1,2-distearoyl-*sn*-glycero-3-phosphocholine (DSPC), 1,2-dioleoyl-*sn*-glycero-3-phosphoethanolamine (DOPE), 1,2-dioleoyl-*sn*-glycero-3-(phosphor-1'-*rac*-glycerol) (DOPG), 1,2-dioleoyl-3-trimethylammonium-propane (DOTAP), and cholesterol (Chol) were purchased from Avanti Polar Lipids (Alabaster, AL). 1-(monomethoxypolyethyleneglycol)-2,3-dimyrystoylglycerol (PEG-DMG) was purchased from NOF-Corporation (Tokyo, Japan). DLinDMA was provided by Pfizer (Cambridge, MA). Boc-Lys-OMe HCl was purchased from Combi-Blocks Inc. (San Diego, CA). Linoleic acid was purchased from TCI-America Inc. (Portland, OR). Quant-iT Ribogreen RNA reagent was purchased from Invitrogen (Carlsbad, CA). The Steady-Glo luciferase assay kit was purchased from Promega (Madison, WI). The Aniara Biophen Factor VII assay kit was purchased from Fisher Scientific (Houston, TX). All other reagents were purchased from Sigma-Aldrich (Milwaukee, WI). Solvents were purchased from VWR (Radnor, PA), and used without further purification.

4.3.2 Lipid Synthesis

4.3.2.1 Synthesis of dialkylamine precursors

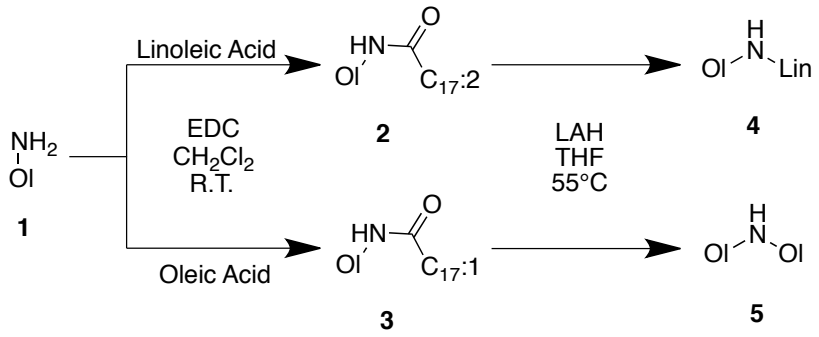

Scheme 4.1: Synthesis of dialkylamine precursors

*Synthesis of **2***

2.3g of linoleic acid (280.45g/mol, 8.2mmol, 1.1eq) and 1.8g 1-Ethyl-3-3-(3-dimethylaminopropyl)carbodiimide (EDC) (155.24g/mol, 11.6mmol, 1.5 eq) were added to 30 mL CH_2Cl_2 and the solution was cooled on ice to 4°C. In a separate vessel, 2g of **1** (oleylamine, 267.49g/mol, 7.48mmol, 1.0 eq) was dissolved in 10 mL CH_2Cl_2. The solution of **1** was then added dropwise over 20 minutes. The reaction was allowed to gradually warm to room temperature while stirring overnight. CH_2Cl_2 was removed by rotary evaporation, and the resulting oil was solubilized in 100mL ethyl acetate (EtOAc) and washed 3x with 20mL 1MHCl and 2x with 20mL brine. The organic layer was then dried over Na_2SO_4 and concentrated to an oil. Further purification was not carried out on this compound. 3.8g (96%). MW calc. ($C_{36}H_{67}NO$) = 529.92 found 530.76. TLC: R_f = 0.7 (99:1 CH_2Cl_2:MeOH).

^{1}H NMR (300 MHz, $CDCl_3$): 5.50-5.30 (m, 6H), 3.30-3.20 (m, 2H), 2.90-2.80 (m, 2H), 2.20-2.10 (m, 2H) 2.10-1.90 (m, 8H), 1.70-1.60 (m, 2H), 1.60-1.50 (m, 2H), 1.40-1.10 (m, 36H), 0.90 (m, 6H).

*Synthesis of **3***

1g of oleic acid (282.46g/mol, 3.5mmol, 1.1 eq) and 0.82g EDC (155.24g/mol, 5.25mmol, 1.5 eq) were added to 20mL CH_2Cl_2, and the solution was cooled on ice to 4°C. In a separate vessel, 0.85g **1** (oleylamine, 267.49g/mol, 3.2mmol, 1.0 eq) was dissolved in 10 mL CH_2Cl_2. The solution of **1** was then added dropwise over 20 minutes. The reaction was allowed to gradually warm to room temperature while stirring overnight. CH_2Cl_2 was removed by rotary evaporation, and the resulting oil was solubilized in 50mL EtOAc and washed 3x with 20mL 1MHCl and 2x with 20mL brine. The organic layer was then dried

over Na_2SO_4 and concentrated to an oil. Further purification was not carried out on this compound. 1.58g (93%). MW calc. ($C_{36}H_{69}NO$) = 531.94 found 532.81. TLC: R_f = 0.7 (99:1 CH_2Cl_2:MeOH).

^{1}H NMR (300 MHz, $CDCl_3$): 5.50-5.30 (m, 4H), 3.30-3.20 (m, 2H), 2.20-2.10 (m,2H), 2.10-1.90 (m, 8H), 1.70-1.60 (m, 2H), 1.60-1.50 (m, 2H), 1.40-1.10 (m, 42H), 0.90 (m, 6H).

*Synthesis of **4***

0.82g of lithium aluminum hydride (LAH) (37.95g/mol, 21.5mmol, 3.0 eq) was suspended in 25mL anhydrous THF and cooled in an ice bath to 4°C. 3.8g of **2** (529.92g/mol, 7.2mmol, 1.0 eq) was solubilized in 20mL anhydrous THF and added dropwise to the LAH solution over 1 hour. The reaction was allowed to warm to room temperature, then heated to 55°C and stirred overnight. After 24 hours, the reaction was cooled back to 4°C in an ice bath, and excess LAH was quenched by the slow addition of 5mL deionized H_2O followed by 1 hour of stirring at 4°C. The solid salts were removed by filtration, and the THF:H_2O mixture was removed by rotary evaporation. The remaining oily solid was solubilized in 100mL diethyl ether and washed 2x with 20mL 1M HCl, 2x with 20mL brine. The organic layer was then dried over Na_2SO_4 and concentrated to an oil. Further purification was not carried out on this compound. 3.35g (91%). MW calc. ($C_{36}H_{69}N$) = 515.94 found 516.18. TLC: R_f = 0.15 (99:1 CH_2Cl_2:MeOH).

^{1}H NMR (300 MHz, $CDCl_3$): 5.50-5.30 (m, 6H), 3.00-2.80 (m, 4H), 2.80-2.70 (m, 2H), 2.10-1.90 (m, 8H), 1.90-1.70 (m, 4H), 1.40-1.10 (m, 38H), 0.90 (m, 6H).

*Synthesis of **5***

0.34g of LAH (37.95g/mol, 8.9mmol, 3.0 eq) was suspended in 20mL anhydrous THF and cooled in an ice bath to 4°C. 1.58g of **3** (531.94g/mol, 3.0mmol, 1.0 eq) was solubilized in 15mL anhydrous THF and added dropwise to the LAH solution over 1 hour. The reaction was allowed to warm to room temperature, then heated to 55°C and stirred overnight. After 24 hours, the reaction was cooled back to 4°C in an ice bath, and excess LAH was quenched by the slow addition of 5mL deionized H_2O followed by 1 hour of stirring at 4°C. The solid salts were removed by filtration, and the THF:H_2O mixture was removed by rotary evaporation. The remaining oily solid was solubilized in 100mL diethyl ether and washed 2x with 20mL 1M HCl, 2x with 20mL brine. The organic layer was then dried over Na_2SO_4 and concentrated to an oil. Further purification was not carried out on this compound. 1.35g (87%). MW calc. ($C_{36}H_{69}N$) = 517.96 found 518.78. TLC: R_f = 0.15 (99:1 CH_2Cl_2:MeOH).

^{1}H NMR (300 MHz, $CDCl_3$): 5.50-5.30 (m, 4H), 2.70-2.50 (m, 4H), 2.10-1.90 (m, 8H), 1.60-1.40 (m, 4H), 1.40-1.10 (m, 44H), 0.90 (m, 6H).

4.3.2.2 Synthesis of LOA-LysC2

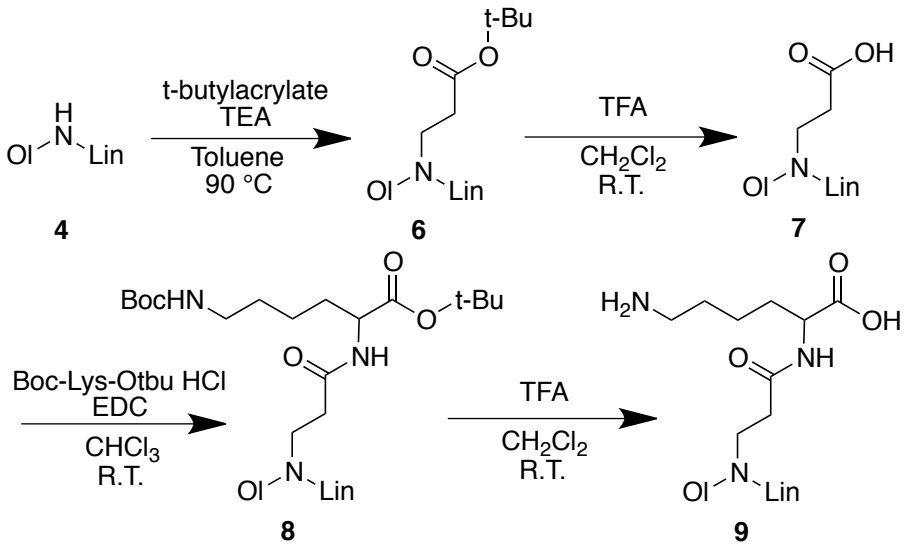

Scheme 4.2: Synthesis of LOA-LysC2

*Synthesis of **6***

3.3g of **4** (515.94g/mol, 6.4mmol, 1.0 eq), 1.6g of t-butylacrylate (128.17g/mol, 12.8mmol, 2.0 eq), and 2.6g triethylamine (TEA) (101.19g/mol, 25.6mmol, 4.0 eq) were solubilized in 10mL toluene and stirred at 90°C for 72 hours. Solvent was removed by rotary evaporation, and the resulting oil was solubilized in 100mL EtOAc, washed 2x with 20mL 1M HCl and 2x with 20mL brine. The organic layer was then dried over Na_2SO_4 and concentrated to an oil. The crude product was purified by HPFC using an elution gradient of 0-8% MeOH in $CHCl_3$. MW calc. ($C_{43}H_{81}NO_2$) = 644.11 found 645.01. 2.76g (67%). TLC: R_f = 0.9 (95:4.5:0.5 CH_2Cl_2:MeOH:NH_3OH).

^{1}H NMR (300 MHz, $CDCl_3$): 5.50-5.30 (m, 6H), 3.50-3.40 (m, 2H), 3.30-3.20 (m, 2H), 3.00-2.80 (m, 4H), 2.80-2.70 (m, 2H), 2.10-1.90 (m, 8H), 1.90-1.70 (m, 4H), 1.50 (s, 9H) 1.40-1.10 (m, 38H), 0.90 (m, 6H).

*Synthesis of **7***

2.7g of **6** (644.11g/mol, 4.2mmol) was stirred in 15mL 1:1 TFA:CH_2Cl_2 at room temperature for 1 hour. TFA and CH_2Cl_2 were removed by rotary evaporation, and the resulting oil was solubilized in 100 mL EtOAc, washed 2x with 20mL 1M $NaHCO_3$ and 2x with 20mL brine. The organic layer was dried over Na_2SO_4 and concentrated to an oil. MW calc. ($C_{39}H_{73}NO_2$) = 588.0 found 588.91. 2.32g (94%). TLC: R_f = 0.3 (95:4.5:0.5 CH_2Cl_2:MeOH:NH_3OH).

^{1}H NMR (300 MHz, $CDCl_3$): 5.50-5.30 (m, 6H), 3.50-3.40 (m, 2H), 3.30-3.20 (m, 2H), 3.00-2.80 (m, 4H), 2.80-2.70 (m, 2H), 2.10-1.90 (m, 8H), 1.90-1.70 (m, 4H), 1.40-1.10 (m, 38H), 0.90 (m, 6H).

*Synthesis of **8***

1.05g of **7** (588.0g/mol, 1.8mmol, 1.0 eq), 0.68g Boc-Lys-Otbu HCl (338.87g/mol, 2mmol, 1.1 eq), 0.42g EDC (155.24g/mol, 2.7mmol, 1.5 eq) were added to 30mL $CHCl_3$ and stirred at room temperature for 24 hours. Solvent was removed by rotary evaporation. The resulting oily solid was solubilized in 100mL EtOAc and washed 2x with 20mL 1M HCl and 2x with 20mL brine. The organic layer was dried over Na_2SO_4 and concentrated to an oil. The crude product was purified by HPFC using an elution gradient of 0-10% MeOH in $CHCl_3$. MW calc ($C_{54}H_{101}N_3O_5$) = 872.40 found 873.31. 1.04g (66%). TLC: R_f = 0.45 (95:4.5:0.5 CH_2Cl_2:MeOH:NH_3OH).

^{1}H NMR (300 MHz, $CDCl_3$): 5.50-5.30 (m, 6H), 4.40 (m, 1H), 3.50-3.40 (m, 2H), 3.30-3.20 (m, 2H), 3.20-3.10 (m, 2H), 3.00-2.80 (m, 4H), 2.80-2.70 (m, 2H), 2.10-1.90 (m, 8H), 1.90-1.70 (m, 8H), 1.55 (m, 2H), 1.40 (s, 18H), 1.40-1.10 (m, 38H), 0.90 (m, 6H).

*Synthesis of **9** (LOA-LysC2)*

1.04g of **8** (872.40g/mol, 1.2mmol, 1.0 eq) was stirred in 10mL 1:1 TFA:CH_2Cl_2 at room temperature for 1 hour. TFA and CH_2Cl_2 were removed by rotary evaporation, and the resulting oil was solubilized in 50 mL EtOAc, washed 2x with 10mL 1M $NaHCO_3$ and 2x with 10mL brine. The organic layer was dried over Na_2SO_4 and concentrated to an oil. The crude product was purified by HPFC using an elution gradient of 0-30% MeOH in $CHCl_3$. MW calc. ($C_{45}H_{85}N_3O_{3)}$ = 716.17 found 717.12. 0.64g (75%). TLC: R_f = 0.15 (72.5:25:2.5 CH_2Cl_2:MeOH:NH_3OH).

^{1}H NMR (300 MHz, $CDCl_3$): 5.50-5.30 (m, 6H), 4.40 (m, 1H), 3.50-3.40 (m, 2H), 3.30-3.20 (m, 2H), 3.20-3.10 (m, 2H), 3.00-2.80 (m, 4H), 2.80-2.70 (m, 2H), 2.10-1.90 (m, 8H), 1.80-1.60 (m, 6H) 1.40-1.10 (m, 42H), 0.90 (m, 6H).

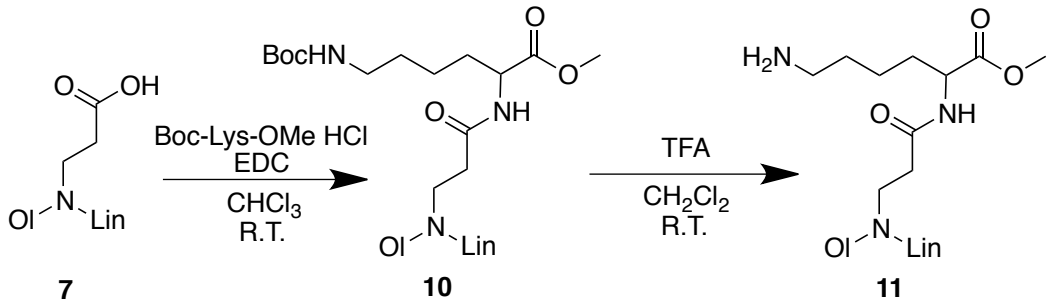

7 **10** **11**

Scheme 4.3: Synthesis of LOA-LysC2-OMe

*Synthesis of **10***

1g of **7** (588.0g/mol, 1.7mmol, 1.0 eq), 0.56g Boc-Lys-OMe HCl (296.79g/mol, 1.9mmol, 1.1 eq), 0.41g EDC (155.24g/mol, 2.6mmol, 1.5 eq) were added to 30mL $CHCl_3$ and stirred at room temperature for 24 hours. Solvent was removed by rotary evaporation. The resulting oily solid was solubilized in 100mL EtOAc and washed 2x with 20mL 1M HCl and 2x with 20mL brine. The organic layer was dried over Na_2SO_4 and concentrated to an oil. The crude product was purified by HPFC using an elution gradient of 0-10% MeOH in $CHCl_3$. MW calc ($C_{54}H_{95}N_3O_5$) = 830.32 found 831.29. 0.85g (60%). TLC: R_f = 0.45 (95:4.5:0.5 CH_2Cl_2:MeOH:NH_3OH).

^{1}H NMR (300 MHz, $CDCl_3$): 5.50-5.30 (m, 6H), 4.40 (m, 1H), 3.70 (s, 3H), 3.50-3.40 (m, 2H), 3.30-3.20 (m, 2H), 3.20-3.10 (m, 2H) 3.00-2.80 (m, 4H), 2.80-2.70 (m, 2H), 2.10-1.90 (m, 8H), 1.90-1.70 (m, 8H), 1.55 (m, 2H), 1.40 (s, 9H), 1.40-1.10 (m, 38H), 0.90 (m, 6H).

*Synthesis of **11** (LOA-LysC2-OMe)*

0.85g of **10** (830.32g/mol, 1.0mmol, 1.0 eq) was stirred in 10mL 1:1 TFA:CH_2Cl_2 at room temperature for 1 hour. TFA and CH_2Cl_2 were removed by rotary evaporation, and the resulting oil was solubilized in 50 mL EtOAc, washed 2x with 10mL 1M $NaHCO_3$ and 2x with 10mL brine. The organic layer was dried over Na_2SO_4 and concentrated to an oil. The crude product was purified by HPFC using an elution gradient of 0-20% MeOH in $CHCl_3$. MW calc. ($C_{45}H_{85}N_3O_{3)}$ = 730.20 found 730.73. 0.6g (82%). TLC: R_f = 0.15 (90:9:1 CH_2Cl_2:MeOH:NH_3OH).

^{1}H NMR (300 MHz, $CDCl_3$): 5.50-5.30 (m, 6H), 4.40 (m, 1H), 3.70 (s, 3H) 3.50-3.40 (m, 2H), 3.30-3.20 (m, 2H), 3.20-3.10 (m, 2H) 3.00-2.80 (m, 4H), 2.80-2.70 (m, 2H), 2.10-1.90 (m, 8H), 1.80-1.60 (m, 6H) 1.40-1.10 (m, 42H), 0.90 (m, 6H).

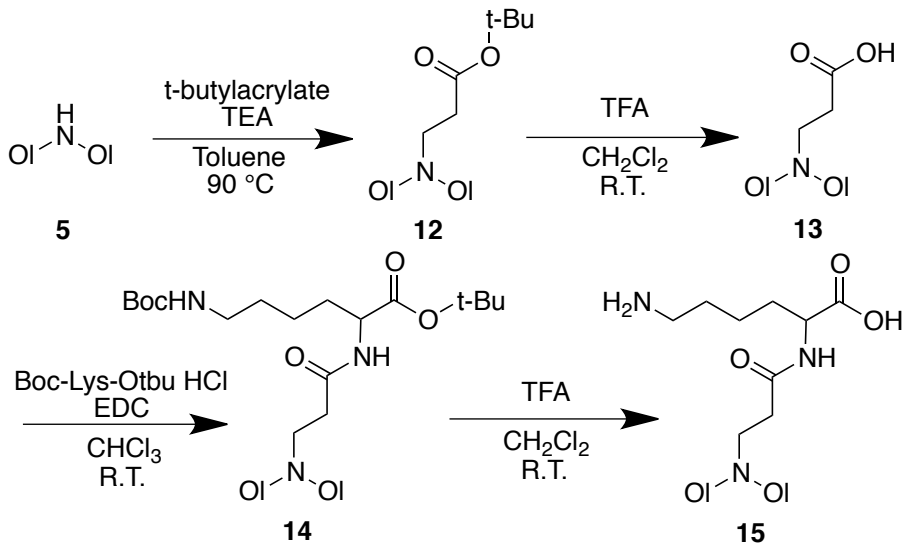

Scheme 4.4: Synthesis of DOA-LysC2

*Synthesis of **12***

2g of **5** (517.96 g/mol, 3.9mmol, 1.0 eq), 1g of t-butylacrylate (128.17g/mol, 7.8mmol, 2.0 eq), and 1.6g triethylamine (TEA) (101.19g/mol, 11.2mmol, 4.0 eq) were solubilized in 10mL toluene and stirred at 90°C for 72 hours. Solvent was removed by rotary

evaporation, and the resulting oil was solubilized in 50 mL EtOAc, washed 2x with 10mL 1M HCl and 2x with 10mL brine. The organic layer was then dried over Na_2SO_4 and concentrated to an oil. The crude product was purified by HPFC using an elution gradient of 0-5% MeOH in $CHCl_3$. MW calc. ($C_{43}H_{83}NO_2$) = 646.12 found 647.02. 1.4g (56%). TLC: R_f = 0.9 (95:4.5:0.5 CH_2Cl_2:MeOH:NH_3OH).

^{1}H NMR (300 MHz, $CDCl_3$): 5.50-5.30 (m, 4H), 3.20 (m, 2H), 3.00-2.80 (m, 4H), 2.80-2.60 (m, 2H), 2.10-1.90 (m, 8H), 1.90-1.70 (m, 4H), 1.50 (s, 9H) 1.40-1.10 (m, 44H), 0.90 (m, 6H).

*Synthesis of **13***

1.35g **12** (646.12g/mol, 2.1mmol) was stirred in 10mL 1:1 TFA:CH_2Cl_2 at room temperature for 1 hour. TFA and CH_2Cl_2 were removed by rotary evaporation, and the resulting oil was solubilized in 50 mL EtOAc, washed 2x with 10mL 1M $NaHCO_3$ and 2x with 10mL brine. The organic layer was dried over Na_2SO_4 and concentrated to an oil. MW calc. ($C_{39}H_{75}NO_2$) = 590.02 found 590.86. 1.05g (85%). TLC: R_f = 0.3 (95:4.5:0.5 CH_2Cl_2:MeOH:NH_3OH).

^{1}H NMR (300 MHz, $CDCl_3$): 5.50-5.30 (m, 4H), 3.20 (m, 2H), 3.00-2.80 (m, 4H), 2.80-2.60 (m, 2H), 2.10-1.90 (m, 8H), 1.90-1.70 (m, 4H), 1.40-1.10 (m, 44H), 0.90 (m, 6H).

*Synthesis of **14***

1g of **13** (590.02g/mol, 1.7mmol, 1.0 eq), 0.64g Boc-Lys-Otbu HCl (338.87g/mol, 1.9mmol, 1.1 eq), 0.4g EDC (155.24g/mol, 2.55mmol, 1.5 eq) were added to 30mL $CHCl_3$ and stirred at room temperature for 24 hours. Solvent was removed by rotary evaporation.

The resulting oily solid was solubilized in 100mL EtOAc and washed 2x with 20mL 1M HCl and 2x with 20mL brine. The organic layer was dried over Na_2SO_4 and concentrated to an oil. The crude product was purified by HPFC using an elution gradient of 0-10% MeOH in $CHCl_3$. MW calc ($C_{54}H_{103}N_3O_5$) = 874.41 found 874.68. 1.05g (71%). TLC: R_f = 0.45 (95:4.5:0.5 CH_2Cl_2:MeOH:NH_3OH).

^{1}H NMR (300 MHz, $CDCl_3$): 5.50-5.30 (m, 4H), 4.40 (m, 1H), 3.50-3.40 (m, 2H), 3.30-3.20 (m, 2H), 3.20-3.10 (m, 2H) 3.00-2.80 (m, 6H), 2.10-1.90 (m, 8H), 1.90-1.70 (m, 8H), 1.40 (s, 18H), 1.40-1.10 (m, 44H), 0.90 (m, 6H).

*Synthesis of **15** (DOA-LysC2)*

1.05g of **14** (874.41g/mol, 1.2mmol, 1.0 eq) was stirred in 10mL 1:1 TFA:CH_2Cl_2 at room temperature for 1 hour. TFA and CH_2Cl_2 were removed by rotary evaporation, and the resulting oil was solubilized in 50 mL EtOAc, washed 2x with 10mL 1M $NaHCO_3$ and 2x with 10mL brine. The organic layer was dried over Na_2SO_4 and concentrated to an oil. The crude product was purified by HPFC using an elution gradient of 0-30% MeOH in $CHCl_3$. MW calc. ($C_{45}H_{87}N_3O_{3)}$ = 718.19 found 719.04. 0.61g (71%). TLC: R_f = 0.15 (72.5:25:2.5 CH_2Cl_2:MeOH:NH_3OH).

^{1}H NMR (300 MHz, $CDCl_3$): 5.50-5.30 (m, 4H), 4.40 (m, 1H), 3.50-3.40 (m, 2H), 3.30-3.20 (m, 2H), 3.20-3.10 (m, 2H) 3.00-2.80 (m, 4H), 2.10-1.90 (m, 8H), 1.80-1.60 (m, 6H) 1.40-1.10 (m, 46H), 0.90 (m, 6H).

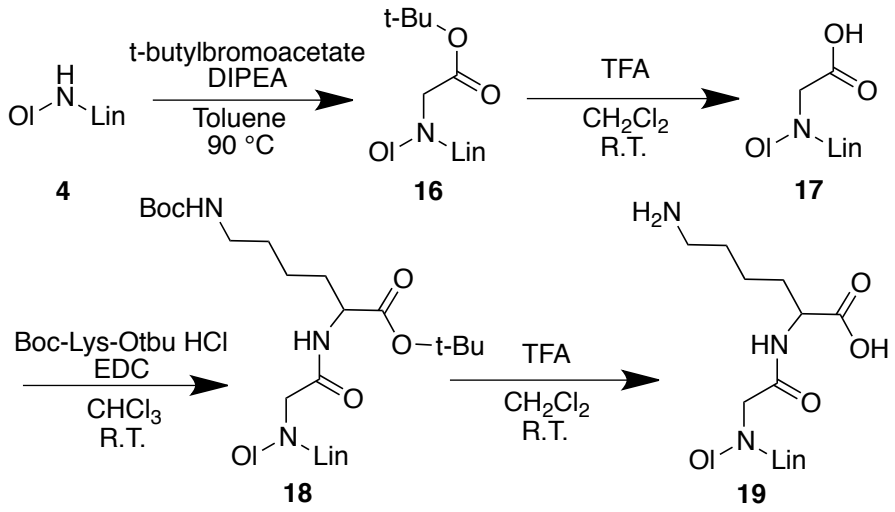

Scheme 4.5: Synthesis of LOA-LysC1

*Synthesis of **16***

2g of **4** (515.94g/mol, 3.9mmol, 1.0 eq), 1.5g of t-butylbromoacetate (195.05g/mol, 7.8mmol, 2.0 eq), and 1.3g DIPEA (129.24g/mol, 9.8mmol, 2.5 eq) were solubilized in 10mL toluene and stirred at 80°C for 48 hours. Solvent was removed by rotary evaporation, and the resulting oil was solubilized in 100 mL EtOAc, washed 2x with 20mL 1M HCl and 2x with 20mL brine. The organic layer was then dried over Na_2SO_4 and concentrated to an oil. The crude product was purified by HPFC using an elution gradient of 0-8% MeOH in $CHCl_3$. MW calc. ($C_{42}H_{79}NO_2$) = 630.08 found 630.36. 1.89g (77%). TLC: R_f = 0.85 (95:4.5:0.5 CH_2Cl_2:MeOH:NH_3OH).

^{1}H NMR (300 MHz, $CDCl_3$): 5.50-5.30 (m, 6H), 3.70-3.60 (s, 2H), 3.30-3.20 (m, 4H), 2.80-2.70 (m, 2H), 2.10-1.90 (m, 8H), 1.90-1.70 (m, 4H), 1.50 (s, 9H), 1.40-1.10 (m, 38H), 0.90 (m, 6H).

*Synthesis of **17***

1.8g of **16** (630.08g/mol, 2.9mmol) was stirred in 10mL 1:1 TFA:CH_2Cl_2 at room temperature for 1 hour. TFA and CH_2Cl_2 were removed by rotary evaporation, and the resulting oil was solubilized in 100 mL EtOAc, washed 2x with 20mL 1M $NaHCO_3$ and 2x with 20mL brine. The organic layer was dried over Na_2SO_4 and concentrated to an oil. MW calc. ($C_{38}H_{71}NO_2$) = 573.98 found 574.42. 1.55g (93%). TLC: R_f = 0.3 (95:4.5:0.5 CH_2Cl_2:MeOH:NH_3OH).

^{1}H NMR (300 MHz, $CDCl_3$): 5.50-5.30 (m, 6H), 3.90-3.80 (s, 2H), 3.40-3.20 (m, 4H), 2.80-2.70 (m, 2H), 2.10-1.90 (m, 8H), 1.90-1.70 (m, 4H), 1.40-1.10 (m, 38H), 0.90 (m, 6H).

*Synthesis of **18***

0.9g of **17** (574.42g/mol, 1.6mmol, 1.0 eq), 0.61g Boc-Lys-Otbu HCl (338.87g/mol, 1.8mmol, 1.1 eq), 0.38g EDC (155.24g/mol, 2.4mmol, 1.5 eq) were added to 30mL $CHCl_3$ and stirred at room temperature for 24 hours. Solvent was removed by rotary evaporation. The resulting oily solid was solubilized in 100mL EtOAc and washed 2x with 20mL 1M HCl and 2x with 20mL brine. The organic layer was dried over Na_2SO_4 and concentrated to an oil. The crude product was purified by HPFC using an elution gradient of 0-10% MeOH in $CHCl_3$. MW calc ($C_{53}H_{99}N_3O_5$) = 858.37 found 859.24. 0.93g (68%). TLC: R_f = 0.45 (95:4.5:0.5 CH_2Cl_2:MeOH:NH_3OH).

^{1}H NMR (300 MHz, $CDCl_3$): 5.50-5.30 (m, 6H), 4.40 (m, 1H), 3.50-3.40 (s, 2H), 3.40-3.30 (m, 2H), 3.20-3.10 (m, 4H), 2.80-2.70 (m, 2H), 2.10-1.90 (m, 8H), 1.90-1.70 (m, 8H), 1.55 (m, 2H), 1.40 (s, 18H), 1.40-1.10 (m, 38H), 0.90 (m, 6H).

*Synthesis of **19** (LOA-LysC1)*

0.9g of **18** (858.37g/mol, 1.0mmol, 1.0 eq) was stirred in 10mL 1:1 TFA:CH_2Cl_2 at room temperature for 1 hour. TFA and CH_2Cl_2 were removed by rotary evaporation, and the resulting oil was solubilized in 50 mL EtOAc, washed 2x with 10mL 1M $NaHCO_3$ and 2x with 10mL brine. The organic layer was dried over Na_2SO_4 and concentrated to an oil. The crude product was purified by HPFC using an elution gradient of 0-30% MeOH in $CHCl_3$. MW calc. ($C_{44}H_{83}N_3O_{3)}$ = 702.15 found 703.01. 0.51g (72%). TLC: R_f = 0.15 (72.5:25:2.5 CH_2Cl_2:MeOH:NH_3OH).

^{1}H NMR (300 MHz, $CDCl_3$): 5.50-5.30 (m, 6H), 4.40 (m, 1H), 3.50-3.40 (s, 2H), 3.30-3.20 (m, 2H), 3.00-2.80 (m, 4H), 2.80-2.70 (m, 2H), 2.10-1.90 (m, 8H), 1.80-1.60 (m, 6H) 1.40-1.10 (m, 42H), 0.90 (m, 6H).

4.3.3 Liposomal Formulation for Biophysical Assays

Chloroform solutions of lipids were dried in 10 x 25 mm glass test tubes by rotary evaporation under reduced pressure followed by high vacuum for 18 hours. The lipid film was rehydrated with 500 μL of 10 mM Tris buffer containing 150 mM NaCl, pH=7.4 (5 mM final concentration). Each preparation was sonicated 30 min at room temperature to form monodisperse liposomes with diameters in the 80-120 nm range. Particle size was measured using a Malvern Zetasizer NanoZS (Malvern, Westborough, MA).

4.3.4 TNS Fluorescence Assay

Ionization behavior of ILL containing liposomes was assayed using a protocol adapted by Zhang et. al.[24] A 5 mM solution of ILL liposomes (40:40:15:5, ILL:Chol:POPC:PEG-DMG) was diluted to 2.67 μM in a 10 mM buffer containing 150 mM

NaCl, pH=3.5–9.5. Fluorescence was measured (Ex/Em = 320/430 nm) using a Spex Fluorolog Fluorimeter (Horiba Scientific, Edison, NJ) to obtain background, then measured again following the introduction of 0.167 μM TNS to give the background subtracted fluorescent signal (F). All experiments were run in triplicate, and normalized to the background subtracted fluorescent signals of DOTAP and DOPC liposomes to correct for changes in TNS fluorescence as a function of pH. The net charge of the ionizable lipid at a given pH is defined as:

$$\text{Net Charge}_{pH} = \frac{F - F_{DOPC}}{F_{DOTAP} - F_{DOPC}} \times 100$$

where F is the fluorescence of the sample at the specified pH, F_{DOPC} is the fluorescence of DOPC liposomes (40:40:15:5, DOPC:Chol:POPC:PEG-DMG) at the specified pH, and F_{DOTAP} is the fluorescence of DOTAP liposomes (40:40:15:5, DOTAP:Chol:POPC:PEG-DMG) at the specified pH.

4.3.5 Membrane Lysis Assay

Membrane lysis activity was assayed using a protocol adapted from Zhang et. al.[24] A 5 mM solution of membrane mimicking liposomes (45:20:20:15, DOPC:DOPE:DOPG:Chol) encapsulating 10 mM TRIS, 12.5 mM ANTS, 45 mM DPX, 20 mM NaCl was diluted to 3.33 μM in a 10 mM isosmotic buffer containing 150 mM NaCl, pH=5.5, 6.5, or 7.4. A 5 mM solution of ionizable liposomes (40:60, ionizable lipid:POPC) was then diluted in to a concentration of 16.67 μM. Baseline ANTS fluorescence (Ex/Em = 360/530 nm) was measured at t = 0 (F_{min}) using a Spex Fluorolog Fluorimeter (Horiba Scientific, Edison, NJ). Following a 30 min incubation at 37 °C, ANTS fluorescence was measured again (F).

Maximum ANTS fluorescence was measured following total membrane lysis using 0.5% $C_{12}E_{10}$ (F_{max}). All measurements were done in triplicate. % Lysis is defined as:

$$\%Lysis_{pH} = \frac{F - F_{Min}}{F_{Max} - F_{Min}} \times 100$$

4.3.6 In Vitro siRNA Transfection Assay

In vitro transfection was assayed using a protocol adapted from Akinc et. al.[25] HeLa cells stably expressing firefly luciferase were seeded (8,000 cells/well) on an opaque black 96-well plate (Greiner Cellstar), and allowed to attach overnight in 90% MEM media with 10% FBS, 100 mcg/ml streptomycin and 100 units/ml penicillin. Lipid/siRNA complexes were made by combining lipid formulations containing 40:40:20 ILL:Chol:DOPE (1 mg/ml total lipid, 25 mM NaOAc buffer, pH=5.0) and siRNA (12.5 μg/ml siRNA, 25 mM NaOAC buffer, pH=5.0) at N:P = 10 for 30 min at room temperature. Cells were transfected with lipoplexes containing anti-luciferase or non-specific siRNA at the given concentrations by adding the lipoplex solution to the cell culture media and incubating for 24 hr. Luciferase expression was measured using the Steady-Glo assay kit (Promega, Madison, WI). Luminescence was measured using an Infinite m1000 Pro microplate reader (Tecan, San Jose, CA). Control experiments were performed with Lipofectamine 2000 using the protocol provided by the vendor (Invitrogen, Carlsbad, CA). Luminescence was normalized to the non-specific siRNA control, and treated wells were compared against untreated wells to evaluate knockdown efficiency. All measurements were done in triplicate.

4.3.7 In Vivo ILL-siRNA Liposomal Formulation

ILL-siRNA formulations were prepared using a batch mixing process as previously described.[23] Formulations contained ILL, Chol, DSPC, and PEG-DMG (40:40:10:10). 2 mg total lipid was dissolved in 250 μL of ethanol and sonicated at 25°C for 5 min. The lipid/ethanol solution was subsequently injected into a magnetically stirred 2.5 mL vial, which contained 100 μg of siRNA dissolved in 250 μL of 50 mM citric acid buffer, pH 4. The lipid suspension was stirred for 10 min and then extruded using a handheld extruder (Avestin, Ottawa, ON, Canada) through 80 nm polycarbonate membranes (Whatman International, Kent, UK) 5 times at room temperature. Ethanol was removed by dialysis against PBS (pH 7.4) without Ca^{2+} and Mg^{2+} for 24h. Encaspulation efficiency of siRNA was quantified by measuring the fluorescence signal using the Quant-iT RiboGreen RNA Assay Kit (Life Technologies, Carlsbad, CA) in the presence or absence of 0.4% Triton-X. Fluorescence was measured using the Fluostar fluorescence plate reader (BMG Labtech, Cary, NC) (Ex/Em = 485/520 nm). Liposome size and zeta potential were measured 3 times per sample on a Zetasizer NanoZS (Malvern, Westborough MA) and averaged.

4.3.8 In Vivo Mouse Factor VII Knockdown Experiments

Six-to eight-week-old, female CD-1 mice (Charles River Laboratories, Wilmington, MA) were administered ILL-siRNA formulations via tail vein injection at an siRNA concentration of 5 mg/kg (15:1 w:w ratio of ILL:siRNA) in a total volume of 200 μL. Control mice received an injection of 200 μL of phosphate buffered saline without calcium or magnesium salts (PBS). 48 hr after administration, animals were anesthetized with isoflurane. Blood was collected by submandibular cheek bleeding. Serum samples were

obtained by allowing the blood to clot for 30 min and then centrifuging for 15 min at 15,000 rpm at 4°C. The supernatant was collected and analyzed for serum levels of Factor VII protein using the Biophen VII chromogenic assay (Aniara, Mason, OH) according to manufacturer's instructions. A standard curve was generated using serially diluted concentrations of PBS-treated animals. Serum Factor VII levels of mice treated with ILL-siRNA formulations were expressed as percentage of PBS-control. Each group consisted of n=3 mice. DLinDMA liposomes (40:40:10:10 DLinDMA:Chol:DSPC:PEG-DMG) served as a positive control.[20]

4.4 Results And Discussion

4.4.1 Chemistry and structure of Ionizable Lysine-Based Lipids

Ionizable lysine-based lipids (ILL) contain a lysine head group linked to a long-chain dialkylamine through an amide linkage at the lysine α-amine (Figure 4.1). The resulting lipid structure contains a primary and tertiary amine, as well as a single carboxylate. As such, the overall net charge of ILL depends upon the ionization state of these protonatable moieties (Figure 4.2). At low pH, all ionizable groups should be protonated, yielding a net charge of +2. As the pH increases, deprotonation of the carboxylate reduces the overall net charge to +1, and subsequent deprotonation of the amines results in a net charge of 0 or -1. We hypothesize that, similar to other ionizable delivery systems, this pH-dependent ionization behavior will promote siRNA encapsulation at low pH and membrane destabilization along the endocytic pathway, while preventing protein opsonization at physiological pH.[12] The presence of the anionic moiety gives these lipids zwitterionic characteristics that may reduce the immunostimulatory effects that are characteristic of cationic lipid systems.[14]

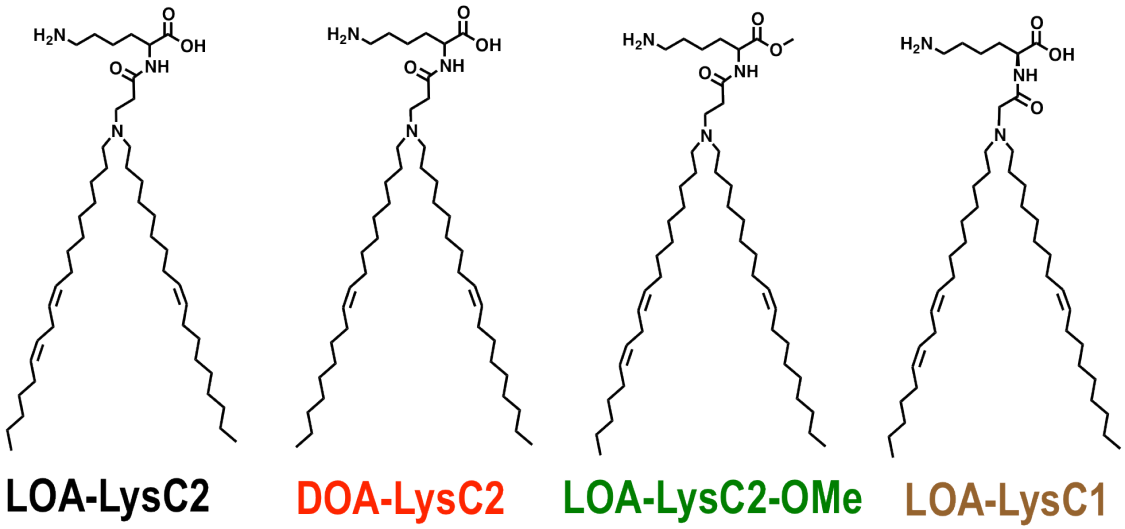

Figure 4.1: Ionizable lysine-based lipid (ILL) structures

We synthesized four distinct lipids to identify the impact of structural modifications on the biophysical and transfection behavior of these lipids (Figure 4.1): LOA-LysC2 contains a linoleyloleylamine (LOA) and a two-carbon spacer between the amide-linked lysine and the LOA core; DOA-LysC2 contains the same two-carbon spacer but a dioleylamine (DOA) hydrophobic region; LOA-LysC2-OMe is identical to LOA-LysC2, except the carboxylic acid is methylated to prevent ionization of this functional group and eliminate the cationic to neutral charge transition; LOA-LysC1 is analogous to LOA-LysC2, but contains a single carbon linker between the amide and the LOA core. This focused lipid library provides a platform to study how lipid hydrophobic fluidity, net charge, and amine pKa impact the biophysical and transfection behavior of ILL.

The general ILL synthetic scheme allows for the orthoganol manipulation of lipid structure. Synthesis begins with the formation of a dialkylamine by coupling a long chain fatty acid to oleylamine, followed by reduction of the resulting amide using lithium aluminum hydride. This long-chain dialkylamine is then functionalized with either t-

butylbromoacetate or t-butylacrylate to create a protected trialkylamino acid with a one- or two-carbon spacer between the tertiary amine and the carboxylate. Following deprotection, the acid group is coupled to the α-amine of a protected lysine. Global or selective deprotection of this compound yields the final ILL product. All compounds were purified by HPFC prior to biophysical characterization or transfection studies.

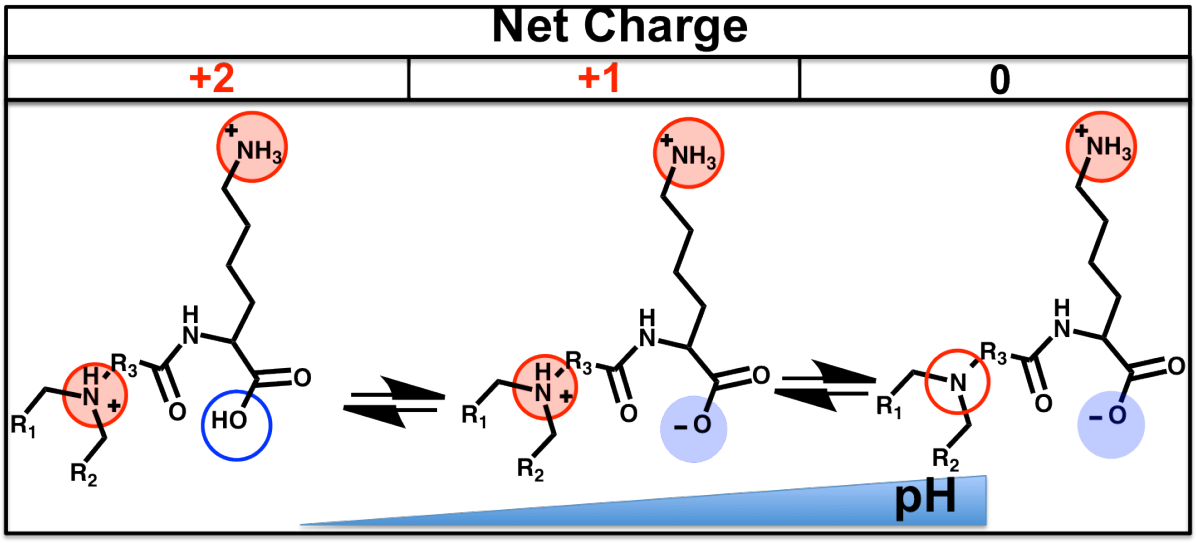

Figure 4.2: Theoretical pH-dependent ionization of ILL

4.4.2 Liposomal formulation for biophysical characterization

ILL liposomes for biophysical characterization were prepared by rehydrating a dried lipid film of the desired composition in 10 mM Tris buffer with 150 mM NaCl, pH=7.4. Two different liposomal formulations were used; 60:40 POPC:ILL and 40:40:15:5 ILL:Chol:POPC:PEG-DMG. Both preparations formed small (80-120 nm), stable liposomes following sonication for 30 minutes at room temperature.

4.4.3 pH-dependent ionization of ILL containing liposomes

The ionization behavior of ILL liposomes (40:40:15:5, ILL:Chol:POPC:PEG-DMG) was studied by comparing their relative surface charge as a function of pH using a TNS assay.[24,26] TNS is an anionic fluorophore whose fluorescence intensity increases drastically in a hydrophobic environment due to the elimination of quenching by water molecules. TNS partitions into cationic lipid membranes to a greater extent than neutral or anionic membranes due to electrostatic interactions. This behavior makes TNS an ideal candidate for exploring the surface charge of ILL containing liposomes across a range of pH. As the ILL headgroup is protonated with decreasing pH, the level of TNS fluorescence should increase due to an increasing concentration of TNS in the hydrophobic environment. The presence of multiple ionizable groups in ILL makes data normalization difficult because the shape of the ionization curve differs depending on lipid structure. As such, normalizing to the maximum and minimum values for each sample does not accurately portray their relative ionization behavior. However, normalization to a formally positive lipid (DOTAP) and a neutral lipid (DOPC) allows us to identify the relative net charge of the ILL as a function of pH. The data for each ILL can then be compared to other ILL, as well as lipids with a single ionizable amine, such as DLinDMA.[20]

TNS fluorescence in the presence of ILL liposomes was measured in 0.5 pH unit increments from pH = 3.0-9.5 (Figure 4.3). Our results indicate that all ILL show pH-dependent ionization, however structural changes clearly impact their ionization behavior. All ILL show a maximum net charge at pH=3.0 and a minimum net charge at pH = 9.5, as expected. LOA-LysC2, which was the template for all synthesized lipids, reaches a maximum net charge of +1.7, and exhibits a broad, double sigmoidal ionization curve,

eventually achieving a minimum value of 0.0 at pH = 9.5. Altering the hydrophobic region of LOA-LysC2 does not impact its ionization behavior, as seen by the matching DOA-LysC2 curve. Altering the length of the linker between the 3° amine and the amide linkage significantly impacts the shape of the ionization curve, but has no impact on the maximum or minimum lipid charge. This is illustrated by the ionization behavior of LOA-LysC1 liposomes. The shorter linker in LOA-LysC1 appears to lower the pKa of the 3° amine, likely due to the electron withdrawing effect of the amide in close proximity. LOA-LysC2-OMe, which has a methylated carboxylic acid moiety, exhibits a significantly different ionization profile due to the absence of the anionic group. At low pH, LOA-LysC2-OMe liposomes achieve a net charge of 2.0, indicating that both amines are fully protonated.

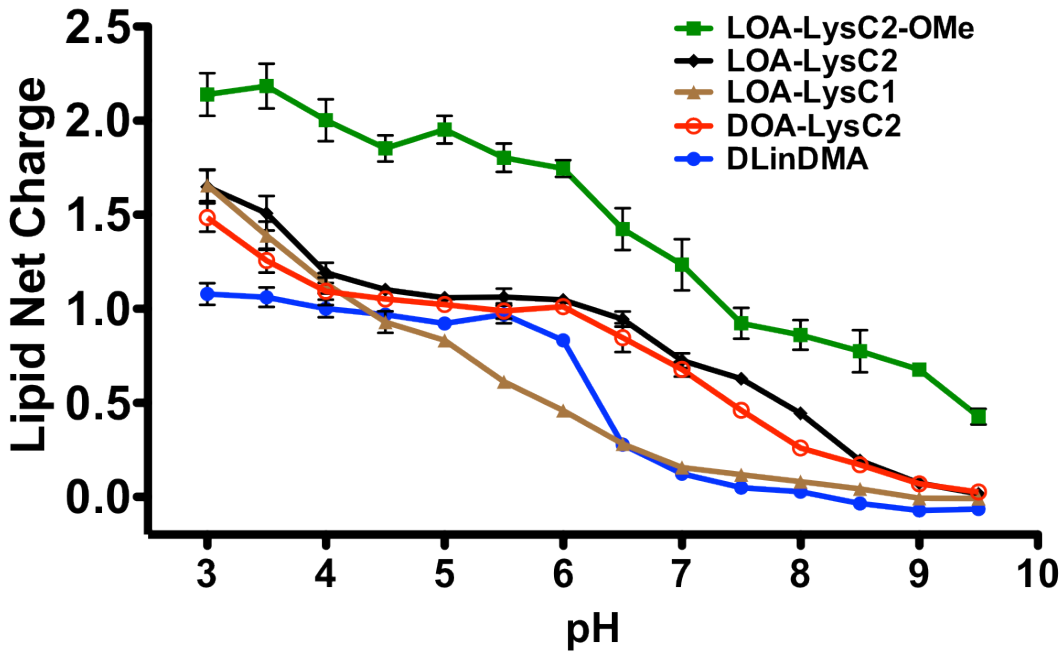

Figure 4.3: pH-dependent ionization of ILL liposomes (40:40:15:5 ILL:Chol:POPC:PEG-DMG)

None of the ILL with an ionizable carboxylate reach a net charge of 2.0 (maximum theoretical net charge) in the tested pH range. However, methylation of the carboxylate

results in a fully ionized head group. This indicates that the carboxylate moiety is either not fully protonated or is somehow interacting with the free amino groups to disrupt interactions with the TNS fluorophore. Interestingly, all of the ILL ionization curves differ significantly from that of DLinDMA, a well characterized ionizable amino lipid[20], which shows a sigmoidal shape with a maximum net charge of 1.0 and a sharp transition to 0.0 between pH = 6.0 and 7.0. ILL do not follow the sigmoid shape observed for other ionizable amino lipids.[12,20,24] These lipids show a broader, more complicated ionization curve, possibly due to the presence of multiple ionizable moieties with varying pKa in each lipid. Additionally, differences in amine substitution (1° versus 3°) or orientation in the bilayer (interfacial versus extended) may affect lipid ionization and alter the pH-dependent surface charge.

4.4.4 Lysis of biomembrane mimicking vesicles by ILL liposomes

It is hypothesized that the charge state of lipids impacts their ability to disrupt anionic biomembranes along the endocytic pathway and deliver contents to the cytosol.[7,12,24] Cationic lipids can ion-pair with naturally occurring anionic lipids, inducing a phase transition from the stable L_α to the unstable H_{II} phase, promoting endosomal escape.[18,27] The efficiency of this process is believed to be key to the effective delivery of liposomal contents to the cytosol.[7,8,18,20] However, formally cationic systems are generally immunostimulatory and have short plasma half-lives due to protein opsonization and subsequent clearance by the reticuloendothelial system, making them poor candidates for systemic delivery.[8] Alternatively, ionizable lipids that become cationic at pH < 7.4 exhibit limited interactions with anionic membranes in circulation, but have strong electrostatic interactions along the endocytic pathway, thereby promoting efficient delivery. Several of these ionizable systems have shown promising *in vivo* data in pre-clinical models.[12,14]

Membrane lysis activity at low-pH is expected to correlate with transfection efficiency, and may help identify lipids with favorable properties for siRNA delivery *in vitro* and *in vivo*. Understanding the pH-dependent interactions between ILL containing liposomes and anionic membranes provides insight into their expected behavior in circulation. We investigated the capacity of ILL containing liposomes to lyse biomembrane mimicking vesicles (BMV) encapsulating the fluorophore/quencher ANTS/DPX as a function of pH. BMV consisted of 45:20:20:15 DOPC:DOPE:DOPG:cholesterol[28], and ILL liposomes contained 40:60 ILL:POPC. pHs of 7.4, 6.5, and 5.5 were chosen to assay lipid behavior physiologically relevant conditions.

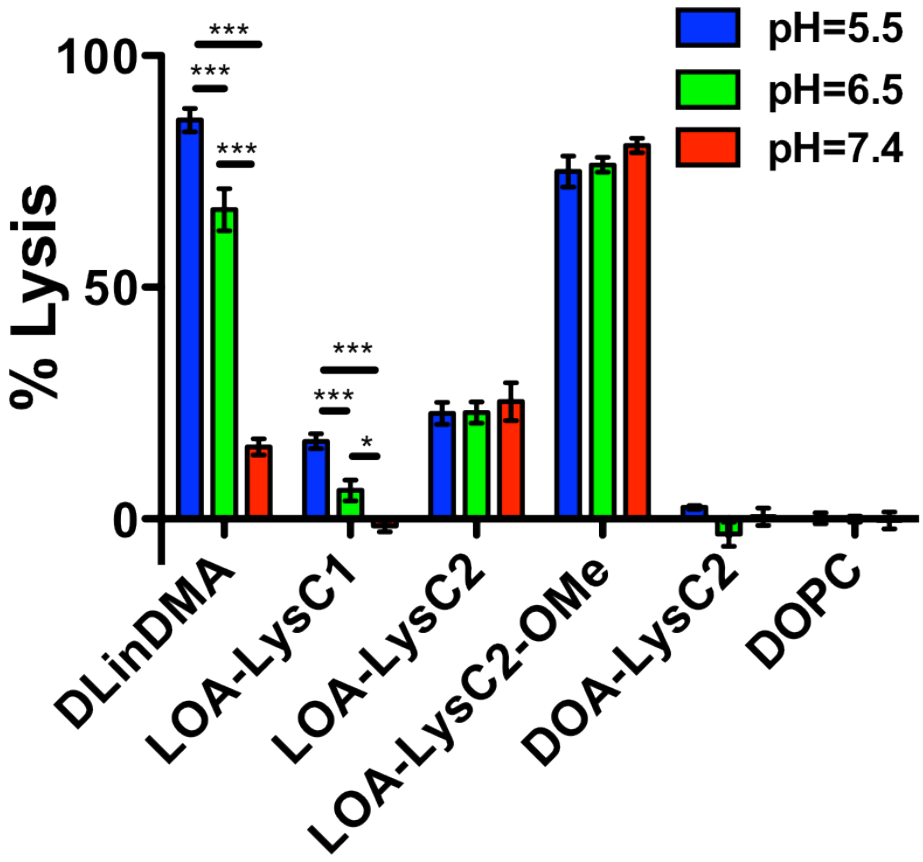

Figure 4.4: Lysis of biomembrane mimicking vesicles (45:20:20:15 DOPC:DOPE:DOPG:Chol) by ILL containing liposomes (60:40 POPC:ILL)

The synthesized ILLs provide a platform for investigating how changes in lipid net charge (LOA-LysC2-OMe), hydrophobic group fluidity (DOA-LysC2), and lipid ionization behavior (LOA-LysC1) impact membrane lysis compared to LOA-LysC2 liposomes. Additionally, we compare the behavior of ILL with DLinDMA, a well characterized ionizable lipid that is effective for *in vivo* siRNA delivery, and DOPC, a zwitterionic membrane phospholipid that is neutral across the tested pH range. DOPC liposomes show no lysis across the tested pH-range, as expected. DLinDMA liposomes show strong pH-dependent lysis characteristics, with a 5-fold increase in lysis at pH = 5.5 (86%) compared to pH = 7.4 (16%). Interestingly, DLinDMA still shows significantly more lysis at pH=7.4 than DOPC, indicating that these lipids are not fully deprotonated at physiological pH (Figure 4.4).

Since all ILLs exhibit pH-dependent ionization, we anticipated that we would observe pH-dependent BMV lysis for all ILL liposomes due to changes in electrostatic interactions as a function of pH. Interestingly, we observed that only LOA-LysC1 shows pH-dependence membrane lysis (Figure 4.4). LOA-LysC1 becomes cationic at a lower pH than all other ILL, possibly explaining this difference in biophysical behavior. At pH=5.5, LOA-LysC1 shows a slightly lower extent of lysis (18%) than LOA-LysC2 (23%), our base lipid for all structural modifications. This may be due to the lower net surface charge of LOA-LysC1 at pH = 5.5. DLinDMA shows a similar pH-dependent lysis profile, however the extent of lysis at pH=5.5 is four-fold higher, indicating it is more membrane active.

LOA-LysC2 and LOA-LysC2-OMe show pH-independent membrane lysis behavior. LOA-LysC2 promotes roughly 23% lysis, and LOA-LysC2-OMe, which is structurally analogous but has a methylated carboxylate, and therefore a higher charge density, shows 79% lysis across the tested pH range (Figure 4.4). The difference in extent of lysis is likely

due to differences in liposomal surface charge; LOA-LysC2-OMe liposomes are more cationic due to the absence of the anionic moiety, and therefore promote stronger electrostatic interactions with BMV. The pH-independent behavior of these two lipids was unexpected based on their ionization behavior; we predicted that the higher net surface charge at low pH would promote electrostatic interactions and increase membrane lysis. Instead, there appears to be a surface charge threshold above which there exists a constant, lipid dependent, extent of lysis. It is interesting to note that LOA-LysC2-OMe liposomes at pH = 7.4 have an identical surface charge to LOA-LysC2 liposomes at pH = 5.5, yet their extent of lysis is three-fold higher. This indicates that, independent of total surface charge, head group structure impacts the ILLs membrane lysis properties. This may be due to changes in lipid orientation, amine group presentation, or head group hydration in the bilayer caused by the presence of an anionic moiety in the LOA-LysC2 head group.

Decreased fluidity in the hydrophobic lipid tails is known to attenuate lipid mixing and fusion between lipid bilayers.[20] Comparing the membrane lysis behavior of LOA-LysC2 and DOA-LysC2, which contains a more rigid dioleyl hydrophobic region, we see that decreasing the fluidity of the ILL tails prevents membrane lysis across the entire pH range (Figure 4.4). In this case, the stability of the ILL liposome is likely preventing electrostatic-driven membrane fusion and lysis from occurring.

4.4.5 In vitro screening of ILL-siRNA complexes

We investigated ILL lipoplexes as siRNA delivery systems in a stably transfected HeLa-Luc cell line. Anti-luciferase and non-specific siRNA was complexed with ILL liposomes (40:40:20, ILL:Chol:DOPE) at N:P = 10. This ratio showed equivalent knockdown with lower toxicity compared to higher N:P ratios (data not shown).

Concentration dependent knockdown was assayed by incubating cells 0.11 – 90 nM of siRNA for 24 hrs at 37 °C. Our results show that all ILLs show potent, dose dependent knockdown (Figure 4.5). Structural differences impact the transfection efficiency of these systems, and their efficacy generally correlates with their capacity to lyse BMV. LOA-LysC2 and LOA-LysC2-OMe, which showed the highest BMV lysis across all tested pH values, exhibited nearly identical knockdown behavior. Both ILLs exhibited an IC_{50} of 1.1 nM. DOA-LysC2 and LOA-LysC1, both of which showed lower BMV lysis, exhibited IC_{50} values of 11.5 nM and 16.6 nM respectively. No significant toxicity was seen in any formulation at the tested concentrations.

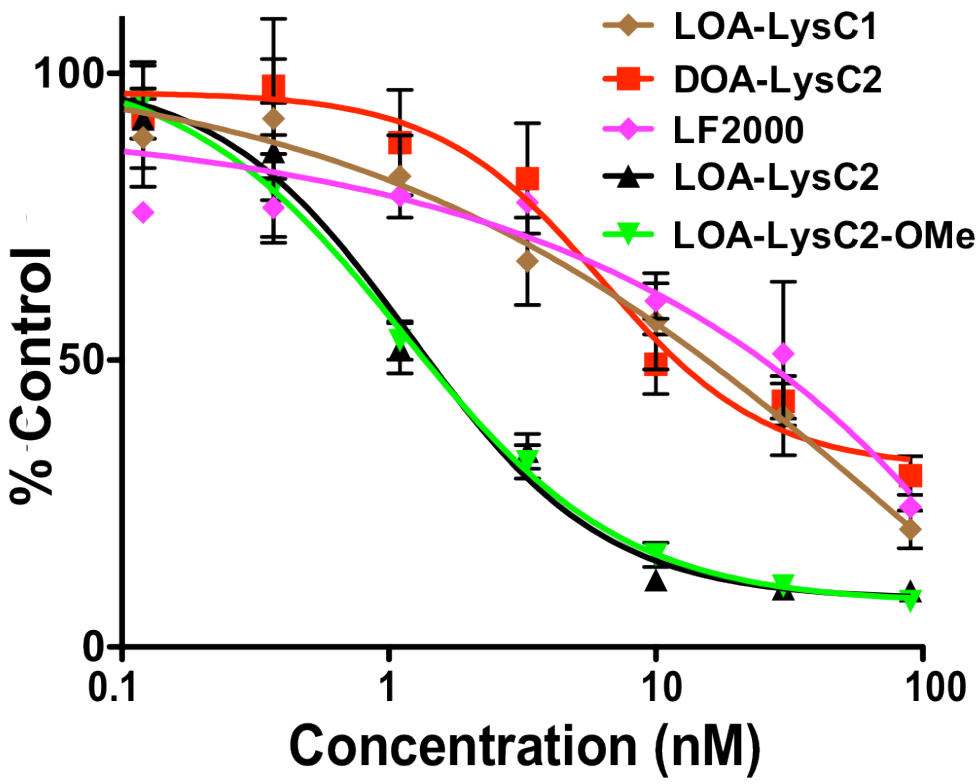

Figure 4.5: siRNA mediated knockdown of *Renilla* luciferase in stably transfected HeLa-Luc cells. ILL lipoplexes (40:40:20 ILL:Chol:DOPE) at N:P = 10 were used for all experiments.

Though transfection efficiency generally correlates with the trends seen in the BMV lysis data, there are discrepancies in the overall behavior. For example, LOA-LysC2-OMe shows significantly higher BMV lysis than LOA-LysC2, but has almost identical transfection behavior. Also, DOA-LysC2 showed no BMV lysis but still showed potent transfection. These differences may be due to differences in the lipid formulation between the lysis and transfection experiments. Inclusion of fusogenic DOPE lipids in transfection formulations likely increases the transfection efficiency by promoting membrane disruption. However, the order of magnitude difference in IC_{50} between ILLs that effectively lyse BMV and those that do not indicate that this characteristic may be important independent of liposomal formulation.

4.4.6 Factor VII knockdown in vivo with ILL liposomes

All ILL were tested for their ability to deliver siRNA *in vivo*. The mouse Factor VII model was chosen as the primary *in vivo* screen for ILL liposome mediated delivery of siRNA to hepatocytes via systemic injection.[25] Stable siRNA encapsulating liposomes suitable for systemic delivery were formulated using 40:40:10:10 ILL:Chol:DSPC:PEG-DMG at a 15:1 lipid:siRNA (w:w) ratio. The encapsulation efficiency and particle sizes of the resulting particles were 83% to 93% and 86 nm to 104 nm (Table 4.1). siRNA against the blood clotting protein Factor VII was administered at 5 mg/kg via tail vein injection. At 48 hrs post injection, blood was drawn and protein levels were assayed. Factor VII levels were unchanged compared to a PBS control for all tested ILL formulations (Figure 4.6). A positive control formulation containing DLinDMA showed potent knockdown, thereby verifying the validity of the assay.

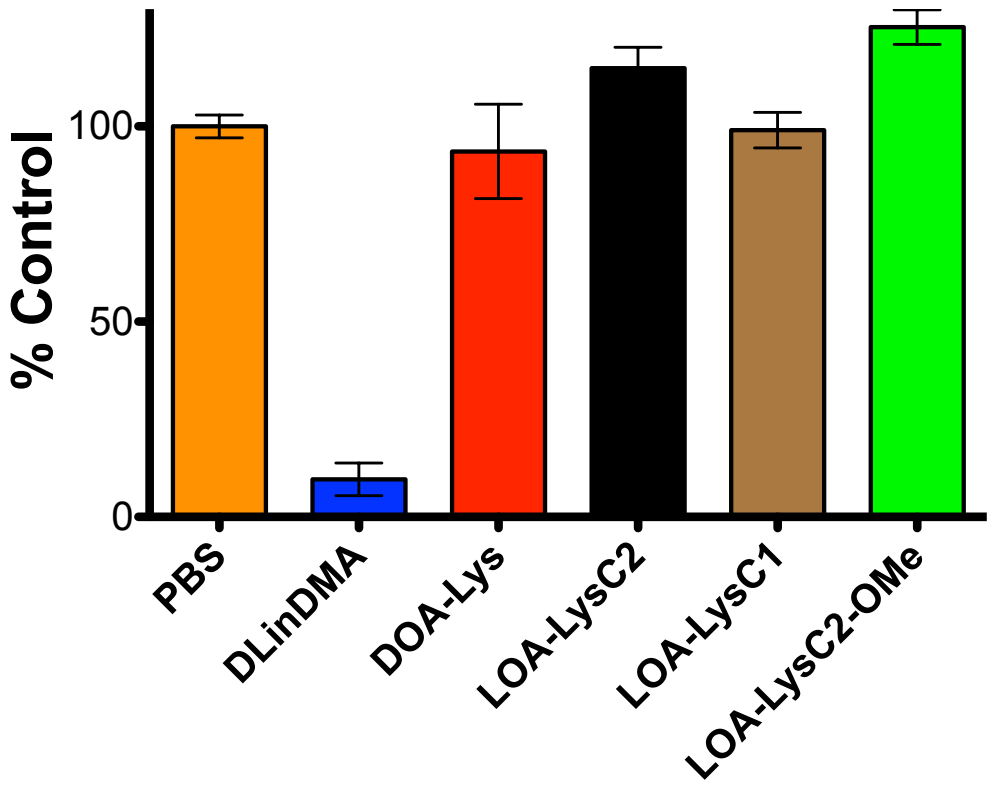

Figure 4.6: siRNA-mediated knockdown of Factor VII *in vivo* in a murine model. ILL-siRNA formulations were administered at 5 mg/kg via tail vein injection (15:1 w:w ILL:siRNA), and Factor VII levels were assayed 48 hours following administration. ILL formulation – 40:40:10:10 ILL:Chol:DSPC:PEG-DMG

Despite their potency *in vitro*, ILL show no *in vivo* knockdown in hepatocytes. The difficulty of translating effective *in vitro* transfection reagents to viable *in vivo* siRNA delivery systems is well documented; cationic systems are rapidly cleared by the RES, preventing accumulation and transfection in hepatocytes.[7,8] Additionally, structure-activity relationships for ionizable lipids have shown that slight changes in lipid structure significantly impact their *in vivo* efficacy.[9,12,20] Though our ionization data indicates that ILL are more cationic at low pH, the two most membrane active ILL (LOA-LysC2-OMe and LOA-LysC2) show no pH dependent lysis behavior. Despite their promising *in* vitro transfection data, this indicates that these two ILL may be too cationic at pH = 7.4 to avoid protein or membrane interactions in circulation, stimulating RES uptake and preventing

hepatocyte targeting. LOA-LysC1, which exhibits pH-dependent membrane lysis, has a lower extent of lysis at low pH that may prevent transfection *in vivo*. DOA-LysC2 appears to be less membrane active than all other ILL, possibly explaining its lack of efficacy. Changes to the liposomal formulation of LOA-LysC2 and LOA-LysC2-OMe did not improve results (data not shown). However, a broad, systemic manipulation of liposomal formulation, particularly the percentage of ILL as well as the choice of helper lipids or inclusion of targeting moieties may help to improve efficacy in these ILL systems.

Ionizable Lysine Lipid	Size (nm)	PDI	Encapsulation Efficiency (%)
LOA-LysC2	89.7	0.16	91.6
DOA-LysC2	98.0	0.18	93.6
LOA-LysC1	85.8	0.13	83.5
LOA-LysC2-OMe	103.6	0.15	92.7

Table 4.1: Size, PDI, and encapsulation efficiency of ILL liposomes (40:40:10:10 ILL:Chol:DSPC:PEG-DMG)

4.5 Summary And Conclusions

Here, we have described the synthesis and characterization of ionizable lysine-based lipids (ILL), a novel class of lipids with pH-dependent biophysical behavior. The goal of this work was to investigate how ionizable lipids with polyvalent, zwitterionic head groups behave compared to ionizable cationic systems. Four distinct ILLs were synthesized, and structural variations between ILLs impacted their biophysical behavior as well as their ability to deliver siRNA *in vitro*. All ILLs became increasingly cationic with a reduction in pH,

however only LOA-LysC1 was neutral at physiological pH. The ionization curves of ILL differ significantly from DLinDMA, likely due to the more complex, polyvalent head groups. All ILLs show potent siRNA mediated luciferase knockdown *in vitro* in a stably transfected HeLa-Luc cell line, with LOA-LysC2-OMe and LOA-LysC2 exhibiting IC_{50} values of roughly 1 nM. Interestingly, our *in vitro* data correlated well with our membrane lysis results, indicating that electrostatically driven membrane disruption promotes transfection. All ILLs form small diameter, monodisperse liposomes across multiple liposomal formulations, and efficiently encapsulate siRNA. However, ILL liposomes showed no *in vivo* knockdown in hepatocytes using a mouse Factor VII model. Given their potent transfection capabilities *in vitro*, the lack of *in vivo* efficacy may be due to poor targeting of liposomes to hepatocytes. Further optimization of these systems, through systemic manipulation of liposomal formulation or chemical modification of the ILL structures, may lead to higher *in vivo* efficacy.

4.6 References

1. Torchilin, V. P. Recent advances with liposomes as pharmaceutical carriers. *Nature Reviews Drug Discovery* **4**, 145–160 (2005).
2. Peer, D. & Lieberman, J. Special delivery: targeted therapy with small rnas. *Gene Ther* (2011).doi:10.1038/gt.2011.56
3. Puri, A., Loomis, K., Smith, B. & Lee, J. Lipid-based nanoparticles as pharmaceutical drug carriers: from concepts to clinic. *Crit Rev Ther Drug Carrier Syst* (2009).
4. Whitehead, K. A., Langer, R. & Anderson, D. G. Knocking down barriers: advances in siRNA delivery. *Nature Reviews Drug Discovery* **8**, 129–138 (2009).
5. Lu, J. J., Langer, R. & Chen, J. A novel mechanism is involved in cationic lipid-mediated functional siRNA delivery. *Mol Pharm* **6**, 763–771 (2009).
6. Schroeder, A., Levins, C. G., Cortez, C., Langer, R. & Anderson, D. G. Lipid-based nanotherapeutics for siRNA delivery. *J Intern Med* **267**, 9–21 (2010).
7. Stanton, M. G. & Colletti, S. L. Medicinal chemistry of siRNA delivery. *J Med Chem* **53**, 7887–7901 (2010).
8. Li, W. & Szoka, F. C. Lipid-based Nanoparticles for Nucleic Acid Delivery. *Pharm Res* **24**, 438–449 (2007).
9. Adami, R. C. *Et al.* An Amino Acid-based Amphoteric Liposomal Delivery System

for Systemic Administration of siRNA. *Mol Ther* **19**, 1141–1151 (2011).
10. Ceballos, C. *Et al.* Cationic Nucleoside Lipids Derived from Universal Bases: A Rational Approach for siRNA Transfection. *Bioconjugate Chemistry* **21**, 1062–1069 (2010).
11. Yang, H., Yi, J., Bang, E. & Jeon, E. Cationic nucleolipids as efficient siRNA carriers. *Org Biomol Chem* (2010).
12. Semple, S. C. *Et al.* Rational design of cationic lipids for siRNA delivery. *Nature Biotechnology* **28**, 172–176 (2010).
13. Love, K. T. *Et al.* Lipid-like materials for low-dose, in vivo gene silencing. *Proceedings of the National Academy of Sciences* **107**, 1864–1869 (2010).
14. Abrams, M. T. *Et al.* Evaluation of Efficacy, Biodistribution, and Inflammation for a Potent siRNA Nanoparticle: Effect of Dexamethasone Co-treatment. *Mol Ther* **18**, 171–180 (2010).
15. Zhang, J., Fan, H., Levorse, D. A. & Crocker, L. S. Interaction of Cholesterol-Conjugated Ionizable Amino Lipids with Biomembranes: Lipid Polymorphism, Structure–Activity Relationship, and Implications for siRNA Delivery. *Langmuir* 110629122925034 (2011).doi:10.1021/la201464k
16. Obata, Y., Suzuki, D. & Takeoka, S. Evaluation of cationic assemblies constructed with amino acid based lipids for plasmid DNA delivery. *Bioconjugate Chemistry* **19**, 1055–1063 (2008).
17. Zelphati, O. & Szoka, F. C. Mechanism of oligonucleotide release from cationic liposomes. *Proc Natl Acad Sci USA* **93**, 11493–11498 (1996).
18. Xu, Y. & Szoka, F. C. Mechanism of DNA release from cationic liposome/DNA complexes used in cell transfection. *Biochemistry* **35**, 5616–5623 (1996).
19. Hafez, I. M., Maurer, N. & Cullis, P. R. On the mechanism whereby cationic lipids promote intracellular delivery of polynucleic acids. *Gene Ther* **8**, 1188–1196 (2001).
20. Heyes, J., Palmer, L., Bremner, K. & Maclachlan, I. Cationic lipid saturation influences intracellular delivery of encapsulated nucleic acids. *Journal of Controlled Release* **107**, 276–287 (2005).
21. Zimmermann, T. S. *Et al.* RNAi-mediated gene silencing in non-human primates. *Nature* **441**, 111–114 (2006).
22. Fricker, G. *Et al.* Phospholipids and Lipid-Based Formulations in Oral Drug Delivery. **27**, 1469–1486 (2010).
23. Walsh, C. L., Nguyen, J. & Szoka, F. C. Synthesis and characterization of novel zwitterionic lipids with pH-responsive biophysical properties. *Chemical Communications* **48**, 5575–5577 (2012).
24. Zhang, J., Fan, H., Levorse, D. A. & Crocker, L. S. Ionization Behavior of Amino Lipids for siRNA Delivery: Determination of Ionization Constants, SAR, and the Impact of Lipid p Kaon Cationic Lipid−Biomembrane Interactions. *Langmuir* **27**, 1907–1914 (2011).
25. Akinc, A. *et al.* A combinatorial library of lipid-like materials for delivery of RNAi therapeutics. *Nature Biotechnology* **26**, 561–569 (2008).
26. Bailey, A. & Cullis, P. Modulation of membrane fusion by asymmetric transbilayer distributions of amino lipids. *Biochemistry* **33**, 12573–12580 (1994).
27. Hafez, I. M. & Cullis, P. R. Roles of lipid polymorphism in intracellular delivery. *Advanced Drug Delivery Reviews* **47**, 139–148 (2001).

28. Koynova, R., Wang, L. & Macdonald, R. C. An intracellular lamellar-nonlamellar phase transition rationalizes the superior performance of some cationic lipid transfection agents. *Proc Natl Acad Sci USA* **103**, 14373–14378 (2006).

Chapter 5: Concluding Remarks and Future Directions

In this dissertation, I present the design, synthesis, and characterization of a series of lipids for use in drug and siRNA delivery systems. The results show how small changes to lipid architecture can significantly alter the biophysical behavior of the lipid, as well as the macromolecular structures these systems form. Further understanding the structure activity relationships in lipid-based drug delivery systems is an essential part of developing new, more effective delivery vehicles for low and high molecular weight drugs.

In Chapter 2, I describe the design and development of a novel class of zwitterionic lipids with head groups containing a cationic amine and anionic carboxylic acid linked by a variable carbon spacer and ester-linked oleic acid tails. These lipids showed structure-dependent, pH-responsive biophysical characteristics when incorporated into liposomes. Additionally, they promote the low-pH encapsulation of siRNA in small, stable liposomes through electrostatic interactions. They showed no immunostimulatory effects *in vivo*, however they were not capable of promoting siRNA delivery both *in vitro* and *in vivo*.

Based on the results of the work in Chapter 2, I extended the idea of an amine/carboxylate containing zwitterionic lipid and synthesized a series of acetate terminated diacyl lipids with saturated aliphatic hydrophobic chains. Chapter 3 describes the synthesis and characterization of these novel lipids. These lipids possess an inverted headgroup charge orientation compared to naturally occurring zwitterionic lipids, which impacts their interactions with ions in solution, and may be useful to modulate the release kinetics of small molecules from liposomes. Interestingly, these lipids show elevated melting temperatures compared to phosphatidylcholine lipid analogs, and exhibit salt dependent biophysical

characteristics. These are the first reported non-phosphate containing zwitterionic lipids for drug delivery, and their interesting properties may prove useful for drug delivery applications.

In Chapter 4, I synthesized and characterized a focused library of ionizable lysine-based lipids, which contain a lysine head group linked to a long-chain dialkylamine. Four distinct lipids were synthesized to determine the impact of hydrophobic fluidity, lipid net charge, and lipid pKa on the biophysical and siRNA transfection characteristics of this novel class of lipids. Our results show that structural variations significantly impact the behavior of liposomes containing these lipids. Increasing the fluidity of the hydrophobic region or the net charge of the lipid significantly increases their ability to interact with membranes and deliver siRNA *in vitro*. However, these systems were not capable of delivering siRNA to hepatocytes *in vivo*.

Our results show that slight structural modifications impact the biophysical behavior of lipids, which in turn dictates their potential utility in drug delivery systems. The synthesis and characterization of novel lipids furthers our understanding of how these molecules behave in macromolecular systems, and help us understand what specific characteristics are required for various drug delivery applications. The work described in this thesis shows how head group modifications alter the pH and salt-dependent behavior of zwitterionic lipids. Interestingly, our results indicate that interfacial charge density and orientation may play an important role in ionic interactions between lipids and their environment. This idea is important for drug delivery, as it alters the kinetics of drug release based on the charge orientation and the lipid bilayer and the net charge of the encapsulated drug. Additionally, it is important for siRNA delivery, because ionic interactions promote membrane

destabilization and fusion, two steps that are believed to be essential for the successful delivery of siRNA to the cytosol.

The impact of charge density and orientation on zwitterionic lipid-based siRNA delivery systems will be further explored in a new class of lipids with head groups containing two adjacent tertiary amines and a terminal carboxylate. We believe that the higher cationic charge density at the membrane interface will promote membrane destabilization, while the presence of the carboxylate at least partially mitigates the immunostimulatory effects of the cationic lipid. The assays described in this dissertation will be used to determine the biophysical, transfection, and immunostimulatory characteristics of these new lipids. These results will further our understanding of the relationship between lipid head group charge density and orientation on lipid behavior in siRNA delivery systems.

Publishing Agreement

It is the policy of the University to encourage the distribution of all theses, dissertations, and manuscripts. Copies of all UCSF theses, dissertations, and manuscripts will be routed to the library via the Graduate Division. The library will make all theses, dissertations, and manuscripts accessible to the public and will preserve these to the best of their abilities, in perpetuity.

Please sign the following statement:

I hereby grant permission to the Graduate Division of the University of California, San Francisco to release copies of my thesis, dissertation, or manuscript to the Campus Library to provide access and preservation, in whole or in part, in perpetuity.

Cali Walsh
Author Signature

6/13/12
Date